ISTANBUL TECHNICAL UNIVERSITY ★ GRADUATE SCHOOL OF SCIENCE ENGINEERING AND TECHNOLOGY

PRODUCTION OF DYE SENSITIZED SOLAR CELL AND OPTIMIZATION OF PRODUCTION PARAMETERS

M.Sc. THESIS
Ramazan ŞİMŞEK

Department of Nano-Science and Nano-Engineering

Nano-Science and Nano-Engineering Programme

Thesis Advisor: Asst. Prof. Dr. Ali KILIÇ

AUGUST 2015

ISTANBUL TECHNICAL UNIVERSITY ★ GRADUATE SCHOOL OF SCIENCE ENGINEERING AND TECHNOLOGY

PRODUCTION OF DYE SENSITIZED SOLAR CELL AND OPTIMIZATION OF PRODUCTION PARAMETERS

M.Sc. THESIS
Ramazan ŞİMŞEK
513131020

Department of Nano-Science and Nano-Engineering

Nano-Science and Nano-Engineering Programme

Thesis Advisor: Asst. Prof. Dr. Ali KILIÇ
Textile Technologies and Design Faculty

AUGUST 2015

İSTANBUL TEKNİK ÜNİVERSİTESİ ★ FEN BİLİMLERİ ENSTİTÜSÜ

BOYA UYARIMLI GÜNEŞ PİLLERİNİN ÜRETİMİ VE ÜRETİM PARAMETRELERİNİN OPTİMİZASYONU

YÜKSEK LİSANS TEZİ
Ramazan ŞİMŞEK
513131020

Nano-Bilim ve Nano-Mühendislik Ana Bilim Dalı
Nano-Bilim ve Nano-Mühendislik Programı

Tez Danışmanı: Yrd. Doç. Dr. Ali KILIÇ
Tekstil Teknolojileri ve Tasarımı Fakültesi

AĞUSTOS 2015

Ramazan ŞİMŞEK, a M.Sc. student of **ITU Graduate School of Science Engineering and Technology** student ID 513131020, successfully defended the thesis entitled "**PRODUCTION OF DYE SENSITIZED SOLAR CELL AND OPTIMIZATION OF PRODUCTION PARAMETERS**", which he prepared after fulfilling the requirements specified in the associated legislations, before the jury whose signatures are below.

Thesis Advisor:	**Asst. Prof. Dr. Ali KILIÇ** Istanbul Technical University
Jury Members:	**Prof. Dr. Ali DEMİR** Istanbul Technical University
	Asst. Prof. Dr. Mustafa ÇAKIR Marmara University

Date of Submission : 14 August 2015
Date of Defense : 17 August 2015

To my wife and sweet daughter,

FOREWORD

I would like to express my gratitude to my thesis supervisor, Asst. Prof. Dr. Ali KILIÇ, for his continuous encouragement and guidance during my graduate studies and for his helpful critiques and discussions on my work.
I would like to thank to TUBİTAK for the great support within TUBİTAK 2211 (2210-D) Domestic Graduate Scholarship Programme for Industry
I would like to thank to ITU for funding via institution of scientific research projects
I would like to thank Prof. Dr. Ahmet GÜL, Dr. Barbaros AKKURT for their supports and guidance.
I especially would like to thank my friends in the TEMAG laboratory especially Mehmet D. ÇALIŞIR for his collaboration and friendship.
I would also like to extend my deepest gratitude to my wife Güler UÇAN ŞİMŞEK stood by me and heartedly supported. I was able to accomplish everything in my life, thanks to her eternal love.
Finally, I would like to thank all of my friends for their emotional support and motivation during this difficult accomplishment.

August 2015

Ramazan ŞİMŞEK
Textile Engineer

TABLE OF CONTENTS

Page

.

ABBREVIATIONS

DSCs	**:** Dye Sensitized Solar Cells
SEM	**:** Scanning Electron Microscopy
XRD	**:** X-Ray Diffractometer
PL	**:** Photoluminescence
UV	**:** Ultraviolet
LED	**:** Light Emitting Diode
RA	**:** Reductive Atmosphere
Cd	: Cadmium
Te	: Telluride
Ga	**:** Gallium
As	**:** Arsenic
CIGS	**:** Copper Indium Gallium Selenite
HTM	**:** Hole Transfer Material
QD	: Quantum Dots
SSSCs	: Semiconductor Sensitized Solar Cells
spiro-OMeTAD	:2,2′,7,7′-tetrakis(N,N-p-dimethoxy-phenylamino)-9,9′-spirobifluorene
LiTFSI	: Lithium bis(trifluoromethanesulfonyl) imide
tBP	: 4-tert-butylpyridine
LHE	: Light Harvesting Efficiency
PFF	: Pore Filling Fraction
SCM- TiO_2	: Single Crystal Mesoporous TiO_2
AcAc	: Acetyl Acetone
IPA	: Isopropanol
TCO	: transparent conductive material

LIST OF TABLES

Page

LIST OF FIGURES

Page

PRODUCTION OF DYE SENSITIZED SOLAR CELL AND OPTIMIZATION OF PRODUCTION PARAMETERS

SUMMARY

Basically, a solar cell is a kind of device that converts light energy into electrical energy through energization of electrons. They are broadly classified in three generations. First-generation solar cells are well-known, silicon-based photovoltaic cells that mainly dominates the solar cell market. This group contains monocrystalline and polycrystalline solar cells. While first generation solar cells have high efficiency, they have some disadvantages such as high manufacturing costs and requirement for well controlled production facilities. Against disadvantages of first generation solar cell, second generation solar cells were developed which are also considered as thin film solar cells. Thin film solar cells have cheaper manufacturing techniques. On the other hand they have lower efficiency than silicon-based solar cells have. Thin film solar cells include modified transition metals such as amorphous silicon (a-Si), Cd–Te, Ga–As and CIGS. It is important to note that, even though these two group of solar cells have some advantageous sides, the raw materials used in manufacturing process of solar cells have high cost or hazardous to environment and human health. Hence further studies on environmentally friendly, cheaper and high efficiency solar cells resulted with third generation solar cells. This group is also called as excitonic solar cells. The excitonic solar cells have different kinds of operation principals and they can also be grouped into nanocrystalline, dye-sensitized solar cells (DSCs) and organic/polymer solar cells. Of these, DSCs have commercial application but it is not in mature state yet.

DSCs show great promise as an inexpensive alternative to conventional p–n junction solar cells. Highly efficient photovoltaic conversions, combined with ease of manufacturing and low production costs, make the DSC technology an attractive approach for large-scale solar energy conversion. These cells are expected to be the next generation of solar cells because of the lower loads to environment during manufacturing. Solidification of DSC was one of the crucial research items. While photovoltaic applications have been dominated by solid-state junction devices, usually made from crystalline or amorphous silicon and profiting from the experience and material availability resulting from the semiconductor industry, there is an increasing awareness of the possible advantages of devices based on mesoscopic inorganic or organic semiconductors commonly referred to as “bulk“ junctions because of their interconnected three-dimensional structure.

DSCs are basically formed from nanocrystalline inorganic oxides, ionic liquids, and organic hole conductor or conducting polymer devices. Energy harvesting is accomplished by the optical absorption and charge separation processes after the association of a sensitizer as a light absorbing material with a wide-band-gap semiconductor of mesoporous or nanocrystalline morphology. They do not require energy-intensive high temperature and high-vacuum processes, and can be compatible

with flexible substrates, and a variety of presentations and appearances which might facilitate market entry, both for domestic devices and in architectural or decorative applications.

It is one of the expected results that the liquid electrolyte may inhibit the stability of DSCs, which led many studies for producing solid state DSCs. On the other hand in order to produce solid state Dye-Sensitized Solar cell (ssDSC) in commercial scale, it is clear that high temperature processing is another obstacle. Thereby, a few studies appeared on low temperature processed-ssDSCs so far. Especially, after coating of TiO_2 paste sintering process is still followed to obtain mesoscopic porous structure.

Commercialization step is looking for some intriguing properties such as flexibility, ease of integration, stability and cost effectiveness. Hence, manufacturing flexible ssDSCs can be realized by meeting the need of using flexible, transparent and conductive electrodes in ssDSCs' structure. In that point, polymeric based transparent materials having durability against high temperature suggested as electrode. Polyethylene terephthalate (PET) and Polyethylene naphthalate (PEN) are current candidates for the electrode of commercial ssDSCs due to durability against temperature up to 150 ^{o}C. Thus, in this thesis study, manufacturing ssDSCs at low temperatures (less than 150 ^{o}C) was set forth as the main research question. Production of fully printable solid state dye sensitized solar cell (ssDSC) was aimed to produce with moderate efficiency. Besides that, a facile way was investigated producing ssDSC for industrial mass production.

In this regard, doctor blade and screen printing technologies were compared to produce ssDSCs. Screen printing is a well-known application from local textile industry for coloration of textile goods, which is basically a kind of application of stenciling. Many experiments were ran with the stencils by defined shapes. Prepared ink was transferred through the holes onto conductive glass to be able to form mesoporous metal oxide layers.

Sensitization of metal oxide layers was performed by photoactive perovskite structures. Methyl ammonium lead iodide was synthesized successfully via reaction of methyl amine, hydroiodic acid. Then, lead iodide was also obtained by reaction of lead nitrate and potassium iodide. As a counter electrode, carbon-based materials was deposited on Zirconia layer acting as a spacer layer. Subsequently, characterization and analysis of ssDSCs produced in this thesis study was performed by using AM1,5G solar simulator. Formation of monolithic ssDSC using screen printing technology was resulted in solar cells in lab scale showed higher efficiency compared to the one produced via doctor blading.

Last of all, ssDSC structure and its components was manufactured successfully by using screen printing and doctor blade techniques enabling large area deposition. Hence, it can be considered as an important step to realize DSCs production in industrial scale.

BOYA UYARIMLI GÜNEŞ PİLLERİNİN ÜRETİMİ VE ÜRETİM PARAMETRELERİNİN OPTİMİZASYONU

ÖZET

Enerji gereksinimine duyulan ihtiyaç her geçen gün giderek artmaktadır. Bu ihtiyacın karşılanması için kullanılan kaynakların tüketimi neticesinde ortaya çıkan karbon salınımının çevreye zararlı olduğu bilinmektedir. Çevreye daha az yük getiren ve ekonomik açıdan daha uygun olan yenilenebilir enerji kaynaklarının kullanımı ön plana çıkmıştır. Bu kaynakların kullanımı ülkemiz için de öncelikli alanlardan biridir. Temiz ve ucuz yenilenebilir enerji kaynağı olan güneş enerjisinin kullanımı için hali hazırda kullanılan silikon bazlı güneş pillerinin üretim teknolojisi ve maliyeti dikkate alındığında insanoğlu daha rantabl çözümler arayışına girmiştir. Dünyanın toplam enerji ihtiyacı 2010 itibariyle $5x10^{20}$J seviyelerini yakaladığı tahmin edilmekte ve bu değerin önümüzdeki 20 yıl boyunca yıllık %2 artış göstereceği öne sürülmektedir. Uluslararası Enerji Ajansı'nın 2010 yılı verilerine göre günlük 85 milyon varil petrol, 3milyon ton kömür tüketilmektedir. Bu miktarda tüketim baz alındığında fosil kaynakların 40-60 yıl arasında ekonomik ömrünün kaldığı hesaplanmaktadır. Diğer yandan insan sağlığı, çevre ve iklim üzerinde her geçen gün bir başka zararı keşfedilen sera gazlarının fosil yakıt tüketiminden kaynaklanması yenilenebilir enerjiye yönelimi zorunlu kılmaktadır. Yenilenebilir enerji şirketler ve ülkeler için önemli bir sektör ve rekabet kalemidir ve yakın gelecekte öneminin daha da artacağı beklenmektedir.

Ülkemiz açısından bakıldığında ise enerji faturasının toplamda 60 milyar doları bulduğu gözlenmektedir. Artan sınai üretim sebebiyle bu rakam her yıl yaklaşık %9 büyüme kaydetmektedir. 2023 itibariyle enerjinin %30'unun yenilenebilir kaynaklarından eldesi hedeflenmiştir. Bu açıdan güneş enerjisi oldukça kritik bir kaynak olarak karşımıza çıkmaktadır. Bunun yanı sıra fotovoltaik teknolojileri pazarı 1997'den beri yıllık %33 civarında büyümektedir ve en iyi senaryolara göre 2100 yılında enerji üretiminin yarısının güneş enerjisi teknolojilerinden karşılanacağı öngörülmektedir. Güneş enerjisi fosil yakıt darboğazındaki ülkemiz açısından ciddi bir alternatiftir. Çünkü Akdeniz havzasında bulunan ülkemizin özellikle güney bölgelerinde havanın yılın 300 günü güneşli, ortalama sıcaklığın 19°C civarında olması sebebiyle fotovoltaik enerji üretimi için büyük avantaja sahiptir.

Güneş pilleri genellikle 3 kategoride (3 nesil) incelenmektedir. Birinci nesil güneş pilleri fosfor ve bor katkılı kristalin silisyum veya germanyum içeren bir p-n eklemi yapısındadır. Pazar payı daralsa da bu piller halen en yaygın olan pillerdir. Elektronik endüstrisinin yan ürünleri güneş pili olarak kullanılmaktadır. Kurulum ve üretim maliyeti yüksek saflıkta silisyum gerektirmesinden yüksektir. Ülkemiz her ne kadar birinci nesil silisyum teknolojilerinde geri kalsa da 2020 yılına kadar Si içeren ve Si içermeyen güneş pili teknolojilerinin aynı pazar yüzdesine sahip olacağı; 2030 yılında Si bazlı güneş pillerinin pazarın %20'nin altına ineceği öngörülmektedir. Bu sebepten Si içermeyen yüksek performans ve yüksek performans/maliyet oranlı ürünler üzerine çalışmalar yoğunlaşmalıdır. Bu beklentiler ışığında yerkürede toplam kaynağı çok az

olan indiyum, galyum, telurid gibi bileşenleri olan güneş pillerinin yerine; daha kolay ve ekonomik yollarla ulaşılabilen ürünlere yoğunlaşılması önem arz etmektedir. İkinci nesil güneş pilleri denilen bu tip piller sandviç yapılı ince film morfolojisinde olup birinci nesle nispeten daha az aktif malzeme gerektirmektedir. Kadmiyum tellurid (CdTe), bakır indiyum galyum diselenid (CIGS) ve amorf silisyum (a-Si) tabanlı güneş pilleri yaygın olarak kullanılan ikinci nesil güneş pillerinden birkaçıdır.

Kadmiyum tellürid esaslı ince film güneş pilleri watt başına maliyet açısından kristalin silisyum en yakın ikinci nesil güneş pilleridir. Ancak kadmiyumun çok zehirli olması ve tellür kaynaklarının azlığı bu pillerin üretiminde en büyük sorundur. Yine de 2013 verilerine göre ince film güneş pillerinin yarısından fazlasını oluşturmaktadır. Bakır indiyum galyum diselenid (CIGS) tabanlı güneş pilleri ikinci nesil ince film güneş pilleri arasında en yüksek verimliliğe sahip olanıdır [6], [7]. CIGS güneş pillerinin absorpsiyon katsayısı silisyum olanlara göre daha fazla olduğu için aynı kalınlıkta silisyuma güre daha fazla ışık emilimi yapar. Bu da daha ince ve daha hafif güneş pillerinin üretilmesine olanak sağlar. Yukarda bahsedilen birinci ve ikinci nesil güneş pillerinin dezavantajlarını göz önüne alarak üçüncü nesil eksitonik güneş pilleri geliştirilmiştir. Eksitonik güneş pilleri silisyum bazlı güneş pillerinin dezavantajlarının birçoğunu ortadan kaldırmıştır. Genel olarak üçüncü nesil güneş pilleri de kendi aralarında 3 farklı grupta değerlendirilmektedir:

- Nanokristalin tabanlı güneş pilleri
- Boya Uyarımlı Güneş Pilleri (BUGP)
- Organik / Polimer tabanlı güneş pilleri

Bahsedilen üçüncü nesil güneş pilleri içerisinde BUGP yeni ticarileşmeye başlamış, üretimi kolay ve hatırı sayılır enerji verimliliği sağlayan sınıfı temsil etmektedir. Bu anlamda BUGP'nin avantajları:

- Açık laboratuvar koşullarında üretilebilmesi, temiz oda gerektirmeyişi
- Bileşenlerinin birçoğunun ülkemiz kaynaklarından sağlanması
- Bileşenlerinin işlenmesi üzerine laboratuvarlarımızın tecrübesi
- Performans açısından mütevazi olsa da performans/maliyet oranında yüksek değerler göstermesi

olarak özetlenebilir.

Bu anlamda 5MW altı yatırımlara yönelik paneller, ev tipi, kapalı ortam pilleri, elektronik cihaz pilleri, cam üzerine işleme gibi alanlarda tercih edileceği öngörülmektedir.

BUGP üzerine araştırmalar 1960 sonlarına gitse de önemli ilerleme Gratzel ve ekibinin geniş aralıkta emilim yapan boyarmaddelerin nanokristalin TiO_2 kompleksinin senteziyle gerçekleştirilmiştir. Bu sayede ilk kez inorganik bazlı güneş pillerinin verimi basit bir mekanizma ve ucuz malzemeler kullanarak mümkün hale gelmiştir. Hava kütle katsayısı 1.5AM ışıması altında verimlilik %10 seviyeleri yakalanmıştır.

Boya uyarılı güneş pillerinin (BUGP) çalışma mekanizması incelendiği takdirde üç temel fonksiyon icra edilmektedir. Bunlar boyar maddenin (BM') fotouyarımı, metal oksite (MO) elektron transferi, redoks çiftinden aldığı elektronla BM'nin rejenerasyonu. Yarı iletken film tabakası elektrolit, boya ve çalışan elektrot ile temas halindedir. Güneşten gelen fotonların boya molekülüne çarpması neticesinde boya molekülünden bir elektron TiO_2 'in iletkenlik bandına aktarılır. Elektron TiO2 üzerinden iletken elektrotlara sonrasında ise dış devreye taşınır. Karşı elektrotta

elektrolitte meydana gelen indirgenme reaksiyonu ile elektron elektrolite taşınır. Son olarak yine uyarılan BM elektrolitten elektron transfer ederek sakin duruma geçer ve süreç tamamlanmış olur. Sistemde yer alan TiO_2 elektron toplayıcı ve boyanın yüzey alanını artırıcı yönde görev yapar. TiO2 çalışan elektrot üzerine kaplanmakta ve TiO_2 üzerine ise BM molekülü tutunmaktadır. BUGP'nin verimliliğini artırmak amacı ile TiO_2'nin spesifik yüzey alanı artırılması önemlidir. Bu sayede BM'ye yüksek düzeyde yüzey alanı sağlamakla görevlidir. Bunun yanı sıra metal oksit tabaka elde edilen serbest elektronları çalışan elektroda iletim görevini de üstlenmiştir. Yukarıda da açıklandığı üzere güneşten gelen ışınların uyarıcıya çarpması neticesinde, boyarmadde uyarılarak son yörüngesindeki elektronlar uyarıcının iletkenlik bandına aktarılır. Daha sonra ise uyarılan elektron uyarıcının iletkenlik bandından, metal oksit tabakanın iletkenlik bandına doğru hareket eder. Metal oksit tabakanın iletkenlik bandına aktarılan elektronlar burada metal oksit tabakanın sahip olduğu 3 boyutlu yapısı ile iletken elektrotlara aktarılarak bir dış devreye geçirilir. Elektronun tüm bu hareketi sırasında bir potansiyel enerjisi vardır ki bu enerji miktarı MO'nun Fermi enerji seviyesine eşittir.

BUGP'nin yapısın incelendiği zaman yapı da yer alan sıvı elektrolitin sızma ya da buharlaşma gibi çeşitli nedenlerle BUGP yapısın terk etmesi BUGP için bir dezavantaj olarak değerlendirilmiştir. Bu durum aynı zamanda BUGP'nin ticarileşmesi yolunda en büyük problemlerden görülmüştür. Bu doğrultuda sıvı elektrolit yerine katı yük taşıyıcı bileşenlerin kullanımı ile katı hal boya uyarımlı güneş pilleri (khBUGP) geliştirilmiştir.

Bu tez çalışması kapsamında her bir bileşeninin baskı tekniği kullanılarak üretildiği khBUGP üretimi amaçlanmıştır. Bu doğrultuda üretilen laboratuvar ölçekli khBUGP'nin endüstriyel boyutta da üretimi için yöntemler araştırılmıştır.

Bu doğrultuda yapılan çalışmalar neticesinde khBUGP başarılı bir şekilde üretilmiştir. Üretilen khBUGP'ler hava kütle katsayısı 1.5AM ışıması altında karakterize edilmiştir. Gerçekleştirilen karakterizasyonlar ve neticesinde yapılan analizler gösterdi ki, serigraf baskı tekniği kullanılarak elde edilen khBUGP, bıçak sıyırma yöntemine kıyasla daha yüksek verimlilik değeri göstermiştir. khBUGP üretiminde kullanılan her iki biriktirme tekniğinin geniş alanda kaplamaya imkan sağlaması, khBUGP'nin endüstriyel boyutta üretimi için önemli bir parametredir. Netice olarak bu tez çalışması kapsamında khBUGP'nin endüstriyel boyutta üretimi için üretim parametrelerinin de optimize edildiği bir yöntem geliştirilmiştir.

1. INTRODUCTION

1.1 Motivation

Global warming and green gas effect is one of the most challenging problem in human life nowadays. In this regard, demands for cleaner earth and also fresh air is getting larger due to environmental pollution step from the combustion of fossil fuels which has frightening climatic consequences. It is also important to note that the greenhouse effect is the consequences of excessive usage of fossil fuels Therefore there is an increasing public awareness of clean energy. So far many alternative solutions provided by scientist. One of the most promising approaches is harvesting energy from sun light. Sun has been endowed for humankind to supply energy to the earth. Total solar energy received by earth is about $3x10^{24}$ J $year^{-1}$ or about 10^4 times more than value which humankind consumes in 2005. In other words, furnishing earth's surface with solar cells in only 0.1% rate with an efficiency of 10% will be enough to satisfy all human need in 2005 [1]. This study is dedicated to investigate the feasible and cost-effective ways to manufacture solar cells.

1.2 Types of Solar Cells

Basically, a solar cell is a kind of device of which duty is to convert directly the light energy into electrical energy through the electron movement. Giribabu et al. [2] categorized solar cells in three generations:

1.2.1 First-generation solar cells

First-generation solar cells are well-known, silicon-based photovoltaic cells that mainly dominates the solar cell market. Monocrystalline and polycrystalline solar cells are included in this group. While first generation solar cells have high efficiency, they have some disadvantages such as high manufacturing costs and complexity of production condition requiring high technology facilities. Those disadvantages of first generation solar cell have been tried to overcomed by second generation solar cells.

1.2.2 Second generation

Second generation solar cells were proposed to overcome disadvantages of firs generation solar cells. Those are basically thin film solar cells. Thin-film solar cells require cheaper manufacturing techniques. However, on the other hand they exhibit lower efficiency than silicon-based solar cells. Thin-film based solar cells contain production and modifying of some transition metals such as amorphous silicon (a-Si), Cd–Te, Ga–As and CIGS. It is important to note that, even though these two group of solar cells have some advantageous sides, the raw materials used in manufacturing process of solar cells have high cost or hazardous to environment and human health.

1.2.3 Third generation

As a result environmentally friendly, cheaper and moderate efficiency solar cell were proposed as third generation solar cells. This group is also called as excitonic solar cells. The excitonic solar cells have different kinds of operation principals and they can also be categorized as nanocrystalline, dye-sensitized solar cells (DSCs) and organic/polymer solar cells. Of those, currently DSCs are commercially produced, but even thıs technology is not mature yet [3].

In this research study, after investigation of operational principals of DSCs, several approaches were proposed to produce low cost and high efficiency DSCs at industrial scale.

1.3 A Feasible Approach in Third Generation Solar Cells: Dye Sensitized Solar Cells (DSCs)

Dye-sensitized solar cells (DSC) show great promise as an inexpensive alternative to conventional p–n junction solar cells[4]. Highly efficient photovoltaic conversions, combined with ease of manufacturing and low production costs, make the DSC technology an attractive approach for large-scale solar energy conversion[5]. These cells are expected to be the next generation of solar cells because of the lower loads toward environments during manufacturing. Solidification of DSC was one of the crucial research items[6]. While photovoltaic industry has been dominated by solid-state junction devices, usually made from crystalline or amorphous silicon and benefited from the experience and material availability coming from the semiconductor industry, there is an increasing awareness of the possible advantages of

devices based on mesoscopic inorganic or organic semiconductors commonly referred to as “bulk“ junctions because of their interconnected three-dimensional structure[1]. DSCs are established by using nanocrystalline inorganic oxides, liquid electrolyte, and hole transfer material (HTM). The explained structure has a wide prospect leading to low cost fabrication without expensive and energy-intensive high temperature and high-vacuum processes. Besides compatibility with flexible substrates is another important and intriguing properties of DSCs facilitating commercialization, both for domestic devices and in architectural or decorative applications[1].

DSCs structures accomplishes the optical absorption and charge separation processes by the association of a sensitizer as a light absorbing material with a wide-band-gap semiconductor of mesoporous or nanocrystalline morphology.

1.3.1 Operational Principle of the DSC

In this part, light harvesting mechanism of conventional solar cells was summarized briefly. Then, operational principal of DSC was explained.

-p-n Junction

A semiconductor is the material having narrow band gap energy, while insulators have wide band gap energy (Figure 1.1). Photons coming from sun in a wave form excite electrons from valence band of semiconductors to the conduction band by giving rise to formation of electron-hole pairs which are so called excitons. The p-n junction is the phenomena used to explain charge separation to generate electric energy via solar irradiation [7], [8].

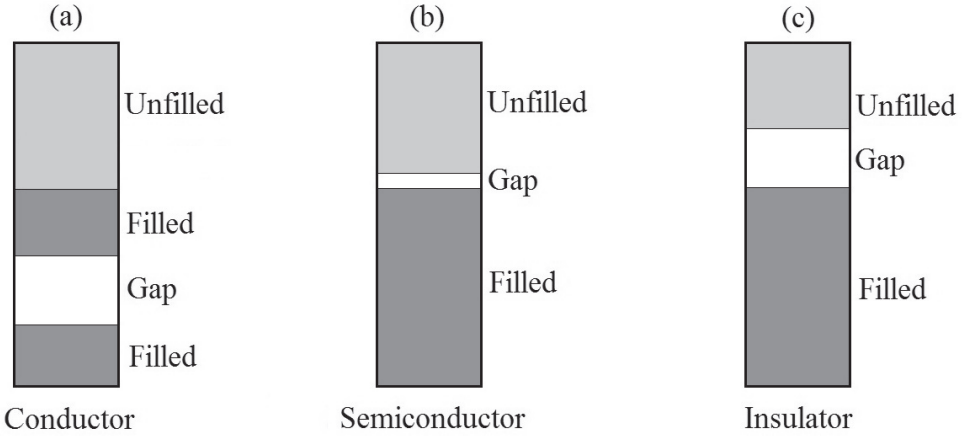

Figure 1.1 : Demonstration of HOMO and LUMO Energy level in a) conductor b) semiconductors c) insulators

Electrons having same energy levels form energy bands which vary from conductive materials to insulators (**Figure 1.2**). In conductors, the highest occupied energy level

is in the middle of an energy band while semiconductors' the highest occupied energy level places just bottom of valance band energy level. However, for insulators, the energy gap is wide notably so they can't achieve electron conduction [7].

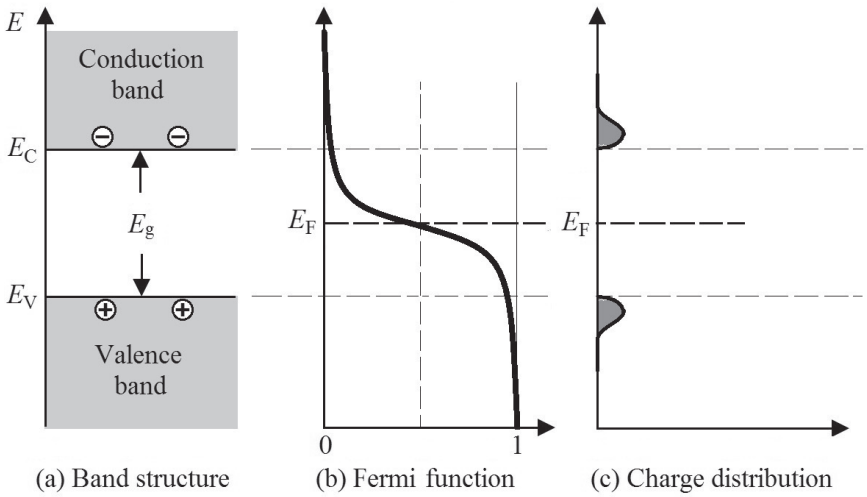

Figure 1.2 : Demonstration of energy bang gap, fermi energy level and charge distribution in semiconductors.

A semiconductor has no conductivity or exhibits too low conductive behavior. However, conductivity of a semiconductor depends on temperature. At low temperature, semiconductors have no charge mobility, but with the increasing temperature, conductivity of semiconductors increases dependently.

Besides temperature dependence of semiconductor conductivity, impurities play an important role to engineer the electrical properties of semiconductors. There are two types of impurities, n-doping and p-doping. Generally, group V atoms are used in n-doping process of silicon and germanium. Dopant atoms give an electron to conduction band of semiconductors. Thus, dopant atoms can be so called as donor atoms due to electron donation. Group V atoms have one more electron compared to group IV atoms, hence the extra electron can release to conduction band of semiconductors via excitations. Because of that, Fermi energy level shift towards conduction energy band as shown in **Figure 1.3**. While intrinsic semiconductors' conductivity depends on temperature, at the same time concentration of electron equals to hole concentration. And it is assumed that free electron concentration equals to donor atoms concentration.

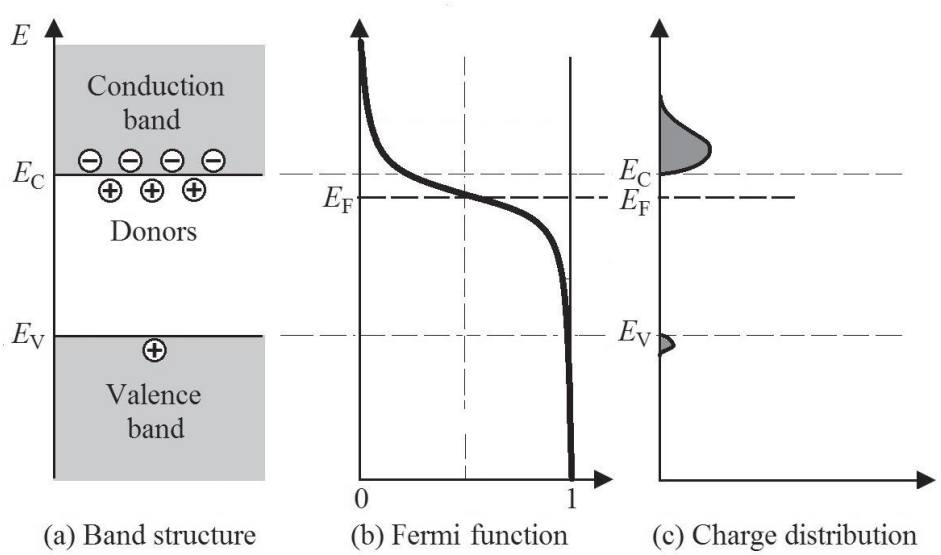

Figure 1.3 : Demonstration of energy band gap, fermi energy level and charge distribution in n-doped semiconductors.

From different view point of that, if silicon and germanium (group IV atoms) are doped with group III atoms, different mechanism will be proceeded, because group III atoms have three electron in their valence band and will have tendency to grab an electron from valence band of semiconductors by forming holes in valence band. In this case, Fermi energy level will be shifted towards valance band as shown in Figure 1.4. If the temperature is not so low, all acceptor atoms will be rendered to negative ions, and it will be assumed that density of holes equals to acceptor atoms' density [7].

Fermi-Dirac Statistic states the electron concentration (n_o) in conduction band of semiconductor with respect to formula below:

$$n_o = N_C f(E_C) \qquad \textbf{(1)}$$

Where Nc is the effective density of states of the conduction band, Nc value vary with respect to the semiconductor type, and $f(E_C)$ is the Fermi function which states the electron distribution in the temperature of 0^oK.

Fermi function can be written for room temperature as

$$f(E_C) = \frac{1}{e^{(E_C - E_f)/K_b T} + 1} \approx E^{-(E_C - E_F)/K_b T} \qquad \textbf{(2)}$$

As a consequence, concentration of electron in intrinsic semiconductor can be expressed as

$$n_o = N_c E^{-(E_C - E_F)/K_b T} \quad (3)$$

With same approaches, hole concentration can be written as

$$p_o = N_v E^{-(E_f - E_v)/K_b T} \quad (4)$$

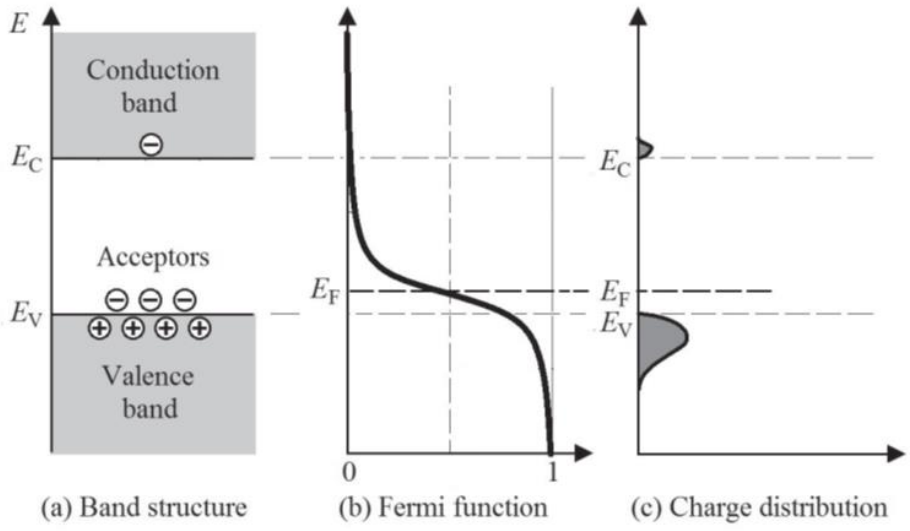

Figure 1.4 : Demonstration of band gap energy, fermi energy and charge distribution in p-doped semiconductors

Where $p_o$is hole concentration, N_v is the effective density of states in the valence band and E_v is the energy level of the valence band [7]. According to formulas and explanations above, electron concentration are affected by difference between energy level of conduction band and Fermi energy level, while hole concentration depends on difference between energy levels of Fermi and valance band, not band gap energy.

-Formation of p-n junctions

p-n junction is an interesting phenomena and it is established if p-type semiconductor and n-type semiconductor, somehow, come together, so *built-in potential* occurs at interface between n-type and p-type semiconductor. The reason behind establishment of built-in potential is difference between Fermi levels of p-type and n-type materials. Because Fermi level of p-type material is closed to energy level of valence band, while n-type semiconductor has Fermi energy level which is closer to conduction band of semiconductor. However, when p-type and n-type semiconductors come together and form p-n junction, Fermi levels of p and n type semiconductors must match each other. Therefore, band bending observes in p-type and n-type semiconductors.

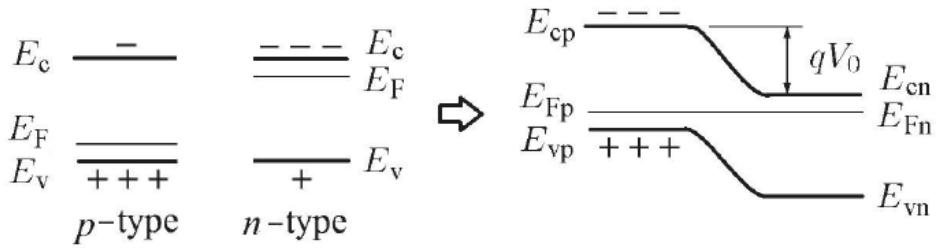

Figure 1.5 : Built-in potential in p-n junction

In Fermi level in Figure 1.5, E_{cp} represents the energy level of conduction band of p-type semiconductor, E_{cn} corresponds to energy level of conduction band of n-type semiconductor. Fermi energy level of n-type semiconductor (E_{F_n}) must be equal to Fermi energy level of p-type semiconductor (E_{F_p}), so energy bands bend by the difference between E_{cp} and E_{cn}. Thereof, built-in potential can be acquired via

$$qV_0 = E_{cp} - E_{cn}$$

When focused on charge transfer at p-n junction, it is clear to note that n-type semiconductor has excess electron due to donor atoms and p-type semiconductor has excess hole due to acceptor atoms. With the p-n junction formation, electron movement takes place and excess electron in n-region start to flow towards p-region by leaving positive charged donor atoms in n-region, same is valid for p-region, holes moves towards n-region and leaves negative charged acceptor atoms in p-region. After reaching equilibrium condition, depletion region occurs at p-n junction border with no excess electron or holes. However, negative charged acceptor atoms and positive charged donor atoms take place at p-n junction. The presence of charged acceptor and donor atoms causes to establishment of electric field which acts as a potential barrier for excess charge carrier in n and p-region. Direction of the electric field is from positively charged donor atoms to negatively charged acceptor atoms. Due to presence of electric field, only diffusion current is valid for p-n junction, because electric field prevents charge carriers' movements through p-n junction from one side to the other [7], [8].

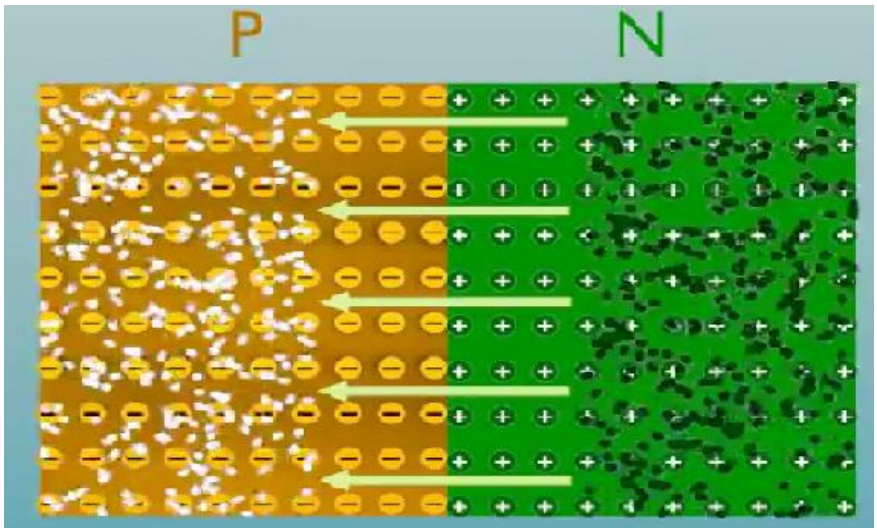

Figure 1.6 : Establishment of Electric Field in P-N Junction

-Energy harvesting mechanism via p-n junction.

The inventors of conversion of solar energy to electric energy is British scientists William Grylls Adams and Richard Evens Day who used selenium for solar cell manufacturing in the 1870s. Besides, first module to obtain electric energy was manufactured by Charles Fritt of New York with the 0.5% efficiency [7], [8].

First promising efficiency come with Gerald Pearson, Darryl Chapin, and Calvin Fuller at Bell Laboratory in 1950s. They used silicon instead of selenium and produced silicon based solar cell with the 5.7% efficiency [7], [8].

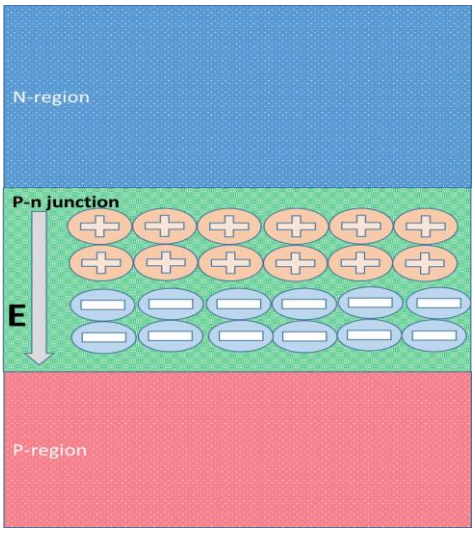

Figure 1.7 : Component of Silicon-Based Solar Cells

Right now, silicon based solar cells dominates solar cell market with exceeding 80% market share.

Basically, solar cell is the solid device which converts energy of photon to electric energy. For the case of silicon solar cells, p doped silicon which is so called as base and n-doped silicon which is so called as emitter are the components of the silicon based solar cells. p-n junction is the most important phenomena for first and second generation solar cells and play an important role to generate electric energy. Built-in electric field is formed by positively charged donor atoms and negatively charged acceptor atoms which is in direction from n-region to p-region. As shown from **Figure 1.7**. When a photon coming from sun excites electrons and forms excitons in p-region, due to built-in electric field, electrons are accelerated against built-in electric field, while holes are moved in the same direction of built-in electric field. Thus, charge separation is acquired and electrons and holes moved in the opposite direction. So electric energy is generated via obtained charge carrier movements through external line. This is the basic explanation of operational principal of solar cells.

A schematic presentation of the operating principles of the DSCs is given in **Figure 1.8** proposed by Gratzel [1]. Main part of the system constitutes of a semiconductor oxide film in mesoscopic scale, electrolyte or an organic hole conductor which is in contact with semiconductor oxide film each other. The material in huge possibility is TiO_2 (anatase), although alternative wide-band-gap oxides such as ZnO[9] and Nb_2O_5[10], MgO[11], CeO_2[12], SnO_2[13] have also been investigated. Sensitizer of which monolayer is attached on the surface of the nanocrystalline semiconductor oxide film. Due to impinging photon, sensitizer which is mainly dye is excited and give rise en electron to be injected to the conduction band of the semiconductor oxide. The electron placing in conduction band of semiconductor percolates and reaches to conductive transparent oxide film. In this case, semiconductor oxide materials act as electron collector and conductive pathway for the electron. An external connection cable carries the electron to the counter electrode of which conductive side is coated with platinum or the other conductive material. Counter electrode is also in contact with electrolyte which is constituted of organic solution containing a redox system, such as the iodide/ tri iodide couple. Due to redox reaction, electrolyte, generally triiodide, is reduced by the donation of electron from counter electrode and it is converted to iodide, on the other hand reduced electrolyte, which is iodide in the most common, play an important role to carry electron to oxidized dye. Again due to redox reaction, iodide is converted to triiodide by giving the electron. The oxidized dye is reduced by electron donation from the electrolyte so it rendered ready to be exited

again. This cycle is repeated in a continuous manner to sustain harvesting energy from sun without any treatment. The neutralization of the sensitizer by electrolyte prevents the recombination of the conduction band electron by the oxidized dye [1][6], [14].

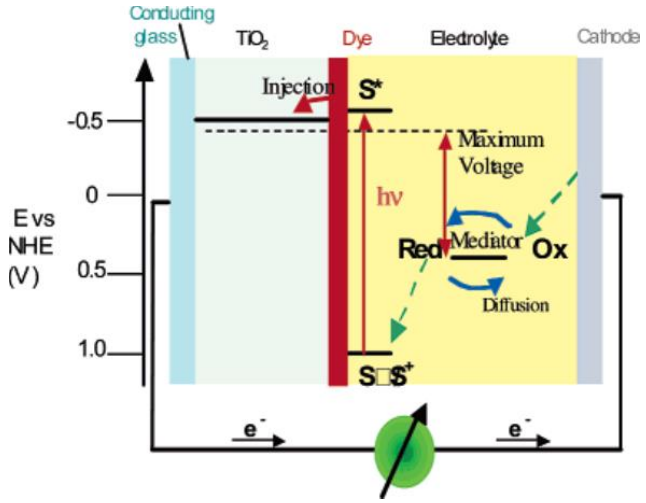

Figure 1.8 : Principle of operation of the dye-sensitized nanocrystalline solar cell

It is worthy to express that excited electrons are expected to be grabbed by electrolyte particle which is ready to be reduced by an electron. In this case, recombination phenomena between excited electron and oxidized sensitizer or electrolyte is expected. Surprisingly, no recombination event was detected and required solar cell process is achieved. This situation is explained by ascribing to process in which electrons excited by photon in the nanoparticles can be surrounded in the mesoscopic scale by electrolyte containing redox couple and act as a barrier for electron recombination due to presenting a resistance on interface of electrolyte and semiconductor oxide. This phenomena contributed to facilitate electron percolation[1], [10], [15] [5].

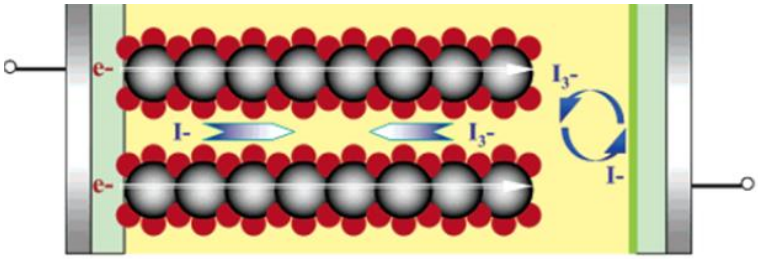

Figure 1.9 : Conduction band electron motion through a network of mesoscopic semiconductor particles. The red dots present cations from the electrolyte.

1.3.1.1 Light Harvesting Phenomena by DSCs

Semiconductor oxide which is in contact with anode electrode give opportunity to sensitizer by supplying great specific surface area. Additionally, it is responsible for carrying electron to the electrodes. With the impinging of photon on the sensitizer, sensitizer is excited and excited electron pass through the conduction band of sensitizer then transferred to conduction band of semiconductor. The electrons injected into semiconductors percolate very rapidly to working electrode. During percolation, electrons have a potential level which is equal to the quasi-fermi level of the semiconductor. It means that energy level of electrons injected to the semiconductor is same as energy level of conduction band of semiconductors. As explained above, the main function of semiconductor oxides;

- Endowing large surface area to sensitizer
- Charge collection
- And charge conduction

Charge collection from sensitizer needs driven force on electron towards semiconductors. So this process consume some energy in amount of most 50-100 meV. It ensures rapid percolation of electron through semiconductors to electrode[1], [6], [10].

Usage of semiconductor material in nano or mesoscopic scale has a tremendous advantages due to large surface area. It is so important for semiconductor endowing large surface area to be coated by sensitizer give rise to enhancement of light absorption ratio[16]

"Light absorption phenomena can be explained by Beer-Lambert's law by using the reciprocal absorption length. The law states that there is a logarithmic dependence between the transmission, T, of light through a substance and the product of the absorption coefficient of the substance, α, and the distance the light travels through the material (i.e., the path length), ℓ. The absorption coefficient can, in turn, be written as a product of either a molar absorptivity (extinction coefficient) of the absorber, ε, and the molar concentration c of absorbing species in the material, or an absorption cross section, σ, and the (number) density N' of absorbers."

$$T=\frac{I}{Io}=e^{-\alpha\ell}=e^{-\sigma\ell N} \qquad (5)$$

And absorption value can be calculated from the expression which is below

$$A = \varepsilon \ell c = \alpha \ell \quad \textbf{(6)}$$

By using same values. The light absorption in terms of the reciprocal absorption length can be calculated with the expression

$$\alpha = \sigma c \quad \textbf{(7)}$$

where σ and c are the optical absorption cross section of the sensitizer and its concentration in the mesoporous film,respectively. The value of σ can be derived from the decadic extinction coefficient ϵ of the sensitizer using the relation

$$\sigma = \epsilon x 1000 \ [\mathrm{cm^2 mol^{-1}}] \quad \textbf{(8)}$$

The light-harvesting efficiency, LHE, is derived from the reciprocal absorption length via

$$LHE\ (\lambda) = 1 - 10^{-\alpha d} \quad \textbf{(9)}$$

1.3.1.2 Incident Photon to Current Conversion Efficiencies

The incident photon to current conversion efficiency (IPCE), sometimes referred to also as "external quantum efficiency" (EQE), is the degree of efficiency and it can be calculated via number of electron pass through external circuit per the monochromatic photon flux that impinge on the DSCs. This key parameter can be expressed as the formula below:.

$$IPCE(\lambda) = LHE(\lambda)\Phi_{\mathrm{inj}}\eta_{\mathrm{coll}} \quad \textbf{(10)}$$

Here LHE(λ) is the light-harvesting efficiency for photons of wavelength λ , Φ_{inj} is the quantum yield for electron injection from the excited sensitizer in the conduction band of the semiconductor oxide, and η_{coll} is the electron collection efficiency. [1], [5]

1.3.1.3 Dynamics of Heterogeneous Electron Injection

The quantum yield of charge injection (Φ_{inj}) is the degree of how effective a sensitizer works and correspond the ratio of flux of photon that excited the electrons to conduction band of semiconductors per whole flux of absorbed photons. Due to radiative or radiationless deactivation channels, some of excited electrons on sensitizer can not injected to conduction band of semiconductor oxide. Taking the sum of the rate constants of these nonproductive channels together as k_{deact} results in

$$\Phi_{inj} = k_{inj} \ / \ (\mathrm{k_{deact}} + k_{inj}) \quad \textbf{(11)}$$

Deactivation of the electronically excited state of the sensitizer is very rapid. Due to that reason, in recent investigation, sensitizers have been designed to retard recombination speed. Developed sensitizer should contain functional groups such as carboxylate, hydroxamate, or phosphonate moieties that anchor the sensitizer to the oxide surface[17].

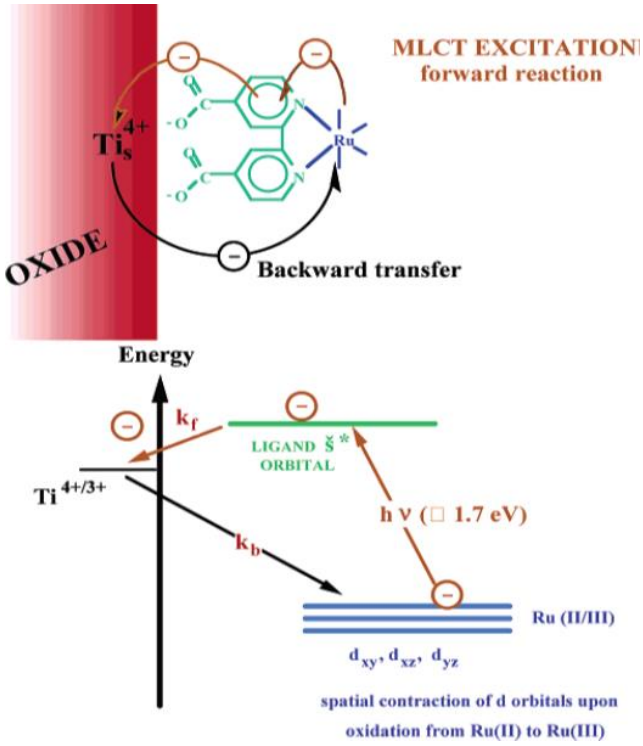

Figure 1.10 : Interfacial electron transfer involving a ruthenium complex bound to the surface of TiO_2 via a carboxylated bipyridyl ligand.

These groups provide that bonding of sensitizer on semiconductor oxide and also they fulfill an additional requirement which is enhanced electronic coupling of the sensitizer lowest unoccupied molecular orbital with the conduction band of the semiconductor[1]. "The lowest energy electronic transition for ruthenium polypyridyl complexes such as those shown in Figure 3 is of metal-to-ligand charge-transfer (MLCT) character." In figure 3, it can be clearly observed the route of excited electron. Firstly, due to inpinging photon, an electron is injected from valance band of Ruthenium to conduction band. Secondly, the excited electron is carried by ligand to interface of ligand and semiconductor. Rapid injection of electron from ligands to semiconductor takes place by consuming such energy. The quantum yield of charge injection generally exceeds 90% [1].

1.3.1.4 Light-Induced Charge Separation

In order to obtain electric current, injected electrons should be collected from conduction band of semiconductor by getting electron through electrode. With this purpose, the back reaction of injected electron with the oxidized sensitizer should be inhibited. As expected, this reaction is undesirable due to back reaction cause efficiency decrease, instead of electrical current, back reaction produces heat. "For the characterization of the recombination rate, an important kinetic parameter is the rate constant k_b. It is of great interest to develop sensitizer systems for which the value of k_{inj} is high and that of k_b low[1]."

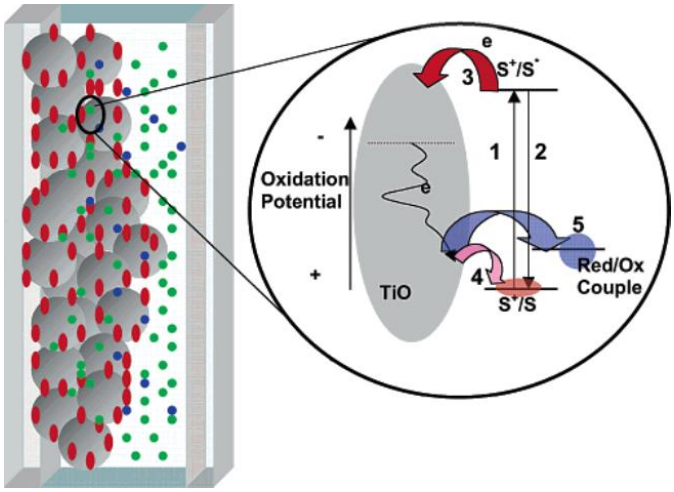

Figure 1.11 : Photo induced processes occurring during photovoltaic energy conversion at the surface of the nanocrystalline titanium.

Figure 1.11. exhibits that films (1) sensitizer (S) excitation by light; (2) radiative and nonradiative deactivation of the sensitizer; (3) electron injection in the conduction band, followed by electron trapping and diffusion to the particle surface; (4) recapture of the conduction band electron by the oxidized sensitizer (S+); (5) recapture of the conduction band electrons by the oxidized form of the redox couple regenerating the sensitizer and transporting the positive charge to the counter electrode. Gray spheres: titania nanoparticles. Red dots: sensitizer. Green and blue dots: oxidized and reduced forms of the redox couple [1]

1.3.1.5 Charge-Carrier Collection

An additional undesired reaction can be observed between injected electron and electrolyte. As expected triiodide should be reduced on counter electrode. However, it

is possible to observe the reduction of triiodide by electrons which take place on conduction band of semiconductors.

$$I_3^- = 2e^-{}_{cb}(TiO_2) \rightarrow 3I^-[1] \quad \textbf{(12)}$$

The other important precaution to enhance efficiency is the inhibition of reaction between electron donor e.g. iodide and excited sensitizer.

$$2S + 3I^- \rightarrow 2S + I_3^-[1] \quad \textbf{(13)}$$

The inhibition of reaction between electron donor and excited sensitizer is fundamental to achieve a high electron collection efficiency and a high cycle life of the sensitizer.[1]

In order to enhance conversion efficiency, all possible precautions and measures should be taken to harvest all injected electrons. IPCEs, referred to also as EQEs, should be as much as high and it should be approach to unity over the near-UV, visible, and near-IR wavelength domain. A key parameter is the electron diffusion length

$$L_n = \sqrt{D_e \tau_r} \quad \textbf{(14)}$$

where De and τ_r are the diffusion coefficient and lifetime of the electron, respectively.[1]

"Quantitative collection of charge carriers can be achieved only if the electron diffusion length is greater than the film thickness (d):"

$$L_n > d \quad \textbf{(15)}$$

The semiconductor oxide layer thickness play an important role to absorb light. It should be much thicker than the light absorption length (1/R). Calculation of light harvesting efficiency by sensitizer can be ensured via:

$$d > {}^1/_{\alpha} \quad [1] \quad \textbf{(16)}$$

The thickness of the semiconductor oxide layer should satisfy the last equation. In experimental investigations, it is observed that the thickness is in micron scale, typically a few microns, depending on the optical cross section of the sensitizer or QD and their concentration in the semiconductor as discussed above.

1.3.2 DSCs Components

1.3.2.1 Semiconductor oxide film

The structure of the nanocrystalline semiconductor oxide electrode used today in the DSC as an electron collector to support a molecular or QD sensitizer. Sequentially, metal oxide nanoparticles are deposited, for example, by screen printing onto a glass or flexible plastic support covered with a transparent conducting layer of fluorine-doped tin dioxide (FTO) or tindoped indium oxide (ITO). Each particle is coated with a monolayer of sensitizer or a QD formed by self-assembly from a staining solution.

The mesoscopic dye-sensitized solar cell (DSC) is a potentially low-cost candidate for future photovoltaic markets. Titanium oxide (TiO_2) has been widely used as the photo anode material in DSC, although a few studies have explored other semiconducting metal oxide such as ZnO[9] and Nb_2O_5[10], MgO[11], CeO_2[12], SnO_2[13].

Titanium Dioxide (TiO_2), a white pigment, is by far the most commonly used. Its extensive usage in paint industry comes from its high refractive index and ease of preparation of particles of very small size (leading to large surface area). As a cheap, readily available material, TiO_2 serves as an attractive candidate for any industrial applications such as paints, paper, coatings, plastics, fibers, cosmetics, etc.

While major emphasis is still on optimizing the performance of solar cells based on TiO_2 films such as white light conversion efficiency, stability, there have also been exploratory studies on nanoporous films of other semiconducting oxides, particularly on ZnO and SnO_2 .

DSC technology based on ZnO has been explored extensively. ZnO is a wide-band-gap semiconductor that possesses an energy-band structure and physical properties similar to those of TiO_2, but has higher electronic mobility that would be favorable for electron transport, with reduced recombination loss when used in DSCs. Many studies have already been reported on the use of ZnO material for application in DSCs. Although the conversion efficiencies of 0.4–5.8% obtained for ZnO are much lower than that of 11% for TiO2, ZnO is still thought of as a distinguished alternative to TiO_2 due to its ease of crystallization and anisotropic growth[18].

According to the literature, T.Miyasaka [19] developed the TiO_2 electrode preparation techniques of DSCs based on low-temperature and the conversion efficiency more than 6%. Seigo Ito [4] et al. utilized 4-tert-butylpyridine, acetonitrile, valeronitrile and

H_2PtCl_6 as experimental materials, screen printing technique was used to prepare the TiO_2 electrode and the conversion efficiency reached to 10%.

Feifei Gao [20] et al. have developed a novel heteroleptic ruthenium sensitizer with a high molar extinction coefficient to considerably enhance the optical absorptivity of mesoporous TiO_2 films, the achievement of over 10.5% power conversion efficiency is very encouraging.

R.Jose [21] et al. utilized electrospinning techniques to prepare and assemble dye-sensitized solar cells and the conversion efficiency reached to 4.7%-5.1%. Tae-Sik Kang [22]et al. fabricated TiO_2 nanotubes using an alumina templating method has been demonstrated. By using a mixture of $Ti(OC_3H_7)_4$ and ethanol, extremely uniform in filtration of the pores was achieved resulting in highly aligned TiO_2 nanotubes, were used to fabricate first generation DSCs. Conversion efficiencies as high as 3.5% at 520 nm were achieved.

Liyuan Han [23] et al. fabricated a highly efficient DSC module with high active area by optimizing the composition of the Pt counter electrode, the electrolyte, the thickness of the TiO_2 films, and the uniformity of the unit cells, and obtained the highest recorded module efficiency of 8.2% with aperture area of 25.45cm^2

DSC efficiency was improved by 4% - 11 % using O_2, CH_4, N_2 or H_2 plasma treatment due to the more absorption of dye molecules by the chemical active state and the generation of excess electrons in the TiO_2 surface. DSC with H_2 plasma-treated TiO_2 showed the most improved result.

Composite networks of TiO_2 nanofibers and nanoparticles were generated using electrospinning and electro hydrodynamic printing. The formation of the fiber-pore structure led to a significant enhancement in absorbance by as much as 3-fold in the visible range. Application of the NP-NF composites in dye sensitized solar cells demonstrated that the fiber-pore structures incorporated in the middle of the electrode improved the efficiency by 10% through forward and backscattering of the light[24]

1.3.2.2 Sensitizer

In DSCs, the key role relating with a sensitizer is absorbing sunlight and converting into electric energy[25], [26]. Regeneration of sensitizer is supported by mediator which may be hole conductor polymer or redox electrolyte couple. In order to achieve this purpose, it need to be bind on semiconductor surface and fulfill such requirements which can be listed below as[27]:

Absorption sensitizer should absorb the light having wave length from near-UV up to 920 nm.

Energetics it is the main purpose that recombination ratio should be minimized and obtained potential difference maximization should be achieved. Due to that reason, the excited state of the adsorbed sensitizer should take place slightly above energy level of the conduction band of TiO_2. In this case, electrons can transfer to the semiconductor oxide with minimum loses. Again for the same purpose, the ground state of the sensitizer should be only slightly below energy potential of mediator.

Kinetics. The process of electron injection from the excited state to the conduction band of the semiconductor should be fast enough to prevent from recombination and occurrences of any side reaction

Stability The adsorbed sensitizer should be stable enough to meet process requirements of DSC for a long time. It is expected to sustain proceeding approximately 20 years of operation under exposure to natural daylight

Interfacial properties. Sensitizer should bind on the semiconductor surface easily and tightly.

Practical properties in order sensitizer to adsorb on semiconductor, it should soluble in the solvent used for dye uptake.

1.3.2.3 Dye as a sensitizer

Karmakar at al[28] are grouped dyes into two classes as inorganic and organic sensitizers. Inorganic dyes used for this purpose are mainly metal complex dyes such as complexes of Ruthenium, Osmium, Iridium, etc. Organic dyes mainly consist of fruit dyes and natural extract dyes. Inorganic dyes have given better results of the two as the stability towards photo degradation is less for organic dyes. The ideal sensitizer for a single junction photovoltaic cell converting standard global AM 1.5 sunlight to electricity should absorb all light below a threshold wavelength of about 920 nm. Moreover, it should also graft the semiconductor oxide surface with help of attachment groups like carboxylate and phosphonate. The attachment group of the dye ensures that it spontaneously assembles as a molecular layer upon exposing the oxide film to a dye solution. Many different compound have been investigated for semiconductor sensitization, such as porphyrins, phtalocyanines, coumarin, carboxylated derivatives of anthracene and polymeric films.

A DSC must sustain producing electricity for 20 years without significant loss of efficiency. Among dye sensitizer, ruthenium complexes are one of the most prominent members of the sensitizer. Therefore, the molecular engineering of suitable ruthenium complexes is getting more attraction due to their excellent stability. Researchers have been spending so much effort to construct the dye with higher efficiency and stability. The most known dye sensitizers are cis-Di-(thiocyanato)bis(2,2'-bipyridyl)-4,4'-dicarboxylate) ruthenium-(II), coded as N3 or N-719 which have high absorption capability and charge-transfer ability. The structure of these sensitizers is shown in Figure 3[1], [25], [28].

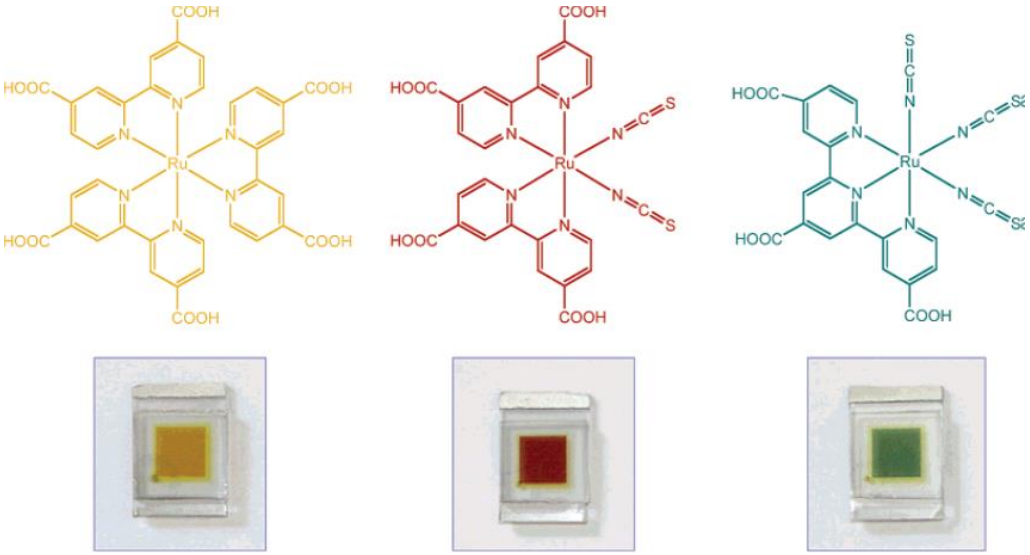

Figure 1.12 : Structure of the ruthenium sensitizers RuL3 (yellow) cis-RuL2(NCS)2 (red) and RuL'(NCS)3 (green)

1.3.2.4 Quantum Dots (QD)

Semiconductor QDs are promising alternatives for dyes to harvest light coming from sun via the DSCs. Semiconductor quantum dots have several type such as II–VI and III–V type and QDs need to have dimension as small as enough to show quantum confinement effects. By playing the size of QDs, it is possible to adjust absorption spectrum. QDs have sizes in nanoscale and it gives them some advantages such as high light absorption ability and it is possible to engineer band gap of QDs in a wide range. The other advantages of QDs is a large intrinsic dipole moment. Since they have features that cannot be ignored, a variety of QDs have been investigated, such as CdS, CdSe, PbS, PbSe, InP, InAs, and Sb_2S_3. Even though QDs solar cells have advantages, yet they couldn't succeeded to obtain promising photovoltaic performance due to such problems such as low stability, low Voc, and fast carrier recombination [23]–[25],

[26]. QDs act as a sensitizer and can be excited by photon giving rise to formation of electron-hole pair. The electron is transferred to the semiconductor oxide, on the other side, the hole is carried by a hole conductor or an electrolyte which are in contact with the nanocrystalline oxide film. Triarylamine hole conductors has been investigated to prove that efficient and rapid hole transportation from PbS QDs, IPCE ratio is higher than value of 50% have been obtained without fine tuning and optimization[33]. It is also important to note that QDs have some advantages such as much higher optical surface area than dye which is molecular sensitizers, depending on the their size. As a disadvantages, QDs occupy a larger area on the semiconductor oxide particles led to decrease the QD concentration in the film[1].

As an alternative to organic dyes, semiconductor quantum dots have also been studied as photosensitizers for application in DSCs, which are accordingly sometimes called semiconductor sensitized solar cells (SSSCs). Quantum dots take the form of nanocrystals of semiconductors compound and therefore, offer the advantage of stability over the metallorganic or even pure organic dyes. More recently, it was reported that the quantum dots were able to generate multiple electron-hole pairs per photon, which would be great beneficial in terms of photovoltaic devices possibly attaining extremely high conversion efficiencies[32][31].

A few attempts have also been made on ZnO. One example is to combine ZnO nanowires with CdSe quantum dots for a photo electrochemical cell, which has demonstrated an internal quantum efficiency of 50–60%, comparable to the results obtained for similar ZnO nanowires sensitized with Ru-complex dye[34]

1.3.3 Perovskite (CH3NH3PbX3) as a Sensitizer

Perovski, a Russian mineralogist first discovered the Perovskite and gave his name to the structure. Perovskite has an ABX_3 formula, where X represent a halogen or oxygen groups. [35]. Currently, perovskite $CH_3NH_3PbI_3$ sensitizers are widely investigated and promising results have been reported due to its super high absorption ability. Organometallic or organic materials became favorite sensitizers for solid-state dye-sensitized solar cells (ssDSC) recently.

If we have a look in a detailed form into perovskite structure, the general chemical formula for perovskite is ABX_3, where ‘A’ and ‘B’ represent two cations having different sizes, and X represent an anion which responsible for binding the two cations, as shown in Figure 1.13 [36].

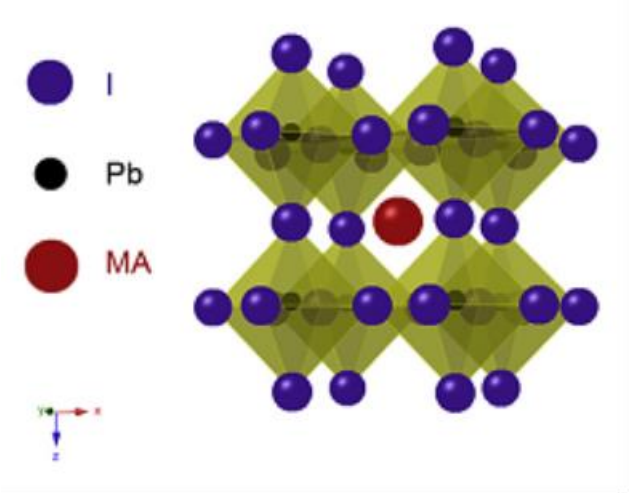

Figure 1.13. Crystal structure of cubic perovskite of general formula ABX_3

For the last two years, halide perovskites (ABX_3), a group of perovskite family, dominated ssDSC structure. Moreover, perovskite structure can be classified as alkali-halide perovskite and organo-metal halide perovskite [37].

In general, alkali-halide perovskite constitutes of the alkali metal A^I (Li^+, Na^+, K^+, Rb^+, Cs^+) and the divalent M^{II} (Be^{2+}, Mg^{2+}, Ca^{2+}, Sr^{2+}, Ba^{2+}, Zn^{2+}, Ge^{2+}, Sn^{2+}, Pb^{2+}, Fe^{2+}, Co^{2+}, Ni^{2+}) with X which is halogen anions (F_, Cl_, Br_, I_). First report about halide perovskite as a sensitizer had been published in 1980. $KPbI_3$ was proposed as a light absorbing material in a solar cell by Salau [37].

On the other hand, organohalide perovskites (ABX_3), which are the hybrid material, comprise of organic cations (A: aliphatic or aromatic ammonium) and divalent metal cations (B: Cu^{2+}, Ni^{2+}, Co^{2+}, Fe^{2+},Mn^{2+}, Pd^{2+}, Cd^{2+}, Ge^{2+}, Sn^{2+}, Pb^{2+}, Eu^{2+},). This group of halide perovskite have been studied intensively, especially during last two years due to its superior photovoltaic properties and potential to use them in low temperature photovoltaic cell manufacturing in industrial scale [36]. Thereby, nowadays especially perovskites containing 4A group metals such as Ge^{2+}, Sn^{2+}, Pb^{2+} are hot topic and many scientists are looking for ways to use them in photovoltaic application to take efficiency of photovoltaic cell one step forward.

1.3.3.1 Solid state Dye Sensitized Solar Cell

It is the approach that the liquid electrolyte may inhibit the production of DSCs in industrial scale. So many studies were conducted to achieve producing ssDSC. First try to produce ssDSC was taken place in 1998[38]. In this study, instead of liquid electrolyte, 2,2′,7,7′-tetrakis(N,N-p-dimethoxy-phenylamino)-9,9′-spirobifluorene

(spiro-OMeTAD) was used as organic hole-transport material (HTM) in solid form. However, power conversion efficiency (PCE) was less than 1%. The low PCE have been attributed to charge recombination at the interface of TiO_2 and (spiro-OMeTAD). Krüger et al.[39] incorporated 4-tert-butylpyridine (tBP) and lithium bis(trifluoromethanesulfonyl) imide (LiTFSI), Li-$[CF_3SO_2]_2N$ in spiro-OMeTAD to inhibit charge recombination and they increased PCE till 2,56%. Krüger et al. sensitized 2 μm TiO_2 mesoporous film with N719.

By using spiro-MeOTAD, several ssDSCs were produced due to solid state of hole transfer material (HTM). At beginning of ssDSC establishment, scientists have been focused on HTM performance. Because spiro-OMeTAD has some deficiency to be used as HTM due to its respectively low hole conductivity. Thus, in order to improve the hole conductivity of spiro-OMeTAD have been realized. PCE was enhanced by increasing conductivity level of spiro-MeOTAD via doping it with tris(2-(1Hpyrazol-1-yl)pyridine)cobalt(III) was proposed [40]. Thus, PCE was enhanced to 7,2% much promising step occurred in ssDSC. The spiro-OMeTAD doped Co^{III} complex was used as an HTM by spin coating on $TiO_2/CH_3NH_3PbI_3$ thin film due to effect of Co^{III} complex to reduce the series resistance, and to increase the hole mobility of HTM layer[40].

Besides that, Inorganic perovskite nano crystals have lately investigated as a sensitizer due to their high light absorption properties. Firstly, Miyasaka et al. [41] introduced organometal halide perovskite as a sensitizer for ssDSC. $CH_3NH_3PbI_3$ and $CH_3NH_3PbBr_3$ were used in ssDSC and obtained PCE of 3,81% and 3,13%, respectively. Although PCE values of the DSCs were moderate respectively, stability of the DSCs was very poor. Because perovskite dissolved in liquid electrolyte in e few minutes. Thereby, PCE values were deteriorated due to disappearance of perovskites on TiO_2. At beginning of this area, Metal chalcogenides have been used in ssDSCs, unfortunately the highest efficiency was achieved to be around 6% [35].

A breakthrough for ssDSC was conducted in 2012 proposing organometal halides $CH_3NH_3PbI_3$ in perovskite structure with the presence of spiro-MeOTAD [42]. Kim et al. sensitized mesoporous TiO_2 film in 0,6 μm thickness with $CH_3NH_3PbI_3$. The ssDSC has showed PCE of 9.7% under the simulated AM1.5G one sun illumination.

In the study, $CH_3NH_3PbI_3$ synthesis process was explained as below:

A hydroiodic acid (30 mL, 0.227 mole, 57 wt. % in water) and methylamine (27.8 mL, 0.273 mol, 40% in methanol, TCI) were stirred in the ice bath for 2 h. After stirring at

0°C for 2 h, the resulting solution was evaporated at 50 °C for 1 h hence, synthesis of CH_3NH_3I was performed. Subsequently, purification takes place to remove any undesired organic compound by washing with diethyl ether and ethanol. In order to obtain $(CH_3NH_3)PbI_3$, the synthesized CH_3NH_3I (0.395 g) and PbI_2 (1.157 g) were mixed in γ-butyrolactone (2 mL, .99% Aldrich) at 60°C for overnight with stirring.

Additionally, TiO_2 paste preparation was reported briefly as below:

Anatase TiO_2 nanoparticles were synthesized in the presence of acetic acid leading to hydrolysis of titanium tetraisopropoxide (TTIP). Thereafter, synthesized TiO_2 was put into autoclave at 230 °C for 12 h. Then, ethanol take place instead of aqueous solvent in the autoclaved TiO_2 colloid solution to obtain non-aqueous TiO_2 paste. Ethylcellulose lauric acid, and terpineol were added into the ethanol solution of the TiO_2 particles, and then ethanol was removed from the solution using a rotary evaporator to obtain viscous pastes. The nominal composition of TiO_2/terpineol/ethylcellulose/lauric acid was 1/6/0.3/0.1.

To produce ssDSC first of all, FTO glasses are cleaned. FTO glasses (Pilkington, TEC-8, 8 V/sq) were put into ultrasonic bath containing ethanol for 15 min and treated in UVO cleaner for 15 min. Afterward, dense TiO_2 blocking layer formation was performed with 0.15 M titanium diisopropoxide bis(acetylacetonate) (75% Aldrich) in 1-butanol (Aldrich) solution by the spin-coating method. After the coated film was cooled down to the room temperature, the same process was repeated twice with 0.3 M titanium diisopropoxide bis(acetylacetonate) solution in butanol. Subsequently, coated FTO glasses with TiO_2 precursor solutions were sintered at 500 °C for 15 min. After sintering, the mesoporous TiO_2 paste was deposited by a doctor-blade method and again one more sintering was performed at 550°C for 1 h to produce mesoporous TiO_2 film. Thicknesses of the TiO_2 films were controlled from 0.5 to ca. 1.5 mm using a micrometer adjustable film applicator. The sintered TiO_2 films were immersed in 0.02 M aqueous $TiCl_4$ solution at 70 °C for 10 min, which was heated at 500 °C for 30 min.

The mesoporous TiO_2 films were coated with perovskite precursor solution, followed by heating at 100°C for 15 min. The composition of hole transport material (HTM) was 0.170 M 2,2',7,7'-tetrakis-(N,N-di-p-methoxyphenyl-amine)-9,9'-spirobifluorene (spiro-MeOTAD, Merck), 0.064 M bis(trifluoromethane) sulfonimide lithium salt (LiTFSI, 99.95%, Aldrich) and 0.198 M 4-tert-butylpyridine (TBP, 96%, Aldrich) in the mixed solvent of chlorobenzene (99.8%, Aldrich) and acetonitrile

(99.8%, Aldrich) (chlorobenzene :acetonitrile 1 : 0.1 v/v). The $(CH_3NH_3)PbI_3$-sensitized TiO_2 films were coated with HTM solution using spin-coating method at 4000 rpm. As a counter electrode, a 60 nm-thick Au was deposited on the top of the HTM over layer by a thermal evaporation, where Au evaporated under ca. 10^{-6} torr vacuum condition.

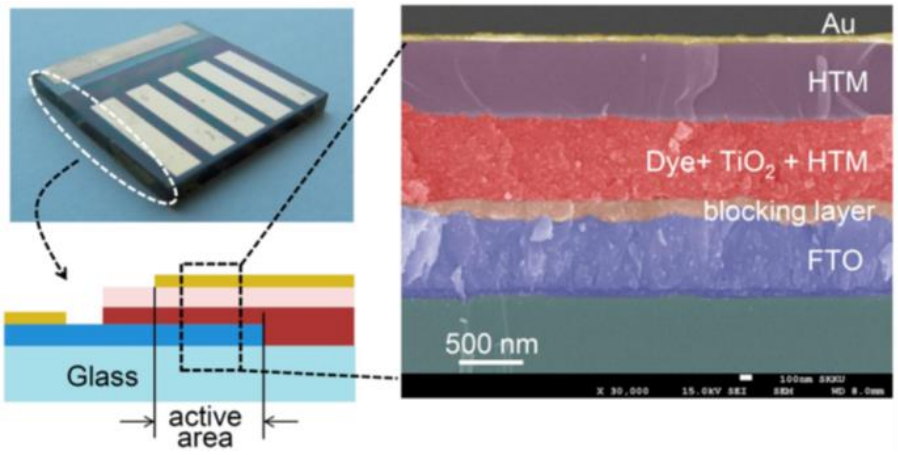

Figure 1.14 : Solid-state DSSC structure showing (left) a real device with the cross-sectional structure and (right) the cross-sectional SEM

Mesoporous TiO_2 layer is coated on blocking layer then sintered at around 500−550 °C. Sintering process is needed to acquire mesoporous metal oxide layer. After obtaining TiO_2 layer, perovskite solution is adsorbed on TiO_2 paste. Then, HTM containing solution coated on inorganic material layer by filling the porous structure. Besides filling porosity, an HTM layer is formed at the top of ssDSC as a capping layer. Infiltration of HTM into mesoporous film is very important. Because infiltration is directly related with pore filling fraction (PFF) which is very important parameter on PCE. In final step, gold or silver conductive layer is formed by thermal evaporator as cathode of ssDSC[35].

Besides, firstly Etgar et al[43] produced HTM-free ssDSC by using $CH_3NH_3PbI_3$ perovskite/TiO_2 heterojunction. In this study, instead of conventional TiO_2 anatase nanoparticle, anatase nanosheets with dominant (001) facets was used as an electron collector. The role of perovskite in HTM-free ssDSC is absorption of sun light and additionally acts as a hole conductor. Elimination of HTM usage gives rise to obtain opportunity to produce ssDSC in industrial scale with low cost. It is important to express that mesoscopic perovskite/TiO_2 heterojunction ssDSC exhibited high performance with short-circuit photocurrent (Jsc) of 16.1 mA cm^{-2}, a fill factor (FF) of 0.57, and open-circuit voltage (V_{oc}) of 0.631 V, with consequence of PCE of 5.5%

under 1 sun intensity. It is the unique part of the study to use anatase nanosheets with dominant (001) facets as an electron collector. However, it is noted that synthesis of anatase nanosheets is a dangerous process.

The other breakthrough came from Burschka et al. by reaching to PCE of 15%. Light harvesting efficiency increased with modification in perovskite synthesis and adsorption techniques.

Perovskite synthesis was performed sequentially. In first step, lead iodide solution was spin-coated on mesoporous titania film and as a subsequent step, TiO_2 and PbI_2 film composite immersed into CH_3NH_3I solution by reacting each other to synthesize $CH_3NH_3PbI_3$ immediately. This process is so called as two-step sequential process have been given rise to a PCE of 15% and a certified value of 14.1% with high reproducibility[44]. It is noteworthy that the two-step method gave opportunity perovskite to be penetrated into mesoporous TiO_2 structure. Thus, higher loading of perovskite is obtained by two-step process resulting in increased LHE [44].

One of the obstacles to obtain high PCE of ssDSC may be the low pore filling fraction (PFF). In order to overcome the deficiency, H.S. Kim et al [45] proposed that instead of mesoporous metal oxide film layer, TiO_2 nanorods or nanotube as anode layer have been used to provide more chance to enhance PFF. Due to complex structure of mesoporous TiO_2 film, infiltration of HTM into TiO_2 layer is in limited scale. To overcome infiltration confinement, authors used highly crystalline rutile TiO_2 nanorods as a photoanode to facilitate penetration of HTM into ordered TiO_2 layer. Rutile crystalline structure of TiO_2 was preferred due to its unique feature such as high electron mobility with easily controllable dimensions. Anode was in 0.6 μm thickness. Rutile TiO_2 nanorod was synthesized by hydrothermal method and spiro-OMeTAD was used as HTM. Photovoltaic (PV) performance values are J_{sc} of 15.6 $mAcm^{-2}$, V_{oc} of 955 mV, and FF of 0.63, yielding PCE of 9.4%. It is expected that due to rutile TiO_2 nanorod structure has less surface area than mesoporous TiO_2 layer, PV performance of the nanorod based device would be much lower than 9,4%. However, remarkable enhancement in PV values especially the high increase in J_{sc} was ascribed to the high absorption coefficient of $CH_3NH_3PbI_3$.

It is obvious that nanorod lengths are time-dependent parameters and can be tuned by controlling the processing time. It is observed that PV performance decreased with increasing nanorod lengths. This is attributed to PFF due to increasing nanorod length yielding empty room in TiO_2 layer.

1.3.3.2 Carbon based monolithic solid state dye-sensitized solar cell

In the conventional DSC structure, the distance between photo anode and counter electrode adjusted by two-side adhesive tape or sealing resin [46]. Separator tape plays very important role to determine the distance. In general, separator tape was used in the DSC structure with liquid electrolyte. On the other side, ssDSC enables to produce solar cell in monolithic structure. Han et al was produced the monolithic-DSC structure by using carbon counter electrode instead of TCO as shown in Figure 1.15. [46],[47]. Han et al used ZrO_2 film as a spacing or separator layer. The spacer insulates photo- and counter-electrodes electrically from each other to inhibit shortcut between two electrodes. The insulating layer that is used as the spacer has also the reflecting functionality of back-scattering the light which is not absorbed by the photoelectrode. The ceramic material as TiO_2 with a rutile crystal structure (r-TiO_2) or large particle size (600 nm) ZrO_2 with tetragonal phase is typically used as the spacer layer in the monolithic DSC device [47]–[49]. Moreover, r-TiO_2 is a poor insulator material compared with ZrO_2 film, characterized with a highly insulating behavior, because of its wide band gap (6 eV).

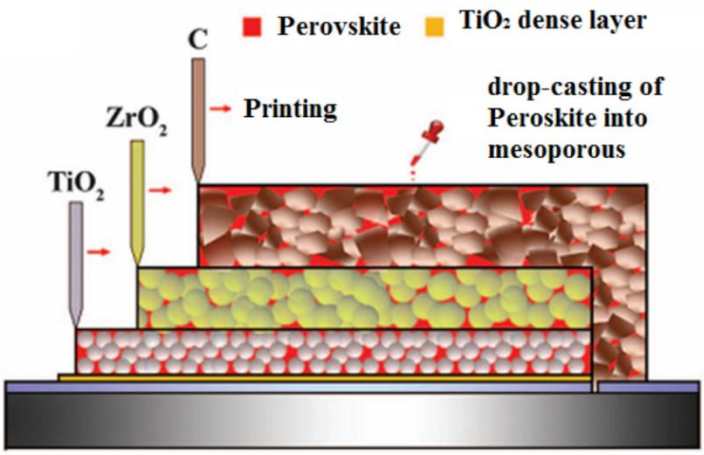

Figure 1.15 : Monolithic Dye-Sensitized Solar Sell Structure without Liquid Electrolyte

Additionally, Vesce et al. [46] used monolithic ssDSC structure with liquid electrolyte. In a common way, ZrO_2 insulating layer deposited mesoporous TiO_2 layer. ZrO_2 printing paste was formulated in presence of ethyl cellulose that act as a rheological agents. Ethyl cellulose plays important role on the paste viscosity, rheology, and porosity.

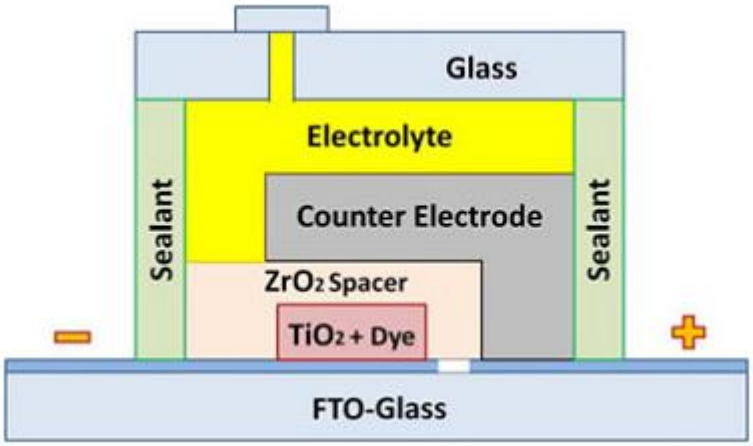

Figure 1.16 : Monolithic Dye-Sensitized Solar Sell Structure with Liquid Electrolyte

Besides, conductivity of counter-electrode is very and it should be as low as possible in order to meet a low charge transfer resistance, that affect the fill factor of the cell together with the shunt resistance. The electrical contact between carbon black particles and the conductivity was improved by using graphite. The counter-electrode needs also a binder to optimize bonding between carbon black and graphite and to increase the adhesion strength on the spacer layer . Since the binder had to sinter at a temperature around 450–500 ◦C and any contamination of the photoelectrode by organic polymers has to be avoided, TiO_2 or ZrO_2 with 10–30 nm particle size are typically chosen as binder [46], [50], [51].

1.3.3.3 Low temperature processed-ssDSCs

In order to produce ssDSC in commercial scale, it is clear that high temperature process is one of the biggest obstacle. Thereby, to establish low temperature processed-ssDSCs on a plastic substrate, a few studies have been conducted till know. Especially, after coating of TiO_2 paste, sintering process can be considered as limiting issue to obtain flexible ssDSC.

Commercialization step is looking for some intriguing properties such as flexibility, ease of integration, stability and cost effectiveness. Hence, manufacturing flexible ssDSCs can be realized by meeting the need of using flexible, transparent and conductive electrodes in ssDSCs' structure. In that point, polymeric based transparent materials having durability against high temperature suggested as electrode. Polyethylene terephthalate (PET) and Polyethylene naphthalate (PEN) are current candidate for the electrode of commercial ssDSCs due to durability against

temperature till 150 ^{o}C. Thus, manufacturing ssDSCs with low temperature process, which has less than 150 ^{o}C, attracting intense interest. It can be thought the key point for commercialization of ssDSCs.

In order to overcome high temperature confinement in ssDSC manufacturing, Snaith et al. [52] proposed that it is possible to produce single crystal mesoporous TiO_2 (SCM-TiO_2) for ssDSC. SCM- TiO_2 has mesoporous structure intrinsically, hence it is not necessary to apply sintering in ssDSC manufacturing process. Due to that reason, SCM- TiO_2 structure enable to produce ssDSC in industrial scale. The produced low temperature sensitized ssDSC showed 7.3% PCE.

At the another ensuing study, again Snaith et al[53] achieved to produce ssDSC in low temperature process condition with the PCE of 12,3%. In author's study, instead of $CH_3NH_3PbI_3$ perovskite structure, $CH_3NH_3PbI_{3-x}Cl_x$ is preferred as a sensitizer. And also Al_2O_3 mosoporous scaffold have been used as a porous layer to load perovskite on. Even though the authors have expressed that they produced low temperature ssDSC, surprisingly, sintering process has been used to acquire blocking layer. It is important to emphasize that having 500^{o}C sintering process in ssDSC manufacturing has huge potential to inhibit mass production of the ssDSC.

Again Snaith et al. [54] conducted another investigation to produce low temperature ssDSC. Authors used florin doped tin oxide (FTO) coated glass as a photoanode. $CH_3NH_3PbI_{3-x}Cl_x$ used as perovskite, spiro-OMeTAD preferred of which responsibility is hole transfer. In TiO_2 synthesis, authors used titanium diisopropoxide bis (acetylacetonate) (TiAcAc) with the aim of increasing conductivity of compact TiO_2 layer. TiAcAc served for filling gaps, which is the reason of conductivity deterioration, to contact TiO_2 nanoparticle. Blocking layer thickness was tuned by concentration of colloidal TiO_2. TiAcAc exposing to 150 ^{o}C temperature decomposed to TiO_x by binding TiO_2 nanoparticle. TiAcAc usage also optimized in the investigation and 10-20 mol% was found as an optimum level. Optimized lt- TiO_2 ssDSC showed high PCE of %15,3.

2. EXPERIMENTAL

In the experimental section, ssDSCs production was conducted by using doctor blade and screen printing technology. Thereby, solutions and pastes to be able to form components of the monolithic ssDSC structure was prepared sequentially. After the pastes and solutions were prepared, ssDSCs structure was built on an ITO coated glass. Besides paste preparation, perovskite synthesis was also performed successfully. Subsequently, sensitization of monolithic ssDSC was conducted according to sequential deposition of perovskite precursors. In this section, all processes pertaining to produce ssDSC was explained according to production sequence.

2.1 Materials

Materials and equipment used in ssDSC production was introduced in this section. Titanium tetraisopropoxide (TTIP,), acetyl acetone (AcAc) was supplied from Sigma Aldrich. Ethanol, Acetic Acid and Isopropanol (IPA,) was used as received from Merc without any further purification. ITO coated conductive glass (TCO) acting as transparent conductive material was locally supplied from Izmir Institute of Technology. Doctor blade and screen printing technology were used as deposition techniques.

P25 TiO_2 nanoparticles were kindly donated by Evonik Turkey. ZrO_2 nanoparticles (Tosoh) was supplied from Prozir Seramdent locally. Terpineol was also supplied locally from Gulcicek and Kali Chemistry. Hydroxyl ethyl cellulose, hydroxyl propyl cellulose kindly granted from Univar Chemistry, ethyl cellulose was also kindly granted by Dow Chemical, Turkey.

$CH_3NH_3PbI_3$ structure was synthesized as the sensitizer for the sensitization of ssDSC. Synthesis process was conducted by the reaction of CH_3NH_3I and PbI_2 which was also synthesized in laboratory conditions. PbI_2 dissolution was conducted by using dimethyl formamid (DMF) was also supplied by Merck.

2.2 Methods

2.2.1 Formation of TiO_2 Dense Layer

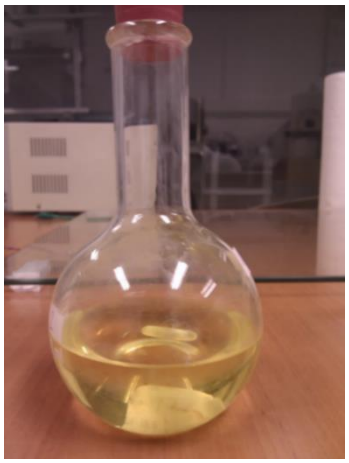

Figure 2.1 : The Prepared Solution for TiO_2 Dense Layer

Dense TiO_2, deposited by spin coating unit, in ssDSC structure is very important because TiO_2 dense layer is responsible from the inhibition of direct contact between photo- and counter electrodes. To obtain a stable TiO_2 solution, a recipe was adopted from the literature [55], [56]. Briefly, 0.3 M titanium tetraisopropoxide (TTIP, Sigma Aldrich) was dissolved in isopropanol (IPA, Merc) and stirred at room temperature for 30 min. Then, acetyl acetone (AcAc, Sigma Aldrich) was added to TTIP solution. TTIP to AcAc molar ration was arranged as 10:3. AcAc was used as stabilizing agent and assisting to fill the gabs occurring on TiO_2 dense layer. The mixture was magnetically stirred for 30 minute. Acetic acid (Sigma Aldrich) was added drop wise to initiate the hydrolysis of TTIP. At the end of the process we followed transparent yellow solution was obtained as seen in Figure 2.1.

The obtained yellowish transparent solution was coated on a conductive ITO coated glass by using spin coating machine with 3000 rpm rotation speed during 30 s. spin coating unit used in formation of TiO_2 dense layer was shown in Figure 2.2.

Figure 2.2 : Spin coating unit used in formation of TiO_2 dense layer.

2.2.2 TiO_2, ZrO_2 and carbon paste preparation

In this thesis study, monolithic ssDSC structure was built on conductive ITO-glass (TCO). It is one of the important steps that forming metal oxide layer on TCO to achieve producing solar cell in monolithic structure. Deposition of metal oxide layers onto TCO was conducted by doctor blade and screen printing technology by using metal oxides pastes. However, metal oxides was in powder form. Additionally, both coating technology use a kinds of viscous liquid so called as paste for deposition. Therefore, In order to proceed both techniques, powder forms of metal oxide were converted into paste form. For paste preparation, a technique was adopted for preparation of metal oxide paste from the literature [51] . According to the method, we followed the recipe shown in Figure 2.3. The Recipe will be called as “Recipe A” in the rest of this research.

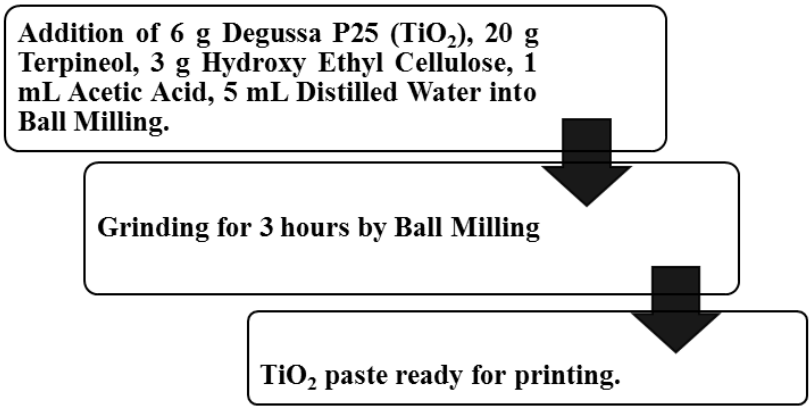

Figure 2.3 : Recipe A: Preparation of TiO_2 Paste

Additionally, one more method was also adopted from the literature [48]. Briefly, the method was introduced in Figure 2.4. The Recipe will be called as “Recipe B” in the rest of this research.

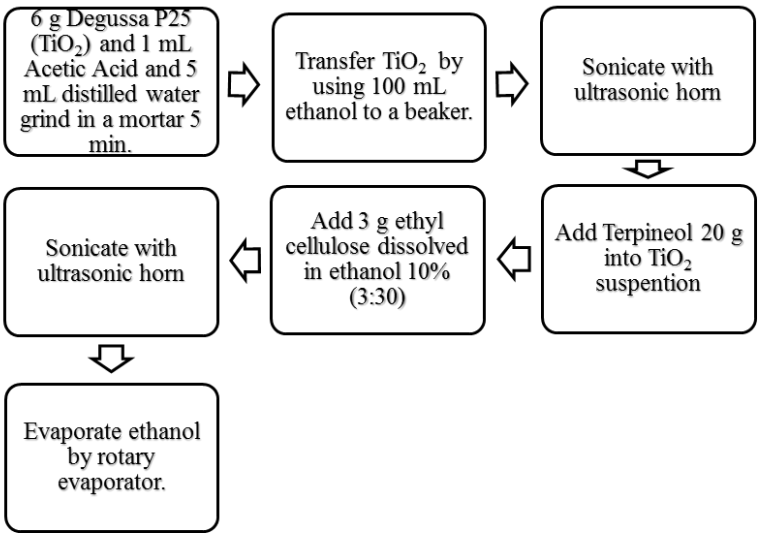

Figure 2.4. Recipe B for TiO_2 paste preparation.

Basically, the differences between two methods are the used materials as thickener such as hydroxy ethyl cellulose and ethyl cellulose and equipment to disperse inorganic powder in nano scale into organic media. The equipment used in TiO_2 paste preparation was introduced in **Figure 2.5**.

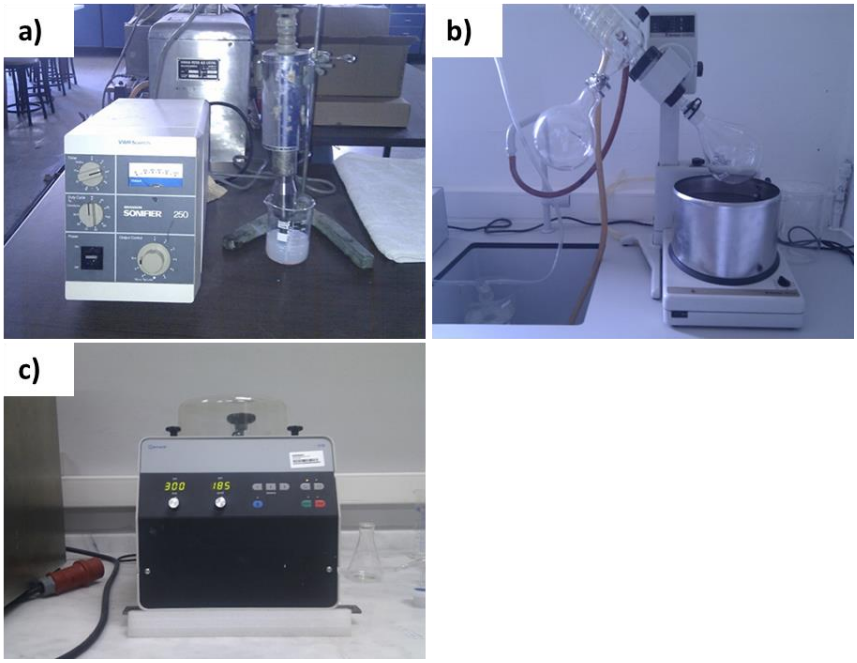

Figure 2.5 : Equipments a) ultrasonic homogenizator b) rotary evaporator c) ball milling used for TiO2 paste preparation.

Han et al. [58] showed hole-conductor-free mesoscopic solar cell by using ZrO_2 space layer instead of organic hole transfer layer. They proposed that a separation layer is needed to proceed selection of excited electron and holes by inhibiting recombination.

In this regard, we also used ZrO_2 nanoparticle as a spacing layer. Thereby, ZrO_2 paste was prepared with a method similar to TiO_2 paste preparation. We only used ZrO_2 instead of TiO_2 nanoparticle in the recipe shown in Figure 2.3 and Figure 2.4.

For counter electrode, carbon paste was also prepared. Again we adopted a technique from literature [48]. Briefly we followed carbon paste preparation recipe shown in Figure 2.6.

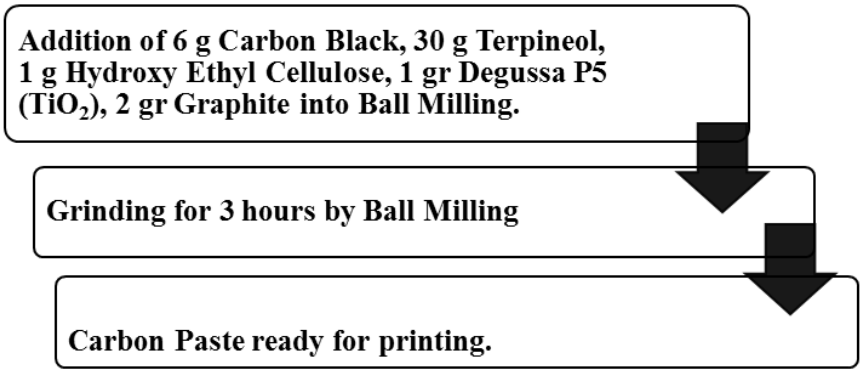

Figure 2.6 : Recipe for carbon paste preparation.

2.2.3 Assembling of ssDSC components

After preparation of all pastes, assembling of monolithic ssDSC was accomplished. Basically, two film deposition techniques, doctor blade and screen printing were used in ssDSC production process.

As a first film deposition technique in ssDSC assembling, doctor blade coating was used via micrometer adjustable film thickness equipment as shown in Figure 2.7.

Figure 2.7 : The equipment used for doctor blade coating.

On the other side, for screen printing deposition of TiO_2, ZrO_2 and carbon pastes, silk screens was used in different constructions. Pore sizes and warp dimensions are critical parameters for film thickness deposited by screen printing technology. In order to manipulate the film properties, the screens in different constructions was used to select

optimum proses conditions in ssDSC production. Optic microscope images of the screens was showed in Figure 2.8.

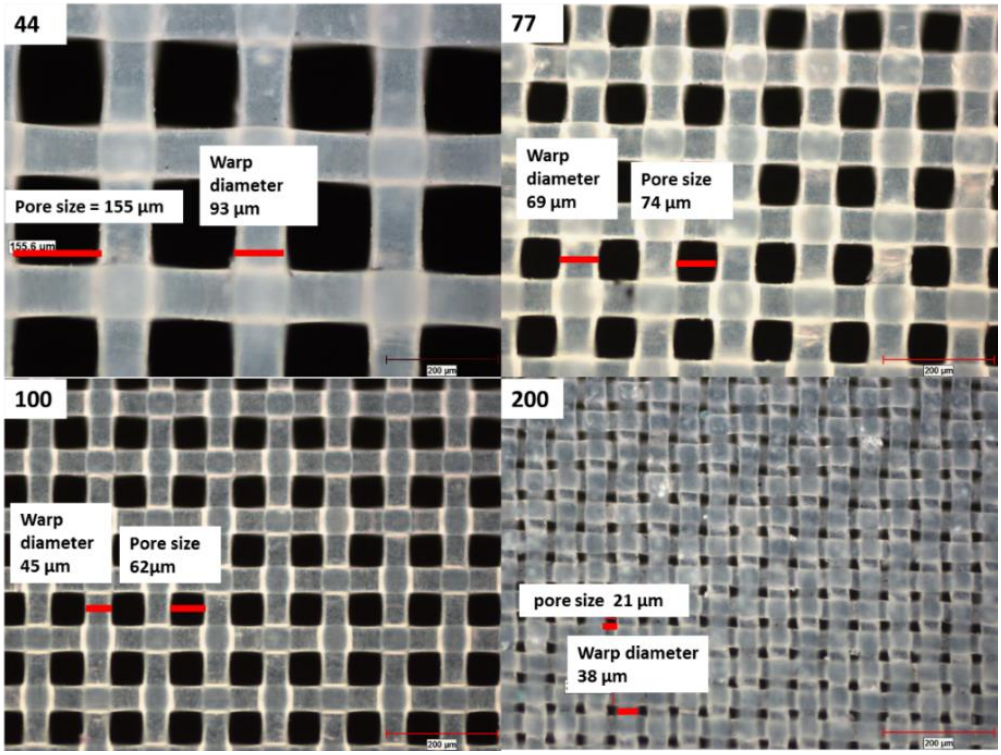

Figure 2.8 : Optic microscope images of silk fabrics used in screen printing technology. 44-77-100-200 represent mesh numbers.

Screen printing of pastes were conducted by using silk mesh screen with different threads per cm. and a squeegee was used to transfer the paste through pores of the silk mesh.

Assembling sequence and architecture of ssDSC was shown in Figure 2.9. ssDSC built up process was achieved via doctor blade and screen printing techniques.

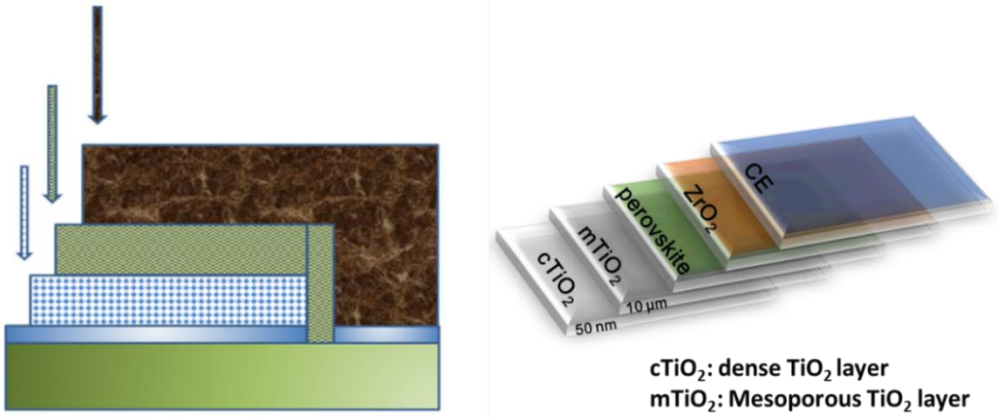

Figure 2.9 : Assembling of ssDSC by screen printing technology

2.2.4 Sensitization of ssDSC

As explained above, it is concentrated on monolithic perovskite based solar cell production because of high potential in scale-up ability of solar cell structure via industry.

In this regard, $CH_3NH_3PbI_3$ perovskite structure was synthesized in accordance with the literature [59]. $CH_3NH_3PbI_3$ was obtained by reaction of CH_3NH_3I and PbI_2. Briefly, first of all, CH_3NH_3I was synthesized via reaction of methylamine (40 wt. % in water) and hydro iodic acid. Reaction was proceed as fallow, in the typical amount of 52 ml of methylamine (40 wt.% in water) and 10 ml of hydro iodic acid (57 wt.% in water) were mixed in a 250 ml beaker placed in ice-bath at 0 ^oC for 2 h by using magnetic stirrer. After completing of reaction, CH_3NH_3I was precipitated by evaporation of water. Precipitated CH_3NH_3I in white color was washed with diethyl ether three times, then CH_3NH_3I dissolved in ethanol and recrystallized in refrigerator to be obtained CH_3NH_3I in clear crystal form.

Subsequently, PbI_2 and CH_3NH_3I were reacted at 3:1 molar ratio of CH_3NH_3I to PbI_2 by dissolving precursors in DMF. It was fallowed two methods for sensitization of ssDSC by perovskite. One of them is the synthesis of perovskite and then drop casting it to the ssDSC, while the other is sequential deposition of perovskite as explained before.

2.2.5 Characterization of ssDSC

Characterization of ssDSC structure was carried out by using 1.5 AM solar simulator equipped with Keithley 2400. TiO_2, ZrO_2 and carbon layer thickness was measured via Veeco Dektak 150 profilometer.

Figure 2.10. Solar simulator used for ssDSC performance evaluation

3. RESULT AND DISCUSSION

3.1. Characterization of Film Morphologies

For characterization, scanning electron microscopy was used for morphological analysis of thin film of ssDSC components. Surface morphology of thin films were examined under using a Zeiss EVO MA10 SEM at 15.00–20.00 kV and with magnifications ranging from 500 to 20 kX. A tungsten filament was used to create the beam and the reported resolution was 35 Å with a 20 kV beam. SEM images of ssDSC components was illustrated in Figure 3.1.

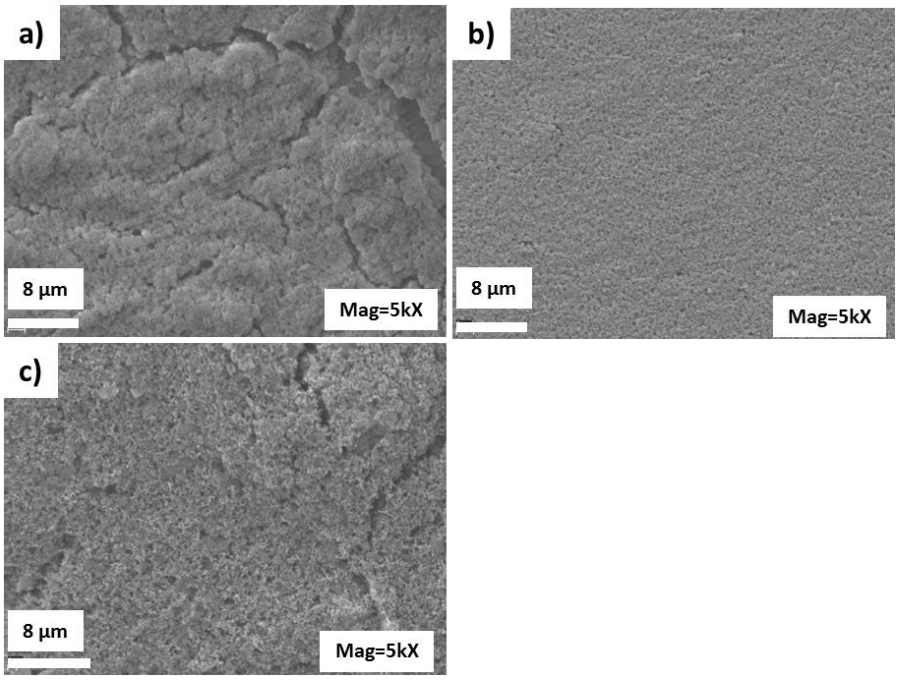

Figure 3.1 : SEM Images of ssDSC Components a) Mesoporous TiO_2 Layer via Recipe A b) Mesoporous TiO_2 Layer via Recipe B c) Carbon Counter Electrode.

As seen from Figure 3.1-a, mesoporous TiO_2 layer was deposited on conductive glass by using Recipe A has cracks on the film structure. TiO_2 film structure with cracks can be evaluated as a limiting factor to harvest electron because of given rise to higher recombination of electrons and holes in the ssDSC structure.

On the other side, Figure 3.1-b shows morphology of TiO_2 layer. It is clear from SEM images that TiO_2 layer has better crack-free morphology via Recipe B comparing to

TiO_2 layer via Recipe A. In this regard, Recipe B stands for a TiO_2 layer formation to go through ssDSC formation. The reason behind the better film formation via Recipe B can be attributable to thickener type used in both recipes. Because, it was observed that while ethyl cellulose dissolved in terpineol with no residues, hydroxyl ethyl cellulose has limited dissolution in terpineol. Besides that the effect of ethyl cellulose on rheological behavior of paste was facilitated the deposition of TiO_2 onto substrate. It also clear from Figure 3.1-c Carbon counter electrode was successfully deposited on TiO_2 layer without any crack formation.

When all issues was considered, we can sum up that cracks on TiO_2 layer might give rise to interconnect between carbon counter electrode and ITO-glass which is unwanted situation due to resulting in recombination of excited charges. So, in the rest of the experiments, we fallowed the Recipe B for paste preparation.

3.2. Discussion: Doctor Blade versus Screen Printing

After selection of recipe for paste preparation, it was proceeded to form ssDSC components. Both techniques was conducted for establishment of ssDSC. Then the produced ssDSCs was analyzed and optimized accordingly. In this section, results and analysis pertaining to both deposition techniques will be given consecutively.

3.2.1. ssDSC via doctor blade

Doctor blade was used as a first ssDSC assembling technique was conducted. ssDSC assembling process by doctor blading was illustrated in Figure 3.2.

It is clear from Figure 3.2, after deposition of spin coating of dense TiO_2 layer, TiO_2 and ZrO_2 mesoporous layer deposited onto TiO_2 dense layer by doctor blading, then sintering at 500 ^oC was conducted. During sintering, organic part of the pastes decomposed and removed from the structure. The brownish color is the indication of decomposition of organic polymers such as ethyl cellulose. After sintering, carbon paste was deposited onto ZrO_2 layer by using doctor blade and again sintering was followed at 400 ^oC. However, after sintering of carbon layer at 400 ^oC, cracks was observed onto carbon layer as seen from Figure 3.2. After completion of ssDSC via doctor blading, it was observed the crack formation of carbon layer than can be attributed to different thermal expansion coefficient of carbon and ZrO_2 layer. It was proposed that the crack formation can be eliminated by addition of TiO_2 particles into ZrO_2 paste, during ZrO_2 paste preparation.

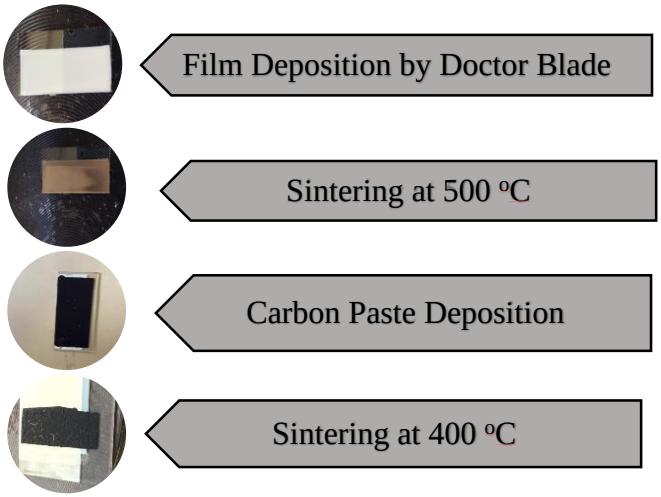

Figure 3.2. ssDSC establishment via Doctor Blade Technique

Afterwards, ZrO_2 paste was prepared with incorporation of TiO_2 particles into ZrO_2 paste and ssDSC structure was established again with modified ZrO_2 paste. Modified ZrO_2 paste has given rise to elimination of crack formation onto carbon layer as seen Figure 3.3. Subsequently, sensitization of ssDSC was performed via drop-casting of perovskite solution. After drop casting, ssDSC was treated at 110 °C, the yellowish color of ssDSC was converted to brownish indicating the crystallization of perovskite which is photoactive phase acting as electron-hole source.

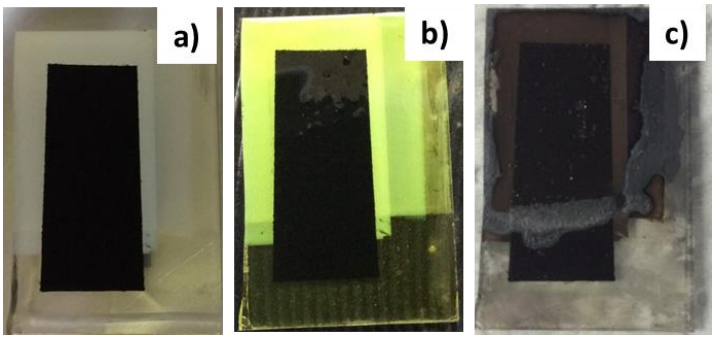

Figure 3.3 : Sensitization of ssDSC structure

Subsequently, efficiency of ssDSC was evaluated via 1.5 AM solar simulator equipped with Keithley 2400. Obtained I-V curves was showed in Figure 3.4.

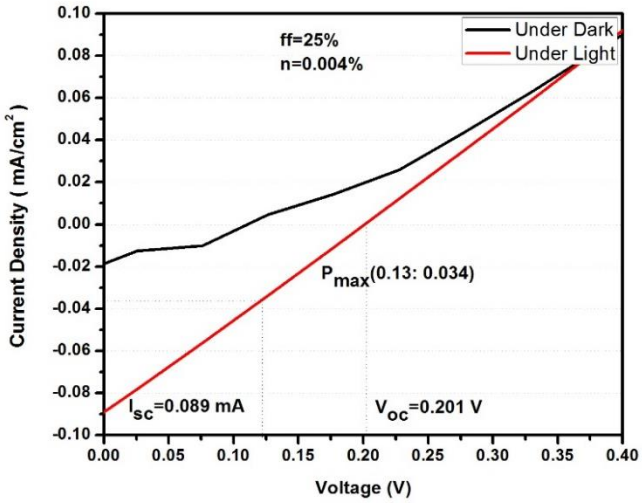

Figure 3.4 : Performance evaluation of ssDSC produced via doctor blade technique.

Perovskite based ssDSC produced by using doctor blade technique was enlightened with solar simulator equipped with Keithley 2400. According to I-V curve obtained by software named as Lab Tracer 2.0, fill factor (ff), open circuit voltage (V_{oc}), short circuit voltage (I_{sc}), maximum power values (P_{max}) and efficiency was calculated. The results showed in Table 3.1.

Table 3.1 : Performance of ssDSC via doctor blade

Method	Efficiency	FF (%)	I_{SC}	V_{OC}
Doctor Blade	0.004	25	0.201	0,089

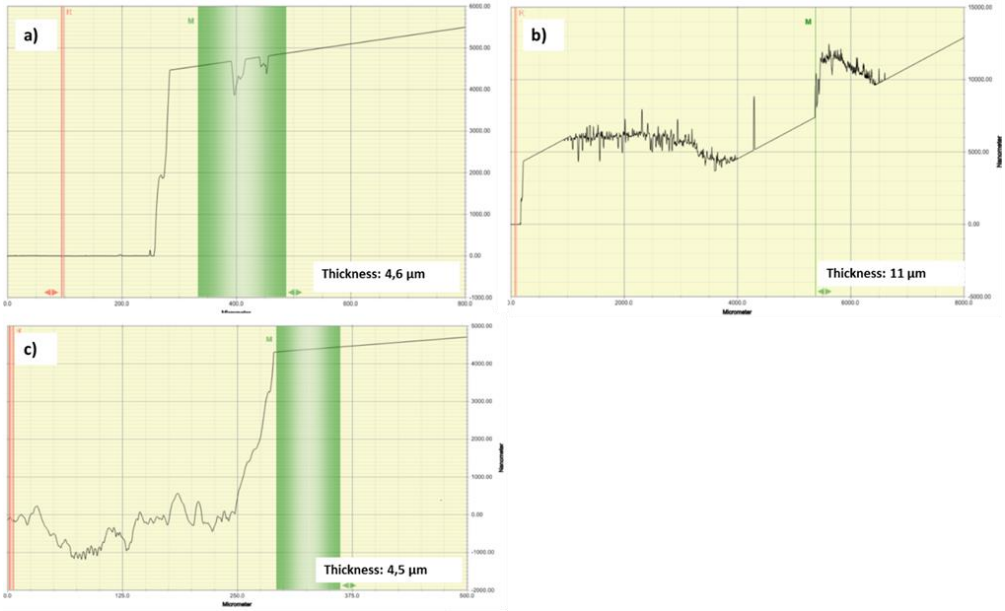

Figure 3.5 : Thickness values of a) TiO_2 b) ZrO_2 c) carbon layer. TiO_2 and ZrO_2 layers were deposited by doctor blade coating technique. Screen printing was used for carbon layer.

As can be seen from Table 3.1, power conversion efficiency (PCE) was quite low with the value of 0,004%. The reason behind the low PCE was analyzed by determination of layer thickness of the ssDSC components. The components of ssDSC-doctor blading layer thickness was measured by profilometer. The results of layer thickness pertaining to TiO_2, ZrO_2 and carbon layer was illustrated in Figure 3.5. The values obtaining from profilometer measurements was exhibited in Table **3.2**.

Table 3.2 : Thickness values of the components constituting ssDSC via doctor blade technique.

ssDSC Components	**TiO_2**	**ZrO_2**	**Carbon**
Thickness (µm)	**4,6**	**11**	**4,5**

As can be seen from Table 3.1, the ssDSC produced by using doctor blade technique show very low efficiency value of 0,004%. The low efficiency can be attributed to thicker component layer of ssDSC exhibited in Table 3.2. Liu et al. [49] conducted a research pertaining to determination of critical parameters such as layer thickness of ssDSC structure. According to the research, produced mesoscopic solar cell structure was in the form of TiO_2/ZrO_2/Carbon, same as the ssDSC produced in this thesis study. They reached efficiency exceeding 13%. They attributed the high efficiency to optimizing thickness of ZrO_2 and TiO_2 layer, application of perovskite into mesoscopic structure, giving rise to improving the light-harvesting ability and the hole transporting resistance. Their optimized values were submicron TiO_2 layer thickness and 1 µm for the spacer layer and 10 µm for the carbon layer thickness.

When we compared to the values depicted in Table **3.2**, it was noticed that the values in literature was quite lower than the values in Table 2. The lower values providing high efficiency might be allowed excited electrons to be captured by electrodes. Because, they proposed that electron diffusion length is about 1 µm. Thereby, thicker layer values much more than 1 µm can inhibit electrons transferring to photo-electrodes.

With this point of view, the optimization process was conducted to be able to obtain lower layer thickness of TiO_2, ZrO_2. It is important to note that ssDSC structure with the architecture shown in Figure 2.9, it is inevitable using patterning to build ssDSC in required form. It was used adhesive tape in doctor blade deposition technique for conduction of patterned deposition of inorganic pastes. However, adhesive tapes usage

limits decreasing TiO_2 and ZrO_2 film thickness layer. Therefore, it was proposed that screen printing technology enabling decreasing layer thickness of TiO_2 and ZrO_2 film and satisfying establishment ssDSC in the required architecture can be feasible deposition method in ssDSC production.

3.2.2. ssDSC via Screen Printing

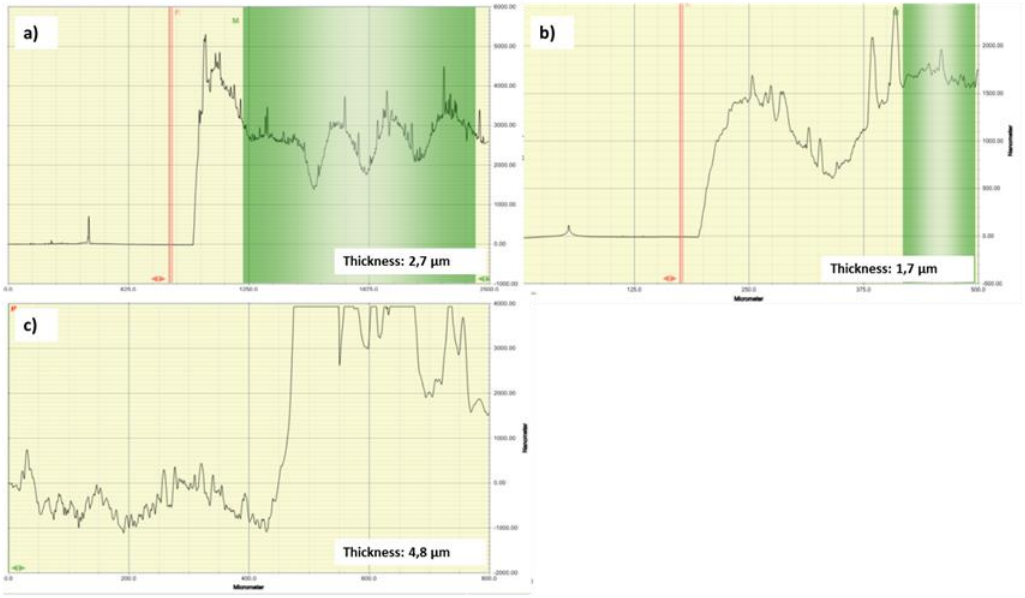

Figure 3.6 : a) TiO_2 b) ZrO_2 c) Carbon layer thickness via screen printing technique.

As a first try in screen printing coating, the same TiO_2 and ZrO_2 paste prepared by Recipe B was used. TiO_2 and ZrO_2 paste was deposited by using 100 mesh and 44 mesh was used for carbon paste deposition, because of carbon paste contains higher particle dimension comparing to TiO_2 and ZrO_2 pastes. Afterwards, TiO_2 and ZrO_2 film thickness was measured by profilometer. The results obtained from profilometer was exhibited in Figure 3.6. and average values of TiO_2 and ZrO_2 film thickness was given in Table 3.3.

Table 3.3 : Thickness values via screen printing technique

Screen Printing	TiO_2	ZrO_2	Carbon
Thickness (µm)	2,7	1,7	4,8

As can be seen from Table 3.3, layer thickness values of TiO_2 and ZrO_2 films were relatively decreased comparing to doctor blade technique. Besides that, surface morphology was investigating by optical microscopy. Optical microscopy image was exhibited in Figure 3.7.

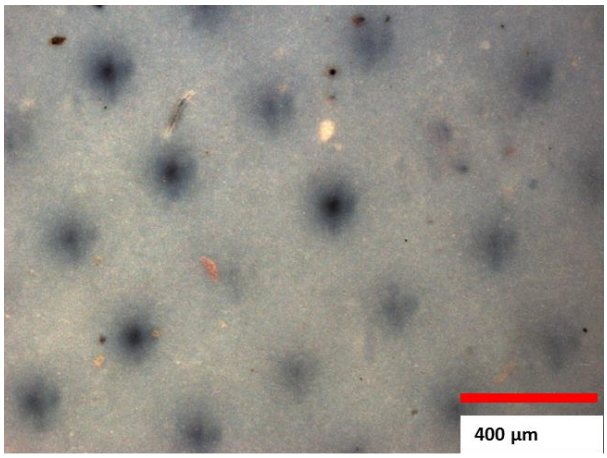

Figure 3.7 : Investigation of morphology of screen printed surface.

When the surface morphology was investigated, it was noticed that surface of TiO_2 and ZrO_2 layer has pin holes which is accepted as surface defects decreasing energy harvesting efficiency. Those pinholes can be attributed to higher viscosity of TiO_2 and ZrO_2 pastes.

In this regard, additional TiO_2 and ZrO_2 pastes optimization for screen printing was also conducted. As emphasized above that surface defects comes from higher viscosity of TiO_2 and ZrO_2 paste, hence, optimization of TiO_2 and ZrO_2 paste were conducted to lower viscosity enabling pin hole- free structure. Additionally, high viscosity of both TiO_2 and ZrO_2 pastes causes increase in layer thickness which is thicker than 1 µm. It is important to note that decreasing TiO_2 layer thickness to submicron and ZrO_2 layer to 1 µm is crucial. For that reason, it was considered that optimization process for paste viscosity was inevitable. With this point of view, new TiO_2 and ZrO_2 paste were prepared based on Recipe B. amount of terpineol was the only difference used in modified paste preparation. Basically, the amount of terpineol was increased for TiO_2 paste preparation to 30 g and 40 g, instead of 20 g. Both TiO_2 paste will be assigned as 6/30 TiO_2 and 6/40 TiO_2 at the rest part of this research.

For the ZrO_2 paste, terpineol amount used in paste preparation increased to 30 g. instead of 20 g and paste name will be assigned as (2+4)/30 ZrO_2 for the rest.

Furthermore, mesh number of screens is another parameters affecting layer thickness. Therefore, different screens with different mesh numbers were used in optimization process. Design of experiments for the paste optimization was exhibited in Table 3.4.

Table 3.4 : Design of Experiments for optimization of screen printing pastes

Experiment	Paste Type	Screen No
1	6/30 TiO_2	77

2	6/30 TiO_2	100
3	6/40 TiO_2	70
4	6/40 TiO_2	100
5	6/40 TiO_2	200
6	(2+4)/30 ZrO_2	77
7	(2+4)/30 ZrO_2	100
8	Carbon	44

All screen printing layer formation was carried out manually by using a squeegee on glass. Layer thickness of samples was measured by profilometer. Thickness values measured by profilometer was illustrated in Figure 3.8, Figure 3.9, Figure 3.10, Figure 3.11 consecutively. Additionally, all layer thickness values were sum up in Table 3.5

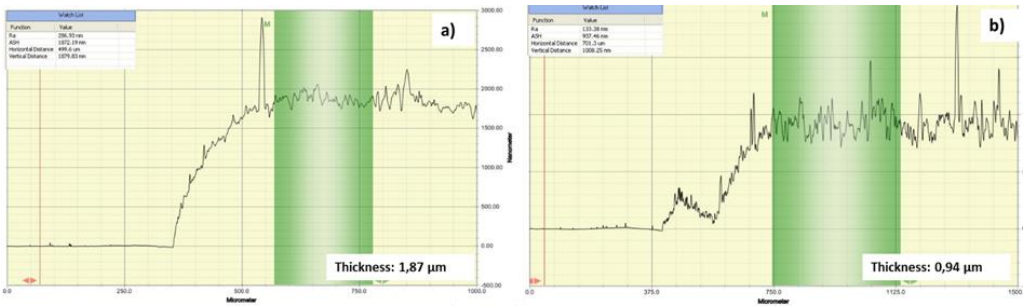

Figure 3.8 : 6/30 TiO_2 paste screen printing layer on glass substrate by using a) 77 mesh b) 100 mesh

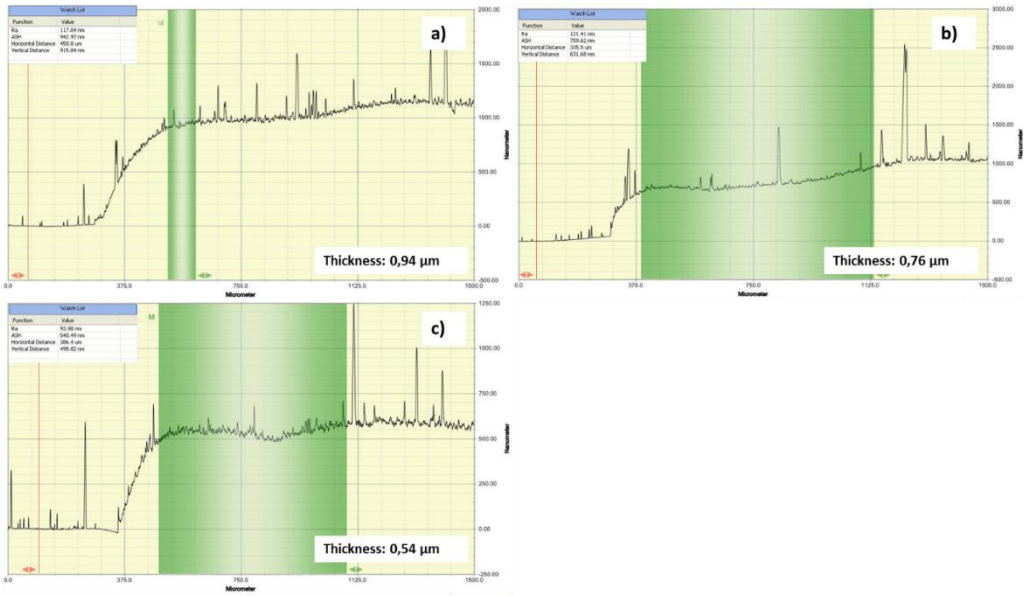

Figure 3.9 : 6/40 TiO2 paste screen printed on glass substrate by using a) 77 mesh b) 100 c) 200 mesh

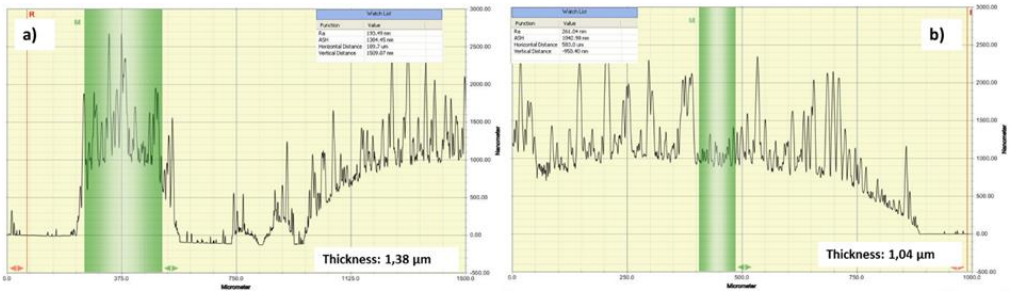

Figure 3.10 : (2+4)/30 ZrO2 paste screen printed on glass substrate by using a) 77 mesh b) 100 mesh

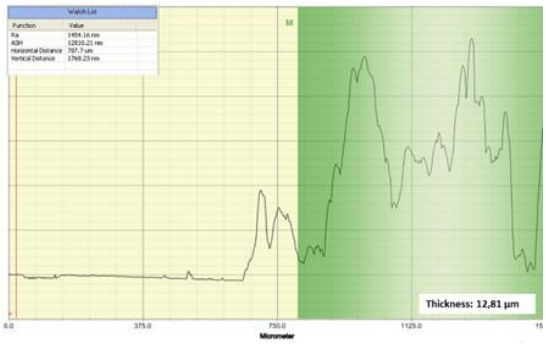

Figure 3.11 : Carbon paste screen printed on glass substrate by using 44 mesh

All experiments were named according to paste type and screen type express in Table 3.5 for more clear understanding. According to layer thickness values obtained profilometer measurements, by considering the research conducted by Liu et al, it was evaluated that Experiment-1 assigned as 6/30-100 TiO_2, experiment 4 assigned as 6/40-100, experiment 5 assigned as 6/40-200 were evaluated worth to try in ssDSC structure as TiO_2 layer. 6/40-200 X2 TiO_2 assigned for double layer of TiO_2 deposited via 6/40-200. For the ZrO_2 layer formation, it was only used experiment 7 assigned as (2+4)/30-100 for spacer layer formation. For the carbon layer deposition, experiment 8 was directly followed. Consequently, ssDSC structure selected for further optimization design was cleared in Table 3.6.

Table 3.5 : Layer thickness obtained by screen printing

Experiment	Paste Type	Screen No	Layer Thickness (µm)
1	6/30 TiO_2	77	1,87
2	6/30 TiO_2	100	0,94
3	6/40 TiO_2	70	0,96
4	6/40 TiO_2	100	0,74
5	6/40 TiO_2	200	0,54
6	(2+4)/30 ZrO_2	77	1,38
7	(2+4)/30 ZrO_2	100	1,04
8	Carbon	44	12

ssDSC structure in Table 3.6 was carried out by screen printing. All screen printing layer formation was performed manually by using a squeegee on dense TiO_2 layer coated ITO-glass. Again layer thickness of real ssDSC samples was measured by profilometer. Surface morphology was also investigated by optical microscope. Optical microscope images combining layer thickness of real devices was presented in Figure 3.12, Figure 3.13, Figure 3.14 and Figure 3.15 respectively.

Table 3.6 : ssDSC produced after optimization of TiO_2 and ZrO_2 layer thickness

Solar Cell Type	TiO_2 Layer	ZrO_2 Layer	Carbon Layer
1	6/30-100 TiO_2	(2+4)/30-100 ZrO_2	Carbon-44
2	6/30-200 TiO_2	(2+4)/30-100 ZrO_2	Carbon-44
3	6/40-100 TiO_2	(2+4)/30-100 ZrO_2	Carbon-44
4	6/40-200 TiO_2	(2+4)/30-100 ZrO2	Carbon-44
5	6/40-200 X2 TiO_2	(2+4)/30-100 ZrO_2	Carbon-44

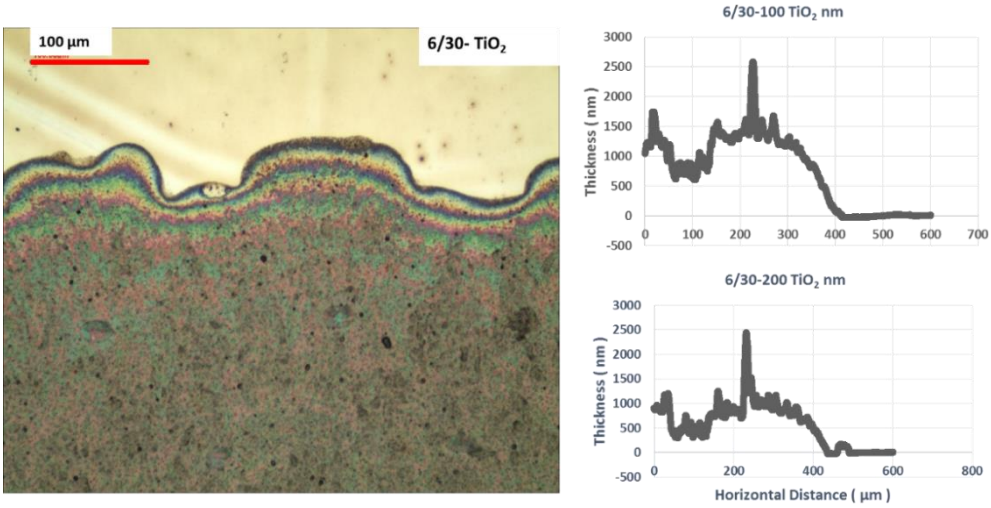

Figure 3.12 : Optical microscopy images combining with profilometer measurement of mesoporous TiO_2 layer via 6/30- TiO_2 paste

Layer thickness results via 6/30 TiO_2 paste from Profilometer was sum up in Table 7.

Table 3.7 : TiO_2 layer thickness by using 6/30 TiO_2 paste

Solar Cell Type	**TiO_2 Layer**	**Layer Thickness (µm)**
1	6/30-100 TiO_2	1,1
2	6/30-200 TiO_2	0,85

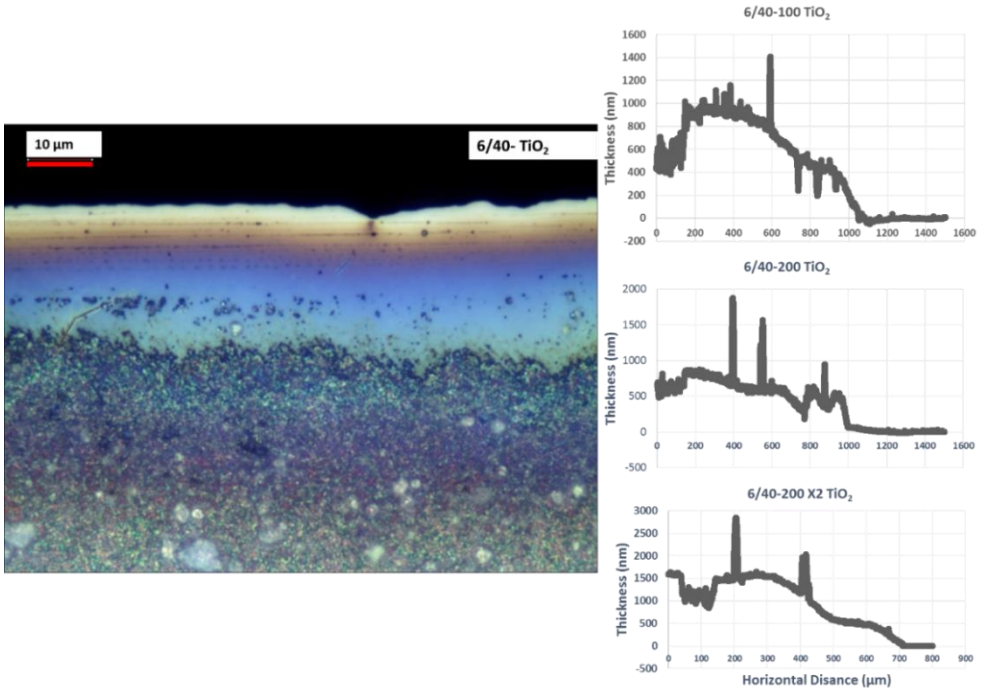

Figure 3.13 : Optical microscopy images combining with profilometer measurement of mesoporous TiO_2 layer via 6/40- TiO_2 paste

Layer thickness results via 6/40 TiO_2 paste from Profilometer was also sum up in Table 8.

Table 3.8 : TiO_2 layer thickness by using 6/40 TiO_2 paste

Solar Cell Type	TiO_2 Layer	Thickness (µm)
3	6/40-100 TiO_2	0,93
4	6/40-200 TiO_2	0,73
5	6/40-200 X2 TiO_2	1,12

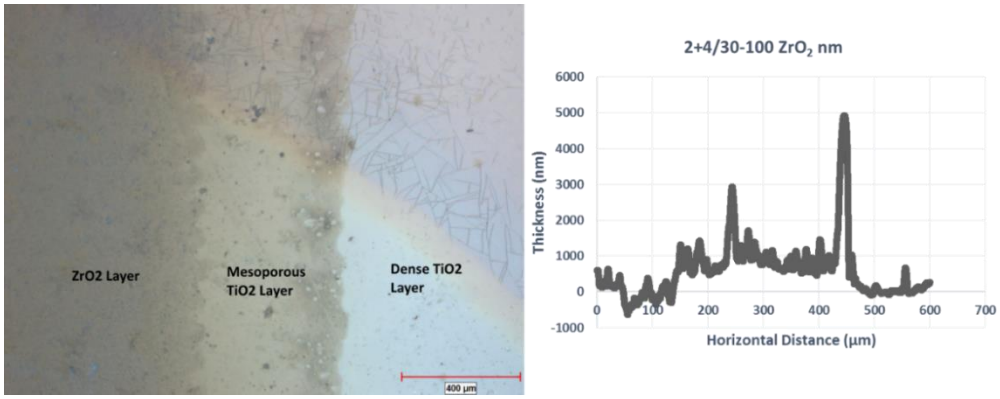

Figure 3.14 : Optical microscopy images combining with profilometer measurement of mesoporous ZrO_2 layer via (2+4)/30- ZrO_2 paste

According to profilometer measurement results, average ZrO_2 layer thickness was calculated as 1 µm.

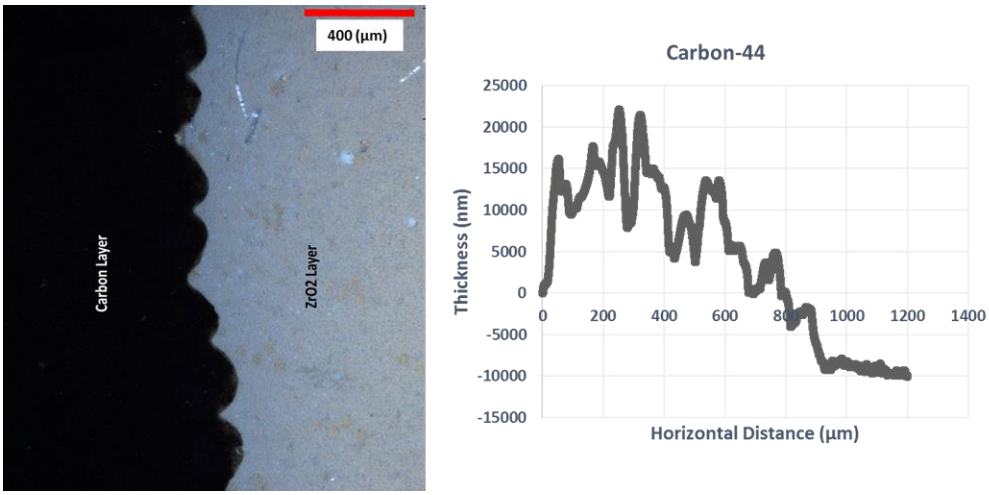

Figure 3.15 : Optical microscopy images combining with profilometer measurement of mesoporous carbon layer.

Profilometer measurement showed average carbon layer thickness as 14 µm for all ssDSC measurements. After construction of ssDSC, all solar cells were sensitized by photoactive $CH_3NH_3PbI_3$ perovskite molecules. Deposition of $CH_3NH_3PbI_3$ onto ssDSC structure was carried out by sequential deposition technique. First of all 0,1 M 1 µL PbI_2 solution dissolved in DMF was dropped onto ssDSC structure. Before deposition, both ssDSC and PbI_2 solution was heated up 70 ^oC, afterward PbI_2 deposited ssDSC was rotated on spin coating unit at 6000 rpm. Then let ssDSC dry at 50 ^oC for 15 min. Subsequently, PbI_2 deposited ssDSC was dipped into solution of CH_3NH_3I dissolved in IPA (10 mg/mL). ssDSC dipped into CH_3NH_3I solution immediately was converted into brownish color which is the indication of formation and crystallization of $CH_3NH_3PbI_2$ in ssDSC structure. After sensitization of ssDSC, absorption characteristics of ssDSC was analyzed by using UV-Vis spectrophotometer.

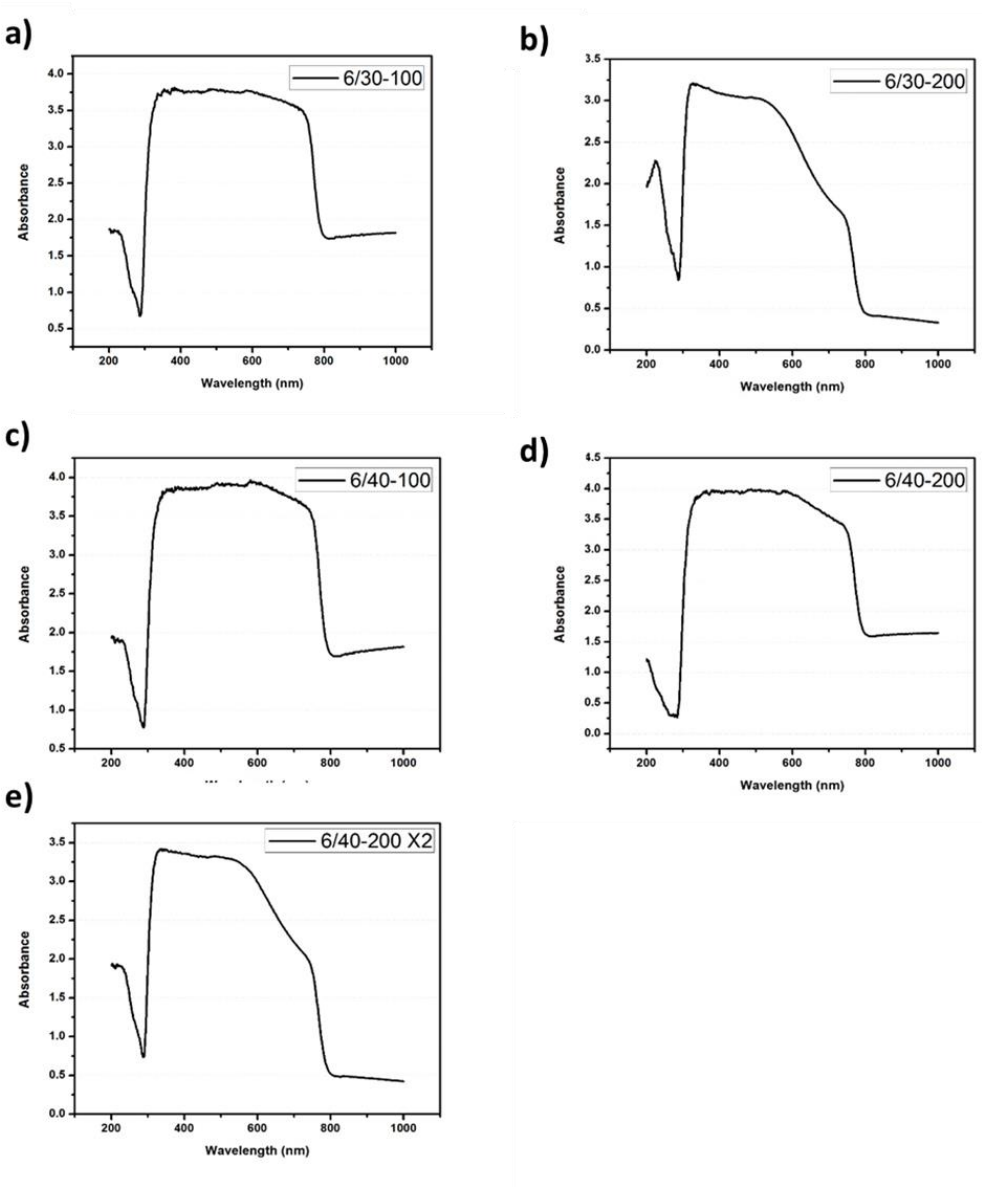

Figure 3.16 : Absorbance Spectrum of Solar Cells Produced by Screen Printing

Absorption curves of ssDSC sensitized by perovskite were exhibited in Figure 3.16. All perovskite based ssDSCs showed better absorption comparing to literature [49].

For the last characterization of ssDSC, power conversion efficiencies (PCE) was measured by solar simulator as explained in experimental section. Photovoltaic performance test results exhibited in Figure 3.17.

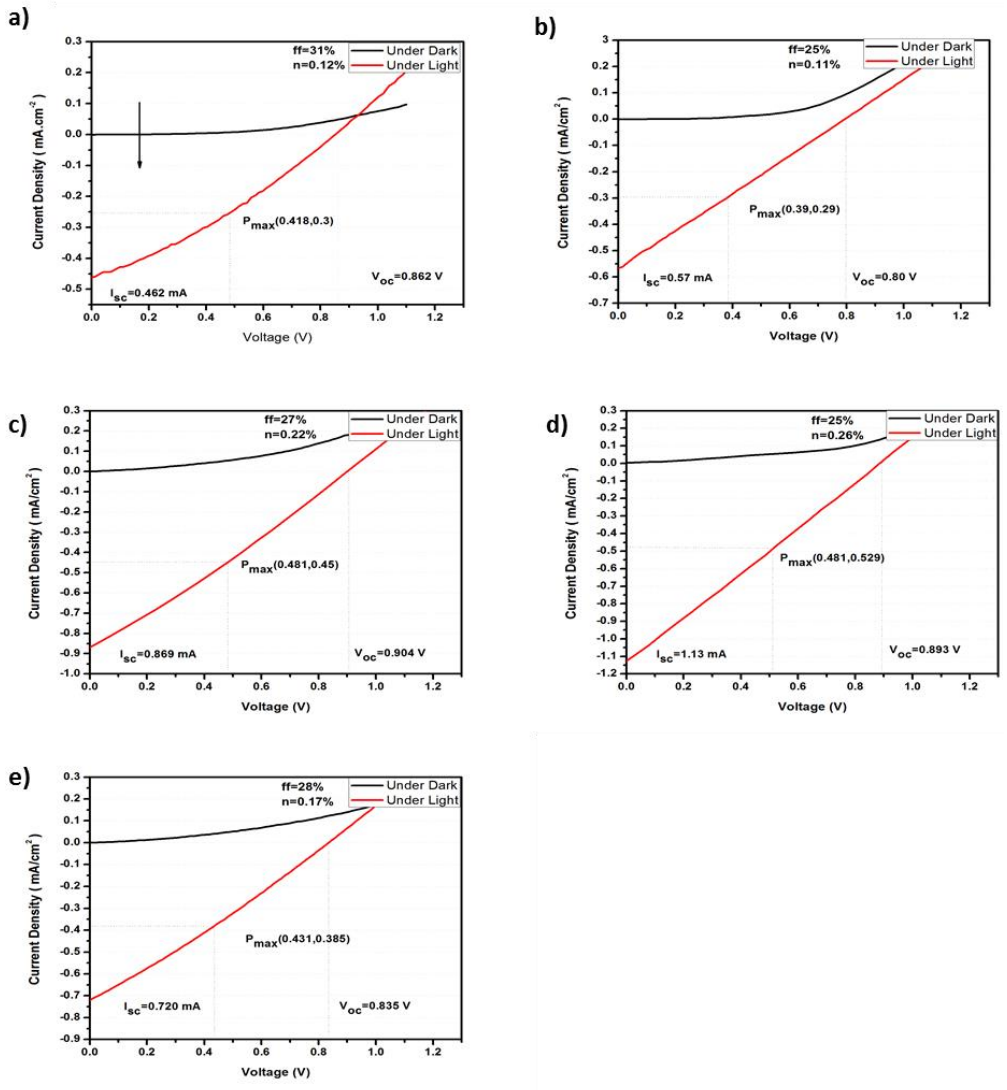

Figure 3.17 : PV measurement of solar cell of which a) 6/30-100 b) 6/30-200 c) 6/40-100 d) 6/40-200 e) 6/40-200 X2

Additionally, PCE results were sum up in

Table 3.9. According to PCE results, all ssDSC showed better PCE comparing to ssDSC produced by doctor blade technique. The higher performance of the ssDSCs can be attributed to decreased layer thickness of ssDSC structure.

Table 3.9 : PV Performance Evaluation of ssDSC Produced by Screen Printing

PASTE	MESH	EFFICIENCY (%)	FF	I_{sc}	V_{oc}
6-30	100	0.12	31	0.462	0.862
6-30	200	0.11	25	0.57	0.8
6-40	100	0.22	27	0.869	0.904
6-40	200	0.26	25	1.13	0.893
6-40 x2	200	0.17	27	0.835	0.72

4. CONCLUSION

In this thesis study, after introducing solar cell structures briefly, focused on dye-sensitized solar cells (DSC) and its component, energy harvesting mechanism and manufacturing process with the aim of industrialization. Among different kind of DSC structure, solid state Dye Sensitized Solar Cells (ssDSC) was evaluated as promising approaches for large scale production. Thus, in this research, whole ssDSC components were successfully manufactured from beginning with particles in nanoscale to macroscopic dimension.

In manufacturing process, two different film formation techniques, doctor blade and screen printing technology was proposed for the industrialization of ssDSC structures. Doctor blade technique was used in first stage because of facile applicability. ssDSC manufactured via doctor blading resulted in low efficiencies around 0,004%. Analysis of ssDSC with lower efficiency showed that mesoporous TiO_2 and ZrO_2 layer thickness plays very important role on power conversion efficiency. In doctor blade techniques, it couldn't be decreased layer thickness of the TiO_2 and ZrO_2 due to patterning issue. Increasing 1 μm layer thickness of TiO_2 and ZrO_2 limits harvesting of excited charges due to limited electron diffusion length value of 1 μm.

Therefore, screen printing technology was proposed as the deposition technique enabling to decrease layer thickness of TiO_2 and ZrO_2 by improving patterning ability. Improved patterning provided manufacturing ssDSC in any required architecture. However, pastes used for doctor blading couldn't be applied in screen printing due to higher viscosity. In this point of view, optimization process was conducted by playing with viscosity of screen printing pastes and construction of screens used in deposition of TiO_2 and ZrO_2 pastes. Profilometer measurement showed that TiO_2 layer in about 500 nm thickness could be produced after optimization process.

After optimization process, ssDSCs in five different construction were manufactured. Afterwards, ssDSC via screen printing showed dramatic increase comparing to ssDSC via doctor blade technique. The dramatic increase can be attributable to decreased layer thickness of TiO_2 and ZrO_2. Additionally, analysis of profilometer results exhibited that deposition of TiO_2 and ZrO_2 layer with tunable thickness may allow

engineering of ssDSC construction in forthcoming studies. It was obtained that the highest efficiency is 0.26% for the best solar cells.

5. FUTURE WORK AND PROPOSALS

In this study, ssDSC manufactured via doctor blading or screen printing showed PCE in the range of 0,004% and 0, 26%. When certified highest PCE of ssDSCs exceeding 20% was considered, long way stand us to go through. One of the issue to enhance PCE is the formation of metal oxide layer without any pin holes on metal oxide layer especially in electron selective layer. It is very important phenomena getting rid of pin holes might pave the ways for higher efficiencies.

In this context, improved metal oxide layer deposition will be the forthcoming studies. For this purpose, ultrasonic-assisted TiO_2 coating was proposed and first work was done by publishing result of the studies. The product of preliminary research was exhibited in Appendiz A.

Another approaches for deposition of pin hole-free metal oxide layer might be solution processed in-situ synthesis of ZnO seeding layer and ZnO nanorod-like structures onto TCO instead of mesoporous TiO_2 layer. in this context, preliminary studies have been proceeding and synthesized ZnO nanorod layer depicted in Figure 5.1 and ZnO nanorod growth was depicted in Figure 5.2.

All synthesis of ZnO layer and nanorod structures was conducted on flexible ITO coated polyethylene terephthalate (ITO-PET) surface by ultrasonic irradiation. It is another important part of this preliminary studies enabling to establish flexible ssDSC structures.

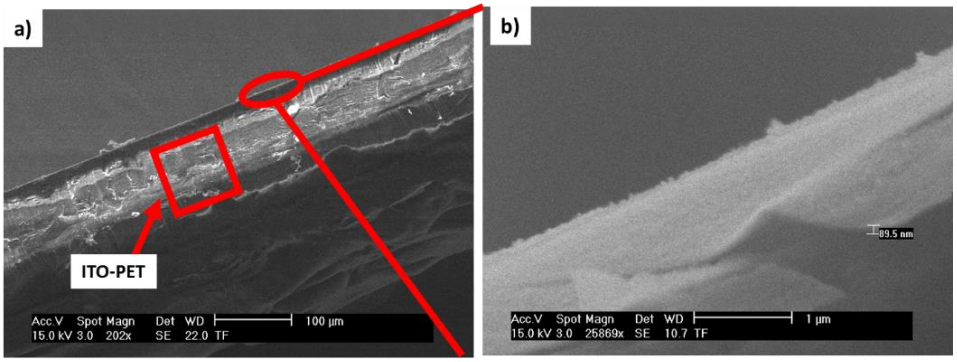

Figure 5.1 : In-situ synthesis of ZnO layer on ITO-PET.

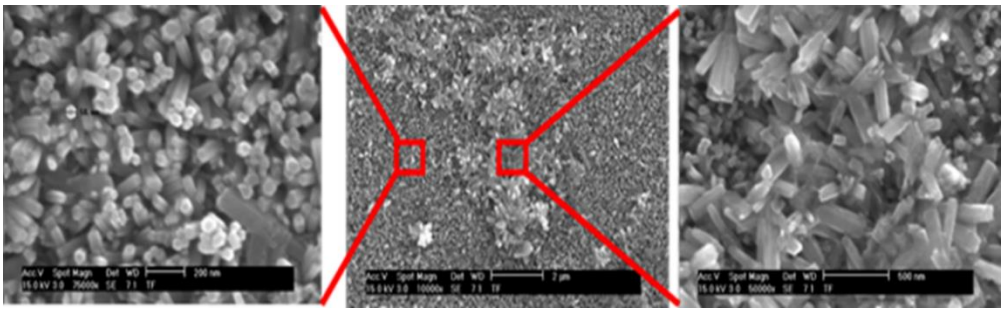

Figure 5.2 : ZnO nanordo Structure growth on ITO-PET surface.

REFERENCES

[1] M. Grätzel, 'Solar energy conversion by dye-sensitized photovoltaic cells', *Inorg. Chem.*, vol. 44, no. 20, pp. 6841–6851, 2005.

[2] L. Giribabu, K. Sudhakar, and V. Velkannan, 'Phthalocyanines: potential alternative sensitizers to Ru (II) polypyridyl complexes for dye-sensitized solar cells', *Curr. Sci.*, vol. 102, no. 7, pp. 991–1000, 2012.

[3] L. Giribabu, K. Sudhakar, and V. Velkannan, 'Phthalocyanines: potential alternative sensitizers to Ru (II) polypyridyl complexes for dye-sensitized solar cells', *Curr. Sci.*, vol. 102, no. 7, pp. 991–1000, 2012.

[4] S. Ito, T. N. Murakami, P. Comte, P. Liska, C. Grätzel, M. K. Nazeeruddin, and M. Grätzel, 'Fabrication of thin film dye sensitized solar cells with solar to electric power conversion efficiency over 10%', *Thin Solid Films*, vol. 516, no. 14, pp. 4613–4619, 2008.

[5] G. P. Smestad, 'Education and solar conversion:: demonstrating electron transfer', *Sol. Energy Mater. Sol. Cells*, vol. 55, no. 1, pp. 157–178, 1998.

[6] M. Fujimoto, T. Kado, W. Takashima, K. Kaneto, and S. Hayase, 'Dye-sensitized solar cells fabricated by electrospray coating using TiO_2 nanocrystal dispersion solution', *J. Electrochem. Soc.*, vol. 153, no. 5, pp. A826–A829, 2006.

[7] C. J. Chen, *Physics of solar energy*. Hoboken, N.J.: John Wiley & Sons, 2011.

[8] A. Goetzberger and V. U. Hoffmann, *Photovoltaic solar energy generation*. Berlin; New York: Springer, 2005.

[9] A. B. Martinson, J. W. Elam, J. T. Hupp, and M. J. Pellin, 'ZnO nanotube based dye-sensitized solar cells', *Nano Lett.*, vol. 7, no. 8, pp. 2183–2187, 2007.

[10] F. Lenzmann, J. Krueger, S. Burnside, K. Brooks, M. Grätzel, D. Gal, S. Rühle, and D. Cahen, 'Surface photovoltage spectroscopy of dye-sensitized solar cells with TiO2, Nb2O5, and SrTiO3 nanocrystalline photoanodes: indication for electron injection from higher excited dye states', *J. Phys. Chem. B*, vol. 105, no. 27, pp. 6347–6352, 2001.

[11] X.-T. Zhang, T. Taguchi, H.-B. Wang, Q.-B. Meng, O. Sato, and A. Fujishima, 'Investigation of the stability of solid-state dye-sensitized solar cells', *Res. Chem. Intermed.*, vol. 33, no. 1–2, pp. 5–11, 2007.

[12] A. Turković and Z. Cmjak Orel, 'Dye-sensitized solar cell with Ce0< sub> 2</sub> and mixed CeO2Sn02 photoanodes', *Sol. Energy Mater. Sol. Cells*, vol. 45, no. 3, pp. 275–281, 1997.

[13] N. Nang Dinh, M.-C. Bernard, A. Hugot-Le Goff, T. Stergiopoulos, and P. Falaras, 'Photoelectrochemical solar cells based on SnO< sub> 2</sub> nanocrystalline films', *Comptes Rendus Chim.*, vol. 9, no. 5, pp. 676–683, 2006.

[14] C.-G. Bostan, N. Dina, M. Bulgariu, S. Craciun, M. Dafinei, C. Chitu, I. Staicu, and S. Antohe, 'Teaching/learning photovoltaic effect in high school', *Romanian Rep. Phys.*, vol. 63, no. 2, pp. 543–546, 2011.

[15] S. Pelet, J.-E. Moser, and M. Grätzel, 'Cooperative effect of adsorbed cations and iodide on the interception of back electron transfer in the dye sensitization of nanocrystalline TiO2', *J. Phys. Chem. B*, vol. 104, no. 8, pp. 1791–1795, 2000.

[16] Y.-G. Kim, J. Walker, L. A. Samuelson, and J. Kumar, 'Efficient light harvesting polymers for nanocrystalline TiO2 photovoltaic cells', *Nano Lett.*, vol. 3, no. 4, pp. 523–525, 2003.
[17] H. Greijer Agrell, J. Lindgren, and A. Hagfeldt, 'Coordinative interactions in a dye-sensitized solar cell', *J. Photochem. Photobiol. Chem.*, vol. 164, no. 1, pp. 23–27, 2004.
[18] Q. Zhang, C. S. Dandeneau, X. Zhou, and G. Cao, 'ZnO Nanostructures for Dye-Sensitized Solar Cells', *Adv. Mater.*, vol. 21, no. 41, pp. 4087–4108, Nov. 2009.
[19] T. Miyasaka, M. Ikegami, and Y. Kijitori, 'Photovoltaic Performance of Plastic Dye-Sensitized Electrodes Prepared by Low-Temperature Binder-Free Coating of Mesoscopic Titania', *J. Electrochem. Soc.*, vol. 154, no. 5, pp. A455–A461, Jan. 2007.
[20] F. Gao, Y. Wang, J. Zhang, D. Shi, M. Wang, R. Humphry-Baker, P. Wang, S. M. Zakeeruddin, and M. Grätzel, 'A new heteroleptic ruthenium sensitizer enhances the absorptivity of mesoporous titania film for a high efficiency dye-sensitized solar cell', *Chem. Commun.*, no. 23, pp. 2635–2637, 2008.
[21] R. Jose, A. Kumar, V. Thavasi, and S. Ramakrishna, 'Conversion efficiency versus sensitizer for electrospun TiO2 nanorod electrodes in dye-sensitized solar cells', *Nanotechnology*, vol. 19, no. 42, p. 424004, 2008.
[22] T.-S. Kang, A. P. Smith, B. E. Taylor, and M. F. Durstock, 'Fabrication of highly-ordered TiO2 nanotube arrays and their use in dye-sensitized solar cells', *Nano Lett.*, vol. 9, no. 2, pp. 601–606, 2009.
[23] L. Han, A. Fukui, Y. Chiba, A. Islam, R. Komiya, N. Fuke, N. Koide, R. Yamanaka, and M. Shimizu, 'Integrated dye-sensitized solar cell module with conversion efficiency of 8.2%', *Appl. Phys. Lett.*, vol. 94, no. 1, p. 013305, 2009.
[24] P. E. Heil, H. Kang, H. Choi, and K. Kim, 'TiO2 nanoparticle-nanofiber composites and their application in dye-sensitized solar cells', in *2010 10th IEEE Conference on Nanotechnology (IEEE-NANO)*, 2010, pp. 482–485.
[25] H. Zhou, L. Wu, Y. Gao, and T. Ma, 'Dye-sensitized solar cells using 20 natural dyes as sensitizers', *J. Photochem. Photobiol. Chem.*, vol. 219, no. 2, pp. 188–194, 2011.
[26] B. E. Hardin, H. J. Snaith, and M. D. McGehee, 'The renaissance of dye-sensitized solar cells', *Nat. Photonics*, vol. 6, no. 3, pp. 162–169, 2012.
[27] S. Sönmezoğlu, C. Akyürek, and S. Akin, 'High-efficiency dye-sensitized solar cells using ferrocene-based electrolytes and natural photosensitizers', *J. Phys. Appl. Phys.*, vol. 45, no. 42, p. 425101, Oct. 2012.
[28] A. S. Karmakar and J. P. Ruparelia, 'A Critical Review on Dye Sensitized Solar Cells.'
[29] D. Bi, L. Yang, G. Boschloo, A. Hagfeldt, and E. M. Johansson, 'Effect of different hole transport materials on recombination in CH3NH3PbI3 perovskite-sensitized mesoscopic solar cells', *J. Phys. Chem. Lett.*, vol. 4, no. 9, pp. 1532–1536, 2013.
[30] R. Lindblad, D. Bi, B. Park, J. Oscarsson, M. Gorgoi, H. Siegbahn, M. Odelius, E. M. Johansson, and H. akan Rensmo, 'The Electronic Structure of TiO2/CH3NH3PbI3 Perovskite Solar Cell Interfaces', *J. Phys. Chem. Lett.*, 2014.
[31] D. R. Baker and P. V. Kamat, 'Photosensitization of TiO2 Nanostructures with CdS Quantum Dots: Particulate versus Tubular Support Architectures', *Adv. Funct. Mater.*, vol. 19, no. 5, pp. 805–811, Mar. 2009.

[32] R. J. Ellingson, M. C. Beard, J. C. Johnson, P. Yu, O. I. Micic, A. J. Nozik, A. Shabaev, and A. L. Efros, 'Highly efficient multiple exciton generation in colloidal PbSe and PbS quantum dots', *Nano Lett.*, vol. 5, no. 5, pp. 865–871, 2005.
[33] R. Plass, S. Pelet, J. Krueger, M. Grätzel, and U. Bach, 'Quantum Dot Sensitization of Organic−Inorganic Hybrid Solar Cells', *J. Phys. Chem. B*, vol. 106, no. 31, pp. 7578–7580, Aug. 2002.
[34] K. S. Leschkies, R. Divakar, J. Basu, E. Enache-Pommer, J. E. Boercker, C. B. Carter, U. R. Kortshagen, D. J. Norris, and E. S. Aydil, 'Photosensitization of ZnO Nanowires with CdSe Quantum Dots for Photovoltaic Devices', *Nano Lett.*, vol. 7, no. 6, pp. 1793–1798, Haziran 2007.
[35] N.-G. Park, 'Organometal perovskite light absorbers toward a 20% efficiency low-cost solid-state mesoscopic solar cell', *J. Phys. Chem. Lett.*, vol. 4, no. 15, pp. 2423–2429, 2013.
[36] P. Gao, M. Grätzel, and M. K. Nazeeruddin, 'Organohalide lead perovskites for photovoltaic applications', *Energy Environ. Sci.*, vol. 7, no. 8, pp. 2448–2463, Jul. 2014.
[37] A. M. Salau, 'Fundamental absorption edge in PbI2:KI alloys', *Sol. Energy Mater.*, vol. 2, no. 3, pp. 327–332, Nisan 1980.
[38] U. Bach, D. Lupo, P. Comte, J. E. Moser, F. Weissörtel, J. Salbeck, H. Spreitzer, and M. Grätzel, 'Solid-state dye-sensitized mesoporous TiO2 solar cells with high photon-to-electron conversion efficiencies', *Nature*, vol. 395, no. 6702, pp. 583–585, 1998.
[39] J. Krüger, R. Plass, L. Cevey, M. Piccirelli, M. Grätzel, and U. Bach, 'High efficiency solid-state photovoltaic device due to inhibition of interface charge recombination', *Appl. Phys. Lett.*, vol. 79, no. 13, pp. 2085–2087, 2001.
[40] J. Burschka, A. Dualeh, F. Kessler, E. Baranoff, N.-L. Cevey-Ha, C. Yi, M. K. Nazeeruddin, and M. Grätzel, 'Tris (2-(1 H-pyrazol-1-yl) pyridine) cobalt (III) as p-type dopant for organic semiconductors and its application in highly efficient solid-state dye-sensitized solar cells', *J. Am. Chem. Soc.*, vol. 133, no. 45, pp. 18042–18045, 2011.
[41] A. Kojima, K. Teshima, Y. Shirai, and T. Miyasaka, 'Organometal halide perovskites as visible-light sensitizers for photovoltaic cells', *J. Am. Chem. Soc.*, vol. 131, no. 17, pp. 6050–6051, 2009.
[42] H.-S. Kim, C.-R. Lee, J.-H. Im, K.-B. Lee, T. Moehl, A. Marchioro, S.-J. Moon, R. Humphry-Baker, J.-H. Yum, and J. E. Moser, 'Lead iodide perovskite sensitized all-solid-state submicron thin film mesoscopic solar cell with efficiency exceeding 9%', *Sci. Rep.*, vol. 2, 2012.
[43] L. Etgar, P. Gao, Z. Xue, Q. Peng, A. K. Chandiran, B. Liu, M. K. Nazeeruddin, and M. Grätzel, 'Mesoscopic CH3NH3PbI3/TiO2 heterojunction solar cells', *J. Am. Chem. Soc.*, vol. 134, no. 42, pp. 17396–17399, 2012.
[44] J. Burschka, N. Pellet, S.-J. Moon, R. Humphry-Baker, P. Gao, M. K. Nazeeruddin, and M. Grätzel, 'Sequential deposition as a route to high-performance perovskite-sensitized solar cells', *Nature*, vol. 499, no. 7458, pp. 316–319, 2013.
[45] H.-S. Kim, J.-W. Lee, N. Yantara, P. P. Boix, S. A. Kulkarni, S. Mhaisalkar, M. Grätzel, and N.-G. Park, 'High efficiency solid-state sensitized solar cell-based on submicrometer rutile TiO2 nanorod and CH3NH3PbI3 perovskite sensitizer', *Nano Lett.*, vol. 13, no. 6, pp. 2412–2417, 2013.

[46] L. Vesce, R. Riccitelli, G. Mincuzzi, A. Orabona, G. Soscia, T. M. Brown, A. Di Carlo, and A. Reale, 'Fabrication of Spacer and Catalytic Layers in Monolithic Dye-Sensitized Solar Cells', *IEEE J. Photovolt.*, vol. 3, no. 3, pp. 1004–1011, Jul. 2013.
[47] H. Han, U. Bach, Y.-B. Cheng, R. A. Caruso, and C. MacRae, 'A design for monolithic all-solid-state dye-sensitized solar cells with a platinized carbon counterelectrode', *Appl. Phys. Lett.*, vol. 94, no. 10, p. 103102, 2009.
[48] Z. Ku, Y. Rong, M. Xu, T. Liu, and H. Han, 'Full printable processed mesoscopic $CH_3NH_3PbI_3/TiO_2$ heterojunction solar cells with carbon counter electrode', *Sci. Rep.*, vol. 3, p. 3132, 2013.
[49] T. Liu, L. Liu, M. Hu, Y. Yang, L. Zhang, A. Mei, and H. Han, 'Critical parameters in TiO2/ZrO2/Carbon-based mesoscopic perovskite solar cell', *J. Power Sources*, vol. 293, pp. 533–538, Oct. 2015.
[50] H. Han, U. Bach, Y.-B. Cheng, and R. A. Caruso, 'Increased nanopore filling: Effect on monolithic all-solid-state dye-sensitized solar cells', *Appl. Phys. Lett.*, vol. 90, no. 21, p. 213510, 2007.
[51] G. Liu, H. Wang, X. Li, Y. Rong, Z. Ku, M. Xu, L. Liu, M. Hu, Y. Yang, P. Xiang, T. Shu, and H. Han, 'A mesoscopic platinized graphite/carbon black counter electrode for a highly efficient monolithic dye-sensitized solar cell', *Electrochimica Acta*, vol. 69, pp. 334–339, May 2012.
[52] E. J. Crossland, N. Noel, V. Sivaram, T. Leijtens, J. A. Alexander-Webber, and H. J. Snaith, 'Mesoporous TiO2 single crystals delivering enhanced mobility and optoelectronic device performance', *Nature*, vol. 495, no. 7440, pp. 215–219, 2013.
[53] J. M. Ball, M. M. Lee, A. Hey, and H. J. Snaith, 'Low-temperature processed meso-superstructured to thin-film perovskite solar cells', *Energy Environ. Sci.*, vol. 6, no. 6, pp. 1739–1743, May 2013.
[54] K. Wojciechowski, M. Saliba, T. Leijtens, A. Abate, and H. J. Snaith, 'Sub-150° C processed meso-superstructured perovskite solar cells with enhanced efficiency', *Energy Environ. Sci.*, vol. 7, no. 3, pp. 1142–1147, 2014.
[55] C. Euvananont, C. Junin, K. Inpor, P. Limthongkul, and C. Thanachayanont, 'TiO 2 optical coating layers for self-cleaning applications', *Ceram. Int.*, vol. 34, no. 4, pp. 1067–1071, 2008.
[56] C. Legrand-Buscema, C. Malibert, and S. Bach, 'Elaboration and characterization of thin films of TiO 2 prepared by sol–gel process', *Thin Solid Films*, vol. 418, no. 2, pp. 79–84, 2002.
[57] S. Ito, P. Chen, P. Comte, M. K. Nazeeruddin, P. Liska, P. Péchy, and M. Grätzel, 'Fabrication of screen-printing pastes from TiO2 powders for dye-sensitised solar cells', *Prog. Photovolt. Res. Appl.*, vol. 15, no. 7, pp. 603–612, Nov. 2007.
[58] A. Mei, X. Li, L. Liu, Z. Ku, T. Liu, Y. Rong, M. Xu, M. Hu, J. Chen, Y. Yang, M. Grätzel, and H. Han, 'A hole-conductor–free, fully printable mesoscopic perovskite solar cell with high stability', *Science*, vol. 345, no. 6194, pp. 295–298, Jul. 2014.
[59] C. Momblona, O. Malinkiewicz, C. Roldán-Carmona, A. Soriano, L. Gil-Escrig, E. Bandiello, M. Scheepers, E. Edri, and H. J. Bolink, 'Efficient methylammonium lead iodide perovskite solar cells with active layers from 300 to 900 nm', *APL Mater.*, vol. 2, no. 8, p. 081504, Aug. 2014.

APPENDICES

Appendices A : The product of preliminary studies for proposed-assisted TiO_2 deposition

J. Coat. Technol. Res.
DOI 10.1007/s11998-015-9718-8

Ultrasonic coating of nanofibrous webs: a feasible approach to photocatalytic water filters

Ramazan Simsek, Yusuf Polat, Esra Serife Pampal, Onur Agma, Ali Kilic

Abstract In this study, we introduce ultrasound-assisted coating as a simple means of functionalizing nanofibrous membranes for photocatalytic (PC) water filtration. TiO_2 nanoparticles, which have an anatase crystalline phase with superior PC activity, were directly synthesized over TPU nanofibers and the coated membranes were characterized using scanning electron microscopy (SEM) and X-ray diffractometry. The SEM images confirmed that the addition of polyethylene glycol reduced the nanoparticle dimensions and yielded greater distribution over the nanofibers. UV–Vis analysis demonstrated that Ag decoration over the coating enhanced the PC performance by up to 69.4% following 2-h UV illumination.

Keywords Nanofibers, Ultrasonic, Coating, Photocatalytic

Introduction

Due to frequent droughts, population increases, and rapid industrialization, the need for safe water is currently at its greatest. According to UN reports, more than 1.5 billion people are currently unable to obtain safe, clean water[1] and, in developing countries, over 2 million people die annually as a result of water-related diseases.[2] Additionally, the impact of the greenhouse effect on the environment, coupled with climate change, is causing the treatment of waste water to become an increasingly pressing issue. Even in well-developed countries, an exorbitant amount of contaminated water is released into water sources such as rivers, lakes, and underground deposits without treatment, leading to pollution problems. In order to identify the most effective engineering solutions, the contaminants within used water, which can be classified as either particulate matter or biological and chemical components, must be examined.[3–5] For particulate matter and biological material, well-known solutions such as coagulation, flocculation, and pressure-driven membranes are widely used. On the other hand, the treatment of chemically contaminated water remains a challenging issue. To date, various oxidation techniques have been proposed. Of these, photocatalytic oxidation (PCO) is a feasible method for the removal of chemical contaminants from wastewater.[6]

As regards the development of an effective PCO technique, titania (or TiO_2) is by far the most widely investigated semiconductor. This is because of its superior PCO performance, along with its unique properties such as chemical stability, biocompatibility, and low cost.[7] Comprising a filled valence band (VB) and an empty conduction band (CB), illumination by a photon with energy larger than the TiO_2 band gap generates an electron in the CB and holes in the VB.[8] Hence, the generated electron and hole produce radicals around the contaminant molecules or directly react with them.[9] Many studies have concentrated on modifying the TiO_2 structure so as to enhance its activity in response to visible light,[5,8,10,11] since titania exhibits a low electron transfer rate to oxygen and a high electron–hole recombination rate. This significantly limits the photo-oxidation rate of organic compounds.[8] Photo-generated electron–hole pairs

R. Simsek, Y. Polat, E. S. Pampal, O. Agma, A. Kilic (✉)
TEMAG Labs, Istanbul Technical University, Gumussuyu, 34437 Istanbul, Turkey
e-mail: alikilic@itu.edu.tr

R. Simsek
Department of Textile Engineering, Faculty of Technology, Marmara University, Istanbul, Turkey

E. S. Pampal
Department of Textile Engineering, Faculty of Engineering, Bartin University, Bartin, Turkey

Published online: 21 July 2015

have a recombination time of the order of 10^{-9} s; however, the chemical interaction with adsorbed pollutant species has a timescale of 10^{-8} to 10^{-3} s.[2,9] The decoration of TiO_2 with metals is a practical means of enhancing the photocatalytic (PC) efficiency, as the recombination of photo-excited electrons is restricted in metal-doped titania. This is because of the appearance of a semiconductor–metal junction, called the Schottky barrier, in which a space-charge separation region is formed. At the metal-titania interface, electron movement occurs because of the difference in Fermi energy level. Electrons move from the high Fermi energy level (TiO_2) toward the lower Fermi energy level of the metal. Thus, charge separation is achieved through the Schottky barrier that appears at the metal-TiO_2 interface. The electron movement leads to excess electrons in the metal, along with excess positive holes in the TiO_2 VB. The resultant depletion layer owing to the Schottky barrier at the metal-TiO_2 interface has the capability to sustain charge separation.[12] Of such metallic modifications, silver (Ag)-incorporated TiO_2 particles have demonstrated enhanced electron–hole separation and interfacial charge transfer ability, as well as increased visible-light excitation.[13] Hence, slower recombination of photo-generated electron–hole pairs and, at the same time, extended excitation wavelengths have been observed.[12]

For application purposes, TiO_2 in powder form is not appropriate, since it requires subsequent cleaning from the water following the initial treatment.[8] Thus, in this study, an ultrasonic coating procedure is proposed that immobilizes the TiO_2 on nanofibrous webs. This system allows for the simultaneous coating of pristine/Ag-doped TiO_2 on previously prepared electrospun webs. Nanofibrous webs provide the largest surface area for coating with an active layer. Theoretically, very high surface roughness for illumination is achievable. Further, the high-energy acoustic cavitation that occurs during ultrasonic treatment provides durable and uniform coating. An extremely high temperature (approximately 5000°C) and pressure (approximately 500 atm) are contained in the cavities, which is a unique feature of the ultrasonic process. These cavities have lifetimes with a timescale of a few microseconds and the shock waves that emerge following cavity collapse in a liquid suspension cause particle collisions, which have sufficient energy to catalyze many reactions.[14–16] Finally, TiO_2 that is synthesized in an ultrasonic bath has more advantageous properties than that synthesized via a conventional sol–gel system, including an extremely high surface area, decreased particle size, and superior PCO activity.[17]

In this study, ultrasonic irradiation was used to decorate silver ions onto TiO_2-coated nanofibrous mats. To the best of our knowledge, this is the first time this approach has been used. Following decoration, the Ag nanoparticles created the possibility for a Schottky barrier to develop, which ensured charge separation. A thermoplastic urethane (TPU) nanofiber mat was used as a template, with the silver nanoparticles as decorative agents on the titania layer. The efficiency of the coated nanofibrous filters was then investigated and evaluated based on the degradation rate of methylene blue (MB) in an aqueous solution. Also, the effect of added polyethylene glycol (PEG) on the TiO_2 distribution and PCO performance was evaluated. In order to evaluate the efficacy of the proposed approach, the performance of ultrasonic-assisted synthesized pristine/silver-decorated TiO_2 and that of a similar commercial product, Degussa, was compared.

Materials and methods

A TPU polymer was purchased from BASF (C95). Dimethyl formamid (DMF %98) and Ethanol (%99) purchased from Merck without any further treatment were used as a solvent for the polymer solution preparation, while $AgNO_3$ and titanium tetra isopropoxide (TTIP) were used as the Ag and TiO_2 sources for the PC activation, respectively. Titanium(IV) oxide (Degussa 21 nm ≥99.5%) was purchased from Sigma Aldrich. All chemicals were used without further purification, as obtained from Sigma Aldrich.

TPU nanofiber electrospinning

A neat polyurethane (13 wt%) solution was prepared by dissolving TPU pellets in DMF at 80°C. Electrospinning was conducted at 24 kV, with a tip-to-collector distance of 150 mm and a solution feed rate of 0.6 mL/h. TPU was selected as the base polymer because of its elasticity.

TiO_2 NP synthesis

Electrospun TPU nanofibrous mats (35 mm × 35 mm) were immersed in preformed solutions (Table 1) under ultrasonic irradiation at a frequency of 40 kHz. Nanocrystalline TiO_2 was synthesized and coated onto the TPU nanofibers simultaneously by hydrolysis of the TTIP in the presence of ultrasonic irradiation. Then, 3 g of silver nitrate ($AgNO_3$) was added to the ultrasonic bath in order to decorate the TiO_2 coating with silver particles. After 5 min of ultrasonic irradiation in solution, the samples were exposed to UV irradiation for 30 min. This was to transform the silver ions into silver atoms, following the method explained in reference (18).

Morphological analysis

The nanoparticle distribution on the nanofibers was examined using a Zeiss EVO MA10 SEM at

Table 1: Process parameters and solution compositions

Filter/sample name	Solution composition	Process
TTIP	100 mL DI water + 2 mL TTIP	45-min ultrasonic
PEG–TTIP	50 mL ethanol + 0.4 mL PEG + 2 mL TTIP + 50 mL distilled water	45-min ultrasonic
PEG–TTIP–Ag	50 mL ethanol + 0.4 mL PEG + 2 mL TTIP + 50 mL distilled water + 3 g $AgNO_3$	45-min ultrasonic
PEG–TiO_2–Ag-UV	50 mL ethanol + 0.4 mL PEG + 2 mL TTIP + 50 mL distilled water + 3 g $AgNO_3$	45-min ultrasonic, 30-min UV

15.00–20.00 kV with magnifications ranging from 500 to 20 kX. A tungsten filament was used to create the beam and the reported resolution was 35 Å with a 20-kV beam. To watch the elemental composition after Ag decoration, the energy dispersive X-ray spectroscopy (EDS) was recorded using SEM (model Zeiss EVO 60) installed in MEMTEK Laboratories, ITU. The crystal structure of the TiO_2 coating was investigated using a Rigaku SmartLab X-ray diffractometer equipped with a rotating anode Cu source with in-line focus geometry, which produces Cu-Kα radiation with a wavelength of 1.54 Å generated at 40 kV and 44 mA. The samples were equatorially scanned within a 2θ range (=20°–80°) at an increment of 0.1°.

MB decomposition test

A custom-made UV irradiation system was used to conduct the PCO performance test. The MB degradation rate under UV illumination was used as a means of evaluating the PCO performance of the nanofibrous samples.[12,19] An explanation of the evaluation technique based on MB concentration loss is available in the literature.[19–22] In order to evaluate the PC activity of the TiO_2, a 10^{-5} M MB aqueous solution was prepared. The as-prepared functionalized nanofibrous mats were floated in the MB aqueous solution for periods of 10 min, 1 and 2 h under UV illumination. The UV lamp used in the study had a wavelength of 365 nm and power of 9 W, and the decomposition rate was evaluated using UV–Visible spectroscopy (Philips UVA PLS/PLA-9 W, irradiation 1.66 W).

Results and discussion

Morphological analysis

Scanning electron microscopy (SEM) was used to analyze the nanofiber diameter and the distribution of the nanoparticles on the nanofibrous webs. As can be seen in Fig. 1a, the average diameter of the TPU nanofibers was found to be 164 ± 33 nm. A smaller fiber diameter would yield a larger surface area, which is important for catalytic reactions. On the other hand, the ultrasonic process did not alter the fibrous structure, as can be seen in Fig. 1b. However, agglomeration occurred in the pristine TiO_2 sample, since TTIP is highly sensitive to water. In the case of the TTIP-based coating sample, TiO_2 particles on the microscopic scale were obtained with no proper distribution. However, the addition of PEG to the solution resulted in TiO_2 particles of nanoscopic dimensions with a more suitable distribution on the nanofibrous web. The homogenous distribution of the nano-scale TiO_2 particles in Figs. 1c and 1d can be attributed to the hydroxyl groups of the PEG which acted as a surfactant resulted in inhibition of agglomeration of synthesized TiO_2 particles.[23,24] Note that dimensional control is extremely important as regards PCO performance, because decreased dimensions enhance the interaction between the TiO_2 particles and dye (MB) molecules, as well as the interaction between the UV light and the TiO_2 particle surfaces. This justifies the strategy of introducing a chemical agent to enhance the PCO activity of the TiO_2.

Additionally, EDS analysis was also conducted to prove Ag decoration on TiO_2. As shown in Fig. 2b, Ag decoration is apparent over TiO_2 particles, whereas without the presence of $AgNO_3$ in precursor, coating was solely composed of C, Ti, and O.

The well-known crystal structures of TiO_2 are anatase and rutile, and it is important to note that the physical properties of a material are dependent on its crystal structure as to highly PC activity. The TiO_2 particles synthesized in the presence of ultrasonic irradiation exhibited an anatase crystalline phase, as seen in Fig. 3. The crystal structure of the sonochemically synthesized anatase TiO_2 may be due to the localized high temperature and high pressure induced by the ultrasonic irradiation. Clearly, the primary advantage of ultrasound-induced anatase TiO_2 synthesis is that the resultant material does not require any additional heat treatment. Thus, this novel method can be evaluated as being both cost effective and rapid, in comparison with other methods such as sol–gel synthesis.

In general, anatase has significantly greater photoactivity than rutile, the other well-known TiO_2 crystalline phase.[25] This behavior is attributed to the band-gap size; anatase and rutile crystalline structures have 3.2 and 3.0 eV band gaps, respectively. The higher band gap is the source of the greater redox potential of the anatase structure. Additionally, anatase crystals have a higher surface hydroxyl area density. Hydroxyls play an important role in slowing the recombination of the photo-generated electron–hole pairs.[12] In addition, Perez et al.[26] have also

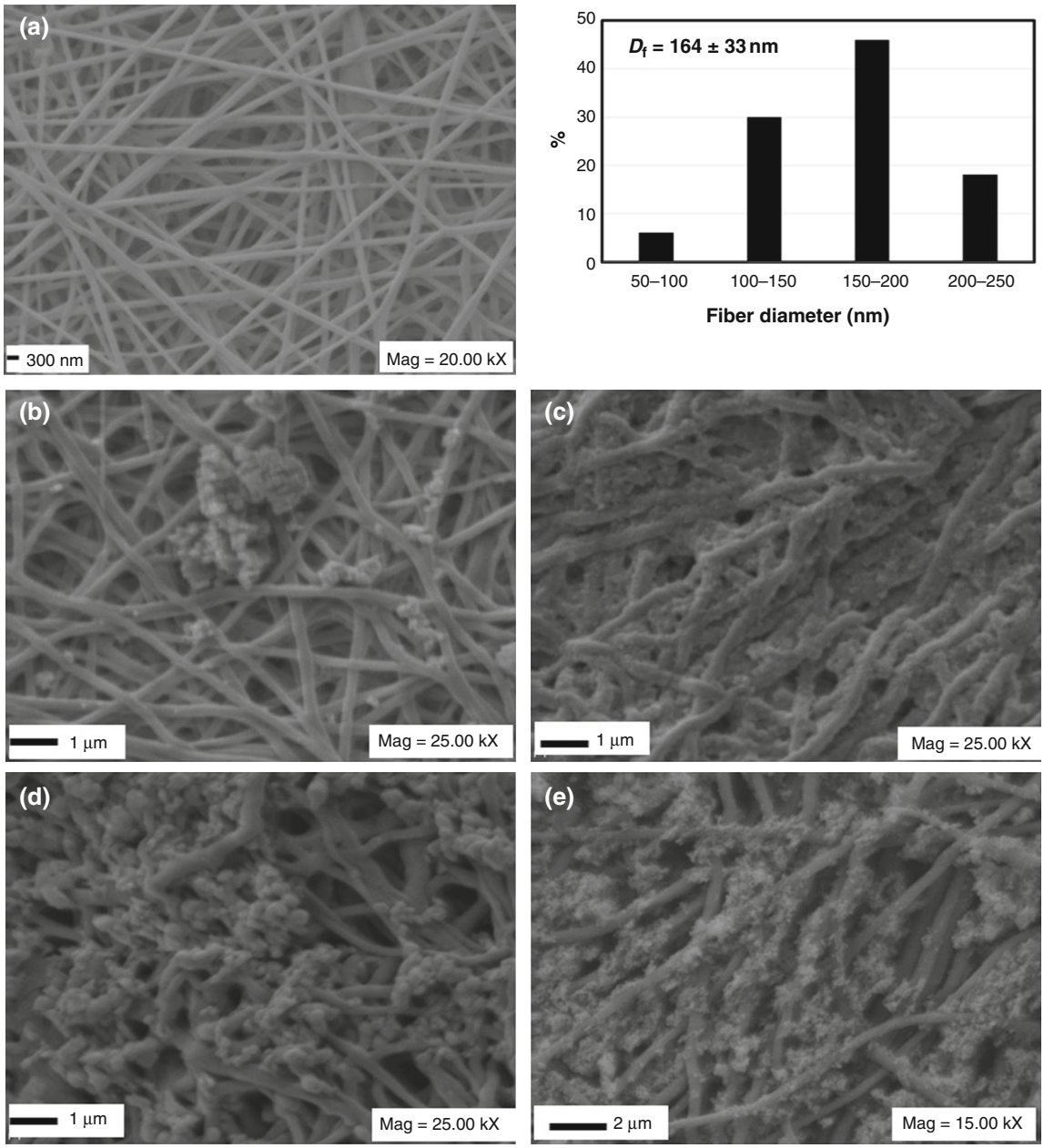

Fig. 1: SEM images of electrospun nanofiber webs: (a) pristine TPU nanofiber; (b) TiO_2 (TTIP-based); (c) TiO_2 (PEG-TTIP); (d) TiO_2 (PEG-TTIP-Ag); and (e) Degussa coated on nanofibers

demonstrated that decreased particle size causes an increase in the band-gap energy of TiO_2. It can then be inferred that the exciton energy levels of TiO_2 with lower particle size are higher than those of TiO_2 samples with greater particle size. It should also be noted that excitons with higher energies may be the source of the superior PC activity observed for this material. As seen in Fig. 2, the as-synthesized TiO_2 nanoparticles with anatase crystalline structures match the results of the study conducted by Perez et al. exactly.[26] It can also be inferred that the PEG addition resulted in the synthesis of TiO_2 with lower dimensions, as indicated by the SEM images. Hence, TiO_2 with reduced dimensions exhibits superior PCO activity because of the higher energy levels of its excitons.

MB decomposition performance of PC filters

UV–Vis spectroscopy measurements were performed after illumination of the MB/water solutions, in which the samples were embedded for periods of 10 min, 1 and 2 h. The as-prepared MB solution was taken as the base line. It is clear from Fig. 4 that the MB solutions

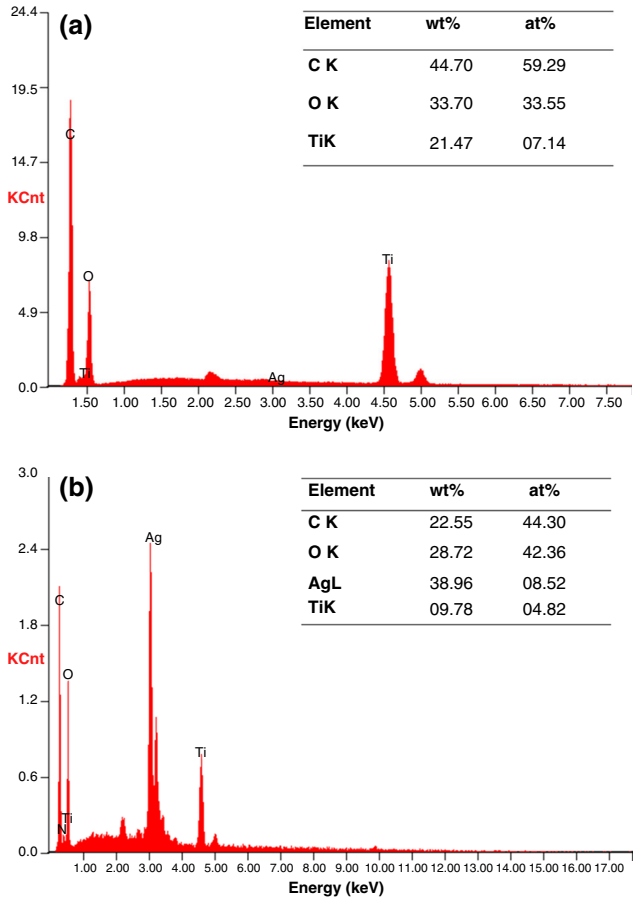

Fig. 2: Elemental composition of coatings via ultrasonic-assisted synthesis (a) TiO_2 (from TTIP, ultrasonicated for 45 min) (b) TiO_2-Ag (from PEG-TTIP-Ag ultrasonicated for 45 min) Silver peaks around 3.05 eV are apparent for decorated samples

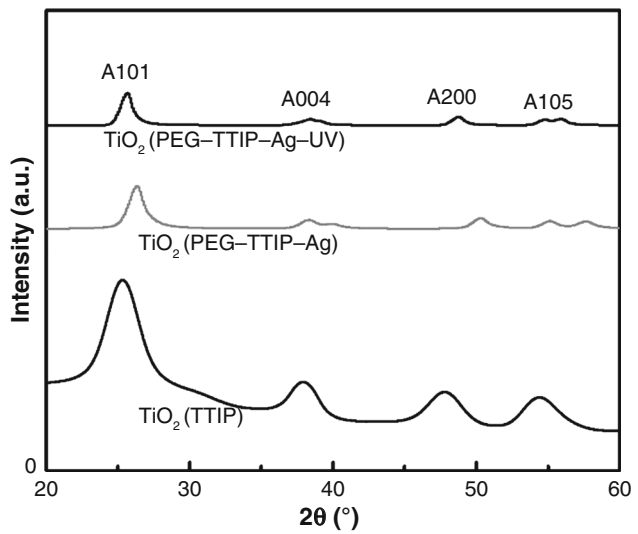

Fig. 3: XRD spectrum of synthesized TiO_2 nanoparticles

treated with functionalized nanofibrous mats were dramatically clarified as a result of the PC activity of the TiO_2 in the solution. As can be seen in Fig. 4a, the presence of the PEG enhanced the PCO efficiency of the filters compared to the performance of the TTIP-based filters. It can then be concluded that PEG addition is an effective strategy for controlling the dimensions of the as-synthesized nanoparticles. Therefore, the PEG-induced highly specific surface area increased the interaction between the TiO_2 and UV light, as well as the interaction between the MB and TiO_2 particles. These increased interactions may be the source of the PCO performance enhancement. Additionally, it can be hypothesized that other reactions may exist which resulted in intermediate products which did not decompose fully. Note that the TTIP-based filter may require a longer period of time for effective performance to be demonstrated, since the UV–Vis spectrum curves indicate absorption in the range of 450–550 and 700–800 nm. On the other hand, the synthesized TiO_2 with added PEG achieved complete MB decomposition.

Considering Fig. 4b, it can be clearly stated that the Ag decoration contributed substantially to the performance of the PC filters, as expected. As explained previously, both charge separation and retarded recombination induced a PCO performance enhancement. Further, additional enhancement of the PCO efficacy was also expected following the reduction of the silver ions to atoms by the UV irradiation. However, the Ag-based filters with no UV irradiation exhibited superior performance to the filter that was exposed to the UV radiation, which was unexpected. Hence, further investigation and improvement of the method used to obtain silver atoms is required in forthcoming studies, in order to explain this result.

In addition, a comparison of the PC effectiveness of the TiO_2 particles synthesized via the sonochemical reaction with that of Degussa (commercial TiO_2 nanoparticles) was conducted. Although Degussa is a well-known and widely used PC, the sonochemically synthesized TiO_2 with silver decoration demonstrated far superior PC activity, as can be seen in Fig. 4c. The excellent performance of the synthesized TiO_2 can be attributed to the reduced dimension and significantly more uniform distribution of the TiO_2 nanoparticles. This uniform distribution was due to the presence of the PEG, and can be considered to be another source of the superior performance of PEG-based PC filters. Following Fig. 4, it is also important to emphasize that PC filters have the capability to degrade organic compounds with a decomposition rate that is directly proportional to the UV irradiation time.

It is clear that MB degradation was observed via the absorbance spectra of the dye molecule throughout the irradiation as shown in Fig. 4. MB degradation rate as a function of irradiation time was also studied. Typically, disappearance of MB is directly correlated with time and can be predicted with Langmuir–Hinshelwood reaction kinetics.[27,28] The examination of MB

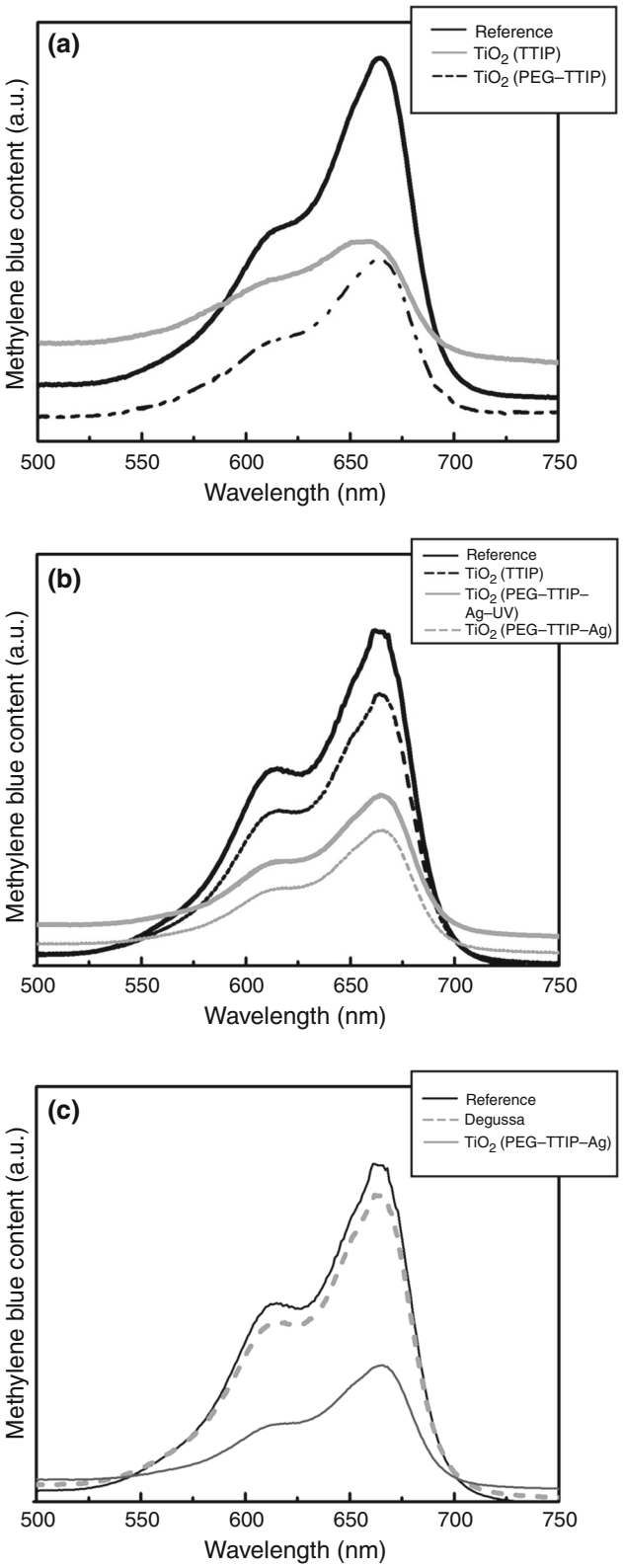

◀ **Fig. 4: Performance evaluation of photocatalytic filters based on methylene blue (MB) degradation after following UV light irradiation for 120 min. (a) Effect of PEG addition on PCO performance, (b) Effect of Ag addition and UV exposure on PCO performance; (c) Comparison of PCO performance of commercial TiO_2 and ultrasonic-assisted synthesized TiO_2**

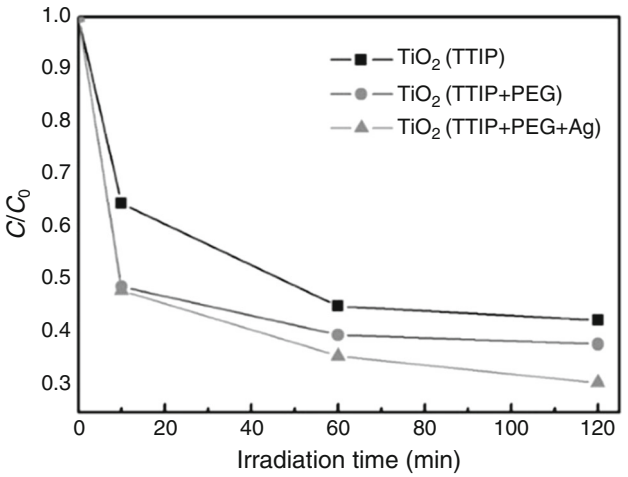

Fig. 5: Photocatalytic degradation of MB as a function of irradiation time for the filters TTIP, TTIP + PEG, TTIP + PEG + Ag

concentration (C/C_0) was conducted with the reaction time via $\ln\left(\frac{C}{C_0}\right) = k \cdot t$, where k is the reaction rate constant; t, time; C_0 is the initial MB concentration; and C is the MB concentration at a specific irradiation time. Figure 5 displays the time dependency of C/C_0 under UV irradiation of the filters. It is important to note that direct photolysis of MB was in negligible scale. On the other hand, it is clear that MB degradation varies as TiO_2 (TTIP + PEG + Ag) > TiO_2(TTIP + PEG) > TiO_2 (TTIP). The variation in MB degradation rate can be attributed to charge separation phenomena, higher exciton energy in anatase crystal structure, decreased particle dimension, and better distribution of nanoparticle on nanofibrous web. Besides that, MB degradation amount can be evaluated by Fig. 5 throughout 120 min. It is evident that 69.4% MB degradation takes place by TiO_2(TTIP + PEG + Ag) filter. Silver decoration resulted in higher performance of the PC filters probably as a result of retarded charge recombination.

Conclusions

An ultrasonically assisted TiO_2 coating has been proposed as an approach to producing PC water filters. This novel technique is promising as it is based on the ceramic coating of polymeric membranes, which enhances both chemical and thermal durability. Further, this system facilitates metal doping/decoration, which enhances PC performance. The dimensions of the as-synthesized TiO_2 particles are controlled by the addition

of PEG, and it has been shown that PEG has beneficial effects on the PCO performance of the TiO_2, leading to smaller particle size and significantly more uniform particle distribution. Additionally, UV–Vis measurements have demonstrated that Ag decoration enhances the performance by approximately 70%, as it causes charge separation at the TiO_2-Ag interface. Further, the PC water filter developed here exhibited superior performance to a similar commercially available product. The findings of this paper will lead to the development of more effective water filtration systems, which have considerable potential applications worldwide.

Acknowledgments The authors gratefully acknowledge the ITU Scientific Research Fund (ITU-BAP) for financial support of this work. Thanks are also due to Prof. Ahmet Gul and Dr. Barbaros Akkurt for their analytical assistance and fruitful discussions.

References

1. Sobsey, MD, Stauber, CE, Casanova, LM, Brown, JM, Elliott, MA, ''Point of Use Household Drinking Water Filtration: A Practical, Effective Solution for Providing Sustained Access to Safe Drinking Water in the Developing World.'' *Environ. Sci. Technol.*, **42** (12) 4261–4267 (2008)
2. Gleick, PH, *Dirty Water: Estimated Deaths from Water-Related Diseases 2000–2020*. Pacific Institute for Studies in Development, Environment, and Security, Oakland, 2002
3. Hoffmann, MR, Martin, ST, Choi, W, Bahnemann, DW, ''Environmental Applications of Semiconductor Photocatalysis.'' *Chem. Rev.*, **95** (1) 69–96 (1995)
4. Hu, X, Li, G, Yu, JC, ''Design, Fabrication, and Modification of Nanostructured Semiconductor Materials for Environmental and Energy Applications.'' *Langmuir*, **26** (5) 3031–3039 (2009)
5. Choi, W, ''Pure and Modified TiO_2 Photocatalysts and Their Environmental Applications.'' *Catal. Surv. Asia*, **10** (1) 16–28 (2006)
6. Devi, LG, Kavitha, R, ''A Review on Non Metal Ion Doped Titania for the Photocatalytic Degradation of Organic Pollutants Under UV/Solar Light: Role of Photogenerated Charge Carrier Dynamics in Enhancing the Activity.'' *Appl. Catal. B Environ.*, **140** 559–587 (2013)
7. Linsebigler, AL, Lu, G, Yates, JT, Jr, ''Photocatalysis on TiO_2 Surfaces: Principles, Mechanisms, and Selected Results.'' *Chem. Rev.*, **95** (3) 735–758 (1995)
8. Park, H, Park, Y, Kim, W, Choi, W, ''Surface Modification of TiO_2 Photocatalyst for Environmental Applications.'' *J. Photochem. Photobiol. C*, **15** 1–20 (2013)
9. Fujishima, A, Rao, TN, Tryk, DA, ''Titanium Dioxide Photocatalysis.'' *J. Photochem. Photobiol. C*, **1** (1) 1–21 (2000)
10. Ohno, T, Mitsui, T, Matsumura, M, ''Photocatalytic Activity of S-Doped TiO_2 Photocatalyst Under Visible Light.'' *Chem. Lett.*, **32** (4) 364–365 (2003)
11. Kato, H, Kudo, A, ''Visible-Light-Response and Photocatalytic Activities of TiO_2 and $SrTiO_3$ Photocatalysts Codoped with Antimony and Chromium.'' *J. Phys. Chem. B*, **106** (19) 5029–5034 (2002)
12. Woan, K, Pyrgiotakis, G, Sigmund, W, ''Photocatalytic Carbon-Nanotube-TiO_2 Composites.'' *Adv. Mater.*, **21** 2233–2239 (2009)
13. Kubacka, A, Ferrer, M, Martínez-Arias, A, Fernández-García, M, ''Ag Promotion of TiO_2 Anatase Disinfection Capability: Study of *Escherichia coli* Inactivation.'' *Appl. Catal. B Environ.*, **84** (1) 87–93 (2008)
14. Suslick, KS, Sonochemistry. *Kirk-Othmer Encyclopedia of Chemical Technology*, 4th edn, vol. 26, pp. 517–541. Wiley & Sons, New York (1998)
15. Suslick, KS, Price, GJ, ''Applications of Ultrasound to Materials Chemistry.'' *Annu. Rev. Mater. Sci.*, **29** (1) 295–326 (1999)
16. Suslick, KS, Didenko, Y, Fang, MM, Hyeon, T, Kolbeck, KJ, McNamara, WB, Mdleleni, MM, Wong, M, ''Acoustic Cavitation and Its Chemical Consequences.'' *Philos. Trans. R. Soc. Lond. Ser. Math. Phys. Eng. Sci.*, **357** (1751) 335–353 (1999)
17. Awati, PS, Awate, SV, Shah, PP, Ramaswamy, V, ''Photocatalytic Decomposition of Methylene Blue Using Nanocrystalline Anatase Titania Prepared by Ultrasonic Technique.'' *Catal. Commun.*, **4** (8) 393–400 (2003)
18. Ghosh, SK, Kundu, S, Mandal, M, Nath, S, Pal, T, ''Studies on the Evolution of Silver Nanoparticles in Micelle by UV-Photoactivation.'' *J. Nanoparticle Res.*, **5** (5–6) 577–587 (2003)
19. Tanguay, JF, Suib, SL, Coughlin, RW, ''Dichloromethane Photodegradation Using Titanium Catalysts.'' *J. Catal.*, **117** (2) 335–347 (1989)
20. Houas, A, Lachheb, H, Ksibi, M, Elaloui, E, Guillard, C, Herrmann, J-M, ''Photocatalytic Degradation Pathway of Methylene Blue in Water.'' *Appl. Catal. B Environ.*, **31** (2) 145–157 (2001)
21. Height, MJ, Pratsinis, SE, Mekasuwandumrong, O, Praserthdam, P, ''Ag-ZnO Catalysts for UV-Photodegradation of Methylene Blue.'' *Appl. Catal. B Environ.*, **63** (3) 305–312 (2006)
22. Yen, C-Y, Lin, Y-F, Hung, C-H, Tseng, Y-H, Ma, C-C, Chang, M-C, Shao, H, ''The Effects of Synthesis Procedures on the Morphology and Photocatalytic Activity of Multi-Walled Carbon Nanotubes/TiO_2 Nanocomposites.'' *Nanotechnology*, **19** (4) 604 (2008)
23. Kato, K, Niihara, K, ''Roles of Polyethylene Glycol in Evolution of Nanostructure in TiO2 Coatings.'' *Thin Solid Films*, **298** (1–2) 76–82 (1997)
24. Alcantar, NA, Aydil, ES, Israelachvili, JN, ''Polyethylene Glycol-Coated Biocompatible Surfaces.'' *J. Biomed. Mater. Res.*, **51** (3) 343–351 (2000)
25. Sun, Q, Xu, Y, ''Evaluating Intrinsic Photocatalytic Activities of Anatase and Rutile TiO_2 for Organic Degradation in Water.'' *J. Phys. Chem. C*, **114** (44) 18911–18918 (2010)
26. Hernández-Perez, I, Maubert, AM, Rendón, L, Santiago, P, Herrera-Hernández, H, Díaz-Barriga Arceo, L, Garibay Febles, V, Palacios Gonzalez, E, González-Reyes, L, ''Ultrasonic Synthesis: Structural, Optical and Electrical Correlation of TiO_2 Nanoparticles.'' *Int. J. Electrochem. Sci.*, **7** 8832–8847 (2012)
27. Gopalakrishnan, K, Joshi, HM, Kumar, P, Panchakarla, LS, Rao, CNR, ''Selectivity in the Photocatalytic Properties of the Composites of TiO_2 Nanoparticles with B- and N-Doped Graphenes.'' *Chem. Phys. Lett.*, **511** (4–6) 304–308 (2011)
28. An, S, Joshi, BN, Lee, MW, Kim, NY, Yoon, SS, ''Electrospun Graphene-ZnO Nanofiber Mats for Photocatalysis Applications.'' *Appl. Surf. Sci.*, **294** 24–28 (2014)

CURRICULUM VITAE

Name Surname: **Ramazan ŞİMŞEK**

Place and Date of Birth: **Kayseri, 10.01.1983**

E-Mail: **ramazansimsek2@gmail.com**

EDUCATION **:**

B.Sc. : Department of Textile Engineering, Ege University, 2005

PUBLICATIONS, PRESENTATIONS AND PATENTS ON THE THESIS:

R. Simsek, Y. Polat, E. S. Pampal, O. Agma, ve A. Kilic, "Ultrasonic coating of nanofibrous webs: a feasible approach to photocatalytic water filters", *J Coat Technol Res*, ss. 1–7, Tem. 2015.

SIMSEK, R., CALISIR, M. D., SEVIM, M. A., & KILIC, A. (2015). Boya Duyarlı Güneş Pillerinde Karbon Elektrot Kullanımı. *1. Ulusal karbon Konferansı.* Istanbul: ITU.

Simsek R., Calisir M. D., Sevim M. A., Kilic A. & Demir A. (2015). "From coloration to energy harvesting. Screen printing technology to establish monolithic dye sensitized solar cell", *5th International Textile Congress*, ITU, Istanbul